Time-Frequency and Time-Scale Analysis of Non-Stationary Biomedical Signals

by

Görkem SERBES

B.S., Electrical & Electronics Engineering, Bahcesehir University, 2006

M.S., Electrical & Electronics Engineering, Bahcesehir University, 2009

Submitted to the Institute of Biomedical Engineering
in partial fulfillment of the requirements
for the degree of
Doctor
of
Philosophy

Boğaziçi University

2014

Time-Frequency and Time-Scale Analysis of Non-Stationary Biomedical Signals

APPROVED BY:

Prof. Dr. Yasemin P. Kahya .....
(Thesis Advisor)

Prof. Dr. Halil Ö. Gülçür .....
(Thesis Co-advisor)

Prof. Dr. Nizamettin Aydın .....

Prof. Dr. Ahmet Ademoğlu .....

Prof. Dr. Cengizhan Öztürk .....

Assoc. Prof. Dr. Albert Güveniş .....

DATE OF APPROVAL: 29 April 2014

ACKNOWLEDGMENTS

Foremost, I would like to express my deepest gratitude to my supervisor Prof. Yasemin P. Kahya and to my co-supervisor Prof. Halil Ö. Gülçür for their guidance and encouragement throughout this thesis study. Their advices were very helpful and are reflected throughout this thesis. Their understanding and support were motivational through the good and the bad times.

I would like to thank to Prof. Nizamettin Aydın. His door was always open for questions and discussions. His guidance helped me in all the time of research and writing of this thesis. It has been a pleasure for me to work with him.

I also would like to thank Prof. Ahmet Ademoğlu, Prof. Cengizhan Öztürk and Assoc. Prof. Albert Güveniş for their participation in my thesis jury and helpful comments.

I am very grateful to have been a Ph.D. student at the Institute of Biomedical Engineering. My thanks also go to my friends and colleagues Cemal Okan Şakar, Betül Erdoğdu Şakar, İpek Şen and Mehmet Kocatürk for their discussions and friendship over the years.

I would like to thank my mother Nükhet, my brother Gencer, every member of my family, and my friends who have always supported and encouraged me all these years. Finally, my deepest thanks go to my wife, Hasret and my lovely son Çınar for their love and their enduring support. Without their patience and encouragement, this thesis would never have been written.

This thesis has been supported by the Ph.D. scholarship (2211) from the Scientific and Technological Research Council of Turkey (TÜBİTAK).

ABSTRACT

Time-Frequency and Time-Scale Analysis of Non-Stationary Biomedical Signals

Fourier transform (FT), which assumes that the analyzed signal is stationary, is not entirely appropriate to analyze biomedical signals since they are in non-stationary nature. To overcome this drawback, FT can be applied over short-windows of time within which the signal can be considered to be stationary. However, this short-time Fourier transform is hampered with a serious time-frequency (TF) trade-off dilemma. Recently, a number of different TF analysis techniques has been developed that provide improved TF resolution. In this dissertation, we consider two strongly non-stationary biomedical signals, lung sound and blood-flow signals, and propose novel and effective systems for the detection of crackles from the former and emboli from the latter. The crackle detection system uses the dual tree complex wavelet transform (DTCWT) for denoising and time-frequency/scale analysis with various windows/wavelets for feature extraction. The emboli detection system processes forward and reverse flow signals using FT, discrete wavelet transform (DWT), and DTCWT. Dimensionality of the extracted coefficients is reduced using Principal Component Analysis, and the new features are used for predicting whether a signal is emboli, speckle or artifact. Since the dyadic TF tiling of classical DWT is not appropriate for processing embolic signals, and since the discrete wavelet packet transform (DWPT) can adaptively decompose the TF axis, we also propose a directional complex DWPT for mapping directional information while processing quadrature signals (QSs). This method has significantly less computational complexity than the existing methods. To overcome the poor frequency resolution, severe frequency aliasing and lack of shift-invariance drawbacks of the DWT, we also propose a novel directional complex DWT. It consists of filter-banks with rational sampling factors and can be applied directly to QSs.

Keywords: Crackles, Emboli, Quadrature Signals, Ensemble Learning.

ÖZET

Durağan-Olmayan Biyomedikal İşaretlerin Zaman-Sıklık ve Zaman-Ölçek Analizi

Fourier dönüşümü (FD) çözümlenen işaretin durağan olduğunu varsayar; bu nedenle de genelde, durağan-olmayan biyomedikal işaretlerin çözümlenmesi için uygun değildir. Bu eksikliği aşmak için, FD'yi, işaretin durağan kabul edilebileceği kısa zaman pencereleri içerisinde uygulayabiliriz. Fakat, bu Kısa Zamanlı FD ciddi bir zaman-frekans değiş-tokuş ikilemine yol açar. Son zamanlarda durağan-olmayan işaretlerin işlenmesi için farklı iyileştirilmiş zaman-sıklık (ZS) çözümleme teknikleri geliştirilmiştir. Bu tezde, durağan olmayan iki biyomedikal işareti, akciğer-ses ve kan-akış işaretlerini ele aldık ve birinciden çıtırtı ikinciden de emboli tespiti yapan yeni ve etkili sistemler önerdik. Çıtırtı tespit sisteminde, gürültü-arındırmada çift ağaç karmaşık dalgacık dönüşümü (ÇAKDD) ve öznitelik çıkarımında çeşitli pencereler/dalgacıklar ile gerçekleştirilmiş zaman-sıklık/ölçek çözümlemesi kullanılmıştır. Ultrason işaretlerinden emboli tespit eden sistemde ise, ileri ve geri akış işaretleri FD, ayrık dalgacık dönüşümü (ADD) ve ÇAKDD kullanılarak işlenmiştir. Elde edilen katsayıların boyutu Temel Bileşen Analizi kullanılarak azaltılmış ve bu yeni ileri ve geri yönlü öznitelikler, işaretin sınıfının emboli, benek veya artifakt olup olmadığının tahmininde kullanılmıştır. Geleneksel ADD'nin diyadik ZS dilimlenmesi embolik işaretlerin işlenmesi için uygun değildir. Ayrık dalgacık paket dönüşümü (ADPD) ile ZS düzlemi esnek biçimde örneklenebilir. Bundan dolayı, quadrature işaretleri (Qİ) işlerken aynı zamanda yön bilgisini elde etme yetisine sahip ve var olan yöntemlere göre daha az işlemsel karmaşıklığı olan yeni bir yönlü ADPD önerilmiştir. Son olarak, diyadik-ADD'nin yetersiz sıklık çözünürlüğü, yoğun sıklık örtüşmesi ve zaman kaymalarına aşırı duyarlılık gibi eksikliklerini gidermek için, oransal örnekleme faktörlerine sahip süzgeç-banklarını kullanan ve doğrudan Qİ'e uygulanabilen yeni bir yönlü ADD önerilmiştir.

Anahtar Sözcükler: Çıtırtı, Emboli, Quadrature İşaretler, Topluluk Öğrenmesi

TABLE OF CONTENTS

ACKNOWLEDGMENTS iii
ABSTRACT iv
ÖZET v
LIST OF FIGURES ix
LIST OF TABLES xiii
LIST OF SYMBOLS xv
LIST OF ABBREVIATIONS xvii
1. INTRODUCTION 1
1.1 Motivation Background and Objectives 1
1.2 Organization of the Thesis and Publications 3
2. PULMONARY CRACKLE DETECTION USING TIME-FREQUENCY AND TIME-SCALE ANALYSIS 6
2.1 Introduction 6
2.2 Materials and Methods 7
2.2.1 Data Acquisition System 7
2.2.2 Feature Extraction Using Time-Frequency and Time-Scale Analysis 8
2.2.2.1 Time-Frequency Analysis 10
2.2.2.2 Time-Scale Analysis 11
2.2.3 Denoising Using Dual Tree Complex Wavelet Transform 12
2.2.4 Individual Learning with Feature Sets 15
2.2.5 Ensemble Learning 16
2.3 Experimental Results 18
2.4 Discussion and Conclusions 21
3. AN EMBOLI DETECTION SYSTEM BASED ON THE DUAL TREE COMPLEX WAVELET TRANSFORM AND ENSEMBLE LEARNING 25
3.1 Introduction 25
3.2 Materials and Methods 29
3.2.1 Doppler Ultrasound Dataset Description 29
3.2.2 Signal Processing Methods 29

3.2.2.1 Fourier Transform 30
3.2.2.2 Discrete Wavelet Transform 30
3.2.2.3 Dual Tree Complex Wavelet Transform 32
3.2.3 Feature Extraction and Dimensionality Reduction Methods . . . 35
3.2.3.1 Feature Extraction 35
3.2.3.2 Dimensionality Reduction 35
3.2.4 Overall Structure of the Emboli Detection System 36
3.2.4.1 Individual Emboli Detection System 36
3.2.4.2 Ensemble of Forward and Reverse Directional Signals . 36
3.3 Experimental Results 39
3.4 Discussion and Conclusions 43
4. DIRECTIONAL DUAL TREE COMPLEX WAVELET PACKET TRANSFORMS FOR PROCESSING QUADRATURE SIGNALS 45
4.1 Introduction 45
4.2 Quadrature Signals 48
4.2.1 Phasing Filter Techniques 49
4.2.1.1 Asymmetrical Implementation of the Phasing Filter Technique 49
4.2.1.2 Symmetrical Implementation of the Phasing Filter Technique 51
4.3 Complex Wavelet Transforms 53
4.3.1 Dual Tree Complex Wavelet Transform 53
4.3.2 Dual Tree Complex Wavelet Packet Transform 56
4.4 Directional Dual Tree Complex Wavelet Packet Transforms 59
4.4.1 Asymmetrical Implementation of the Directional Dual Tree Complex Wavelet Packet Transform 60
4.4.2 Symmetrical Implementation of the Directional Dual Tree Complex Wavelet Packet Transform 64
4.4.3 Shift-Invariance Property of the Proposed Methods 66
4.4.4 The Effect of Non-Analytic Subbands and Energy Leakages in Opposite Frequencies 69
4.5 Simulations and Results 70

4.5.1 Single Frequency Quadrature Signal Simulations 70
4.5.2 Band-Limited Quadrature Signal Simulations 73
4.5.3 Processing Real Quadrature Blood Flow Signals 76
4.5.4 Shift-Invariance Property of Proposed Symmetrical Implementation 79
4.5.5 The Effect of Non-Analytic Bands 81
4.5.6 Computational Costs of the Proposed Algorithms 85
4.6 Discussion and Conclusions 88
5. DIRECTIONAL DUAL TREE RATIONAL-DILATION COMPLEX WAVELET TRANSFORM 90
5.1 Introduction 90
5.2 Rational Dilation Wavelet Transform 93
5.3 Dual Tree Rational-Dilation Complex Wavelet Transform 95
5.4 Directional Dual Tree Rational-Dilation Complex Wavelet Transform . 96
5.5 Experimental Results 97
5.6 Discussion and Conclusions 100
6. CONCLUSIONS AND FUTURE WORKS 103
6.1 General Conclusions 103
6.2 Future Works 105
REFERENCES 108

LIST OF FIGURES

Figure 2.1 Overall block diagram of proposed method for one machine learning algorithm. (BOSUT is the abbreviation of "behavior of signals upon time", BOSUF and BOSUS are the abbreviations for "behavior of signals upon frequency" and "behavior of signals upon scale" respectively. A more detailed explanation of the abbreviations can be found in Section 2.2.2). 8

Figure 2.2 Examples of 512-point signals containing crackles (upper two) and healthy signals (lower two). 9

Figure 2.3 For the WFT analysis using Gaussian window. (a) Original crackle signal, (b) original healthy signal, (c) BOSUT for crackle sample, (d) BOSUT for healthy sample, (e) BOSUF for crackle sample, (f) BOSUF for healthy sample. 13

Figure 2.4 Block diagram for a 2-level DTCWT which demonstrates both analysis and synthesis parts. $X(n)$ is the input signal and $Y(n)$ is the processed signal. 14

Figure 2.5 Projections of the original feature sets before (a), and after denoising (b). Projections of the outputs of time-frequency analysis upon time before (c), and after denoising (d) with Gaussian window. Projections of the outputs of time-frequency analysis upon frequency before (e), and after denoising (f) with Gaussian window ('x' represents crackle, and 'o' represents healthy signals). 14

Figure 2.6 SVM ensemble learning architecture for Gaussian window type. 18

Figure 2.7 Overall accuracy error rate of individual feature sets with undenoised and denoised case for three learning algorithms. (The leftmost column set results belong to the original signal subset calculations. The following 14 column sets belong to the TF feature subset calculations. Final 6 column sets belong to the TS feature subset calculations.) 19

Figure 2.8 True positive error rate of individual feature sets with undenoised and denoised case for three learning algorithms. (The leftmost column set results belong to the original signal subset calculations. The following 14 column sets belong to the TF feature subset calculations. Final 6 column sets belong to the TS feature subset calculations.) 20

Figure 2.9 True positive error rate of three learning methods sets for undenoised and denoised case. (The leftmost column set results belong to the original signal subset calculations. The following 14 column sets belong to the TF feature subset calculations. Final 6 column sets belong to the TS feature subset calculations.) 20

Figure 3.1 Time domain representation of an ES, an artifact and a DS. 28

Figure 3.2 a) A 3 level binary tree implementation, only the analysis part, of the DWT. D_1, D_2 and D_3 are the detail coefficients and A_3 is the approximation coefficients. b) Structure of the analysis part of the DTCWT for 3 levels. $h_0^{(1)}(n)$ is the low-pass filter of real tree and $g_0^{(1)}(n)$ is the low-pass filter of imaginary tree in the first band. $h_0(n)$ and $h_1(n)$ are the low-pass and high-pass filters of the real tree for following bands. $g_0(n)$ and $g_1(n)$ are the low-pass and high-pass filters of the imaginary tree for following bands. 33

Figure 3.3 Proposed Individual Emboli Detection System. 37

Figure 3.4 Proposed Ensemble Emboli Detection System. 38

Figure 3.5 Projections on the LDA components extracted from **(left)** FFT and **(right)** DTCWT data of forward flow view. 42

Figure 4.1 Process of quadrature signals with traditional methods. *D(n)* is the in-phase component and *Q(n)* is the quadrature component. $S_f(n)$ is the forward flow signal and $S_r(n)$ is the reverse flow signal. 47

Figure 4.2 Asymmetrical implementation of the PFT. 50

Figure 4.3 Symmetrical implementation of the PFT. 51

Figure 4.4 Analysis part of Dual Tree Complex Wavelet Transform. 53

Figure 4.5	Real tree of four levels DT-CWPT. For the imaginary tree, the filters $h_i^{(1)}(n)$ must be replaced by $h_i^{(1)}(n-1)$ and $h_i(n)$ filters must be replaced by $g_i(n)$. In both real and imaginary trees, same $f_i(n)$ filters are used for $i \in 0, 1$.	58
Figure 4.6	Asymmetrical Implementation of DDT-CWPT.	64
Figure 4.7	Symmetrical Implementation of DDT-CWPT. C_Q and C_D are the coefficients of *Q(n)* and *D(n)* in the related subband respectively, C_F and C_R are the coefficients of forward and reverse directional signals in the related subband respectively. H[ ] stands for the HT.	65
Figure 4.8	The first 256 points of reconstructed signals with ADDD-CWPT and Asym-PFT.	72
Figure 4.9	Time domain and frequency domain representations of filtered signals.	74
Figure 4.10	*D(n)* and *Q(n)* in time domain.	75
Figure 4.11	Output of ADDT-CWPT and Asym-PFT for synthetic quadrature signal.	76
Figure 4.12	Output of ADDT-CWPT and Asym-PFT for quadrature embolic signal.	77
Figure 4.13	Coefficients of a forward emboli signal obtained with ADDT-CWPT and traditional method.	78
Figure 4.14	Coefficients of a reverse emboli signal obtained with ADDT-CWPT and traditional method.	79
Figure 4.15	Spectrogram of an embolic signal in both directions.	80
Figure 4.16	Traditional quadrature signal processing system with DT-CWPT.	81
Figure 4.17	Coefficients of a forward emboli signal obtained with proposed SDDT-CWPT and traditional method.	82
Figure 4.18	Hilbert transformed coefficients of a forward emboli signal obtained with proposed SDDT-CWPT and traditional method.	83
Figure 4.19	Coefficients of a reverse emboli signal obtained with proposed SDDT-CWPT and traditional method.	84

Figure 4.20	Hilbert transformed coefficients of a reverse emboli signal obtained with proposed SDDT-CWPT and traditional method.	85
Figure 4.21	The signal-difference ratios of 100 embolic signals when the non-analytic bands are removed and not removed.	86
Figure 4.22	A low intensity embolic signal superimposed on a large low frequency artifact.	87
Figure 5.1	A forward blood flow signal (above) and zoomed version of emboli part (below).	92
Figure 5.2	a) The analysis and synthesis filter banks used in RADWT.b) The full structure of RADWT including decomposition and reconstruction phases.	94
Figure 5.3	Frequency response of decomposed subbands and associated wavelets with low Q-factor (left) and high Q-factor (right).	95
Figure 5.4	The decomposition stage of the DT-RADWT.	96
Figure 5.5	The structure of proposed directional DT-RADWT.	97
Figure 5.6	In the upper two rows, forward blood flow signals obtained with the classical PFT and proposed directional DT-RADWT are illustrated respectively. In the third row, zoomed embolic signals obtained with the classical PFT and proposed directional DT-RADWT are illustrated.	98
Figure 5.7	Original signal (red, first row) and the normalized coefficients of each subband (blue, rows 2 to 7) by using low Q-factor wavelet analysis (equivalent to dyadic-DWT).	99
Figure 5.8	Original signal (red, first row) and the normalized coefficients of each subband (blue, rows 2 to 12) by using high Q-factor wavelet analysis.	99
Figure 5.9	Original signal (red, first row) and the recontructed subbands (blue, rows 2 to 7) by using low Q-factor wavelet analysis (equivalent to dyadic-DWT).	101
Figure 5.10	Original signal (red, first row) and the recontructed subbands (blue, rows 2 to 12) by using high Q-factor wavelet analysis.	101

LIST OF TABLES

Table 2.1 Overall accuracies, true positive (TP), and true negative (TN) rates of the individual feature sets and their ensembles for SVMs case. (TFAUT and TFAUF indicate the feature subsets obtained by time-frequency analysis upon time and time-frequency analysis upon frequency respectively. Similarly, TSAUT and TSAUS indicate the feature subsets obtained by time-scale analysis upon time and by time-scale analysis upon scale respectively.) 21

Table 2.2 Overall accuracies, true positive (TP), and true negative (TN) rates of the individual feature sets and their ensembles for MLP case. (TFAUT and TFAUF indicate the feature subsets obtained by time-frequency analysis upon time and time-frequency analysis upon frequency respectively. Similarly, TSAUT and TSAUS indicate the feature subsets obtained by time-scale analysis upon time and by time-scale analysis upon scale respectively.) 22

Table 2.3 Overall accuracies, true positive (TP), and true negative (TN) rates of the individual feature sets and their ensembles for k-NN case. (TFAUT and TFAUF indicate the feature subsets obtained by time-frequency analysis upon time and time-frequency analysis upon frequency respectively. Similarly, TSAUT and TSAUS indicate the feature subsets obtained by time-scale analysis upon time and by time-scale analysis upon scale respectively.) 23

Table 3.1 General accuracy (%) and detection rates (%) of each class obtained with SVMs and k-NN using 150 and 90 training samples. 40

Table 3.2 General accuracy (%) and detection rates (%) of each class with SVMs using the forward directional signal individually and the combined signals. 41

Table 3.3 General accuracy (%) and detection rates (%) of each class with SVMs using the DTCWT features forward directional signal individually and the combined signals with different proportion of PCA variance. 42

Table 4.1 Difference-Ratios of Forward and Reverse Signals for decomposition with different levels. 73

Table 4.2 Signal-Difference Ratios of Forward and Reverse Signals for decomposition with different levels. 75

Table 4.3 Average/Std Signal-Difference Ratios of Forward and Reverse Signals when the non-analytic band are used and not used. 83

Table 4.4 Time enhancement ratios for full tree. 87

Table 4.5 Time enhancement ratios for only analysis part. 88

LIST OF SYMBOLS

a	Scale parameter
a_0^m	Discrete scale step size
$A_1[k]$	Approximation coefficients
b	Time translation parameter
$d(x_s, x_t)$	The distance between samples x_s and x_t
$D_1[k]$	Detail coefficients
$D(n)$	In-phase component
$D_k^l(\omega)$	Frequency response of the decomposed *D(n)* for k^{th} subband in the l^{th} level
DC_k^l	In-phase signal coefficients of the k^{th} subband in the l^{th} level
$f_i(n)$	Extension filter used in DT-CWPT
$f_i'(n)$	Extension filter used in DT-CWPT
$\mathbf{F}[\ \ ]$	Fourier transform operator
$F_s(t, f)$	Short time Fourier transform of $s(t)$
FC_k^l	Forward signal coefficients of the k^{th} subband in the l^{th} level
$g_0(n)$	Low-pass filter of imaginary tree in DTCWT
$g_0^{(1)}(n)$	Low-pass filter of imaginary tree in the first band, in DTCWT
$g_1(n)$	High-pass filter of imaginary tree in DTCWT
$g(t)$	Short time analysis window function
$G_0(\omega)$	Frequency response of low-pass filter of imaginary tree
$G_1(\omega)$	Frequency response of high-pass filter of imaginary tree
$G_k^l(\omega)$	Frequency response of the imaginary tree's k^{th} subband in the l^{th} level
$h_0(n)$	Low-pass filter of real tree in DTCWT
$h_0^{(1)}(n)$	Low-pass filter of real tree in the first band, in DTCWT
$h_1(n)$	High-pass filter of real tree in DTCWT
$\mathbf{H}[\ \ ]$	Hilbert transform operator
$H_0(\omega)$	Frequency response of low-pass filter of real tree

$H_1(\omega)$	Frequency response of high-pass filter of real tree
$H_k^l(\omega)$	Frequency response of the real tree's k^{th} subband in the l^{th} level
$nb_0a_0^m$	Discrete translation step size
$Q(n)$	Quadrature-phase component
$Q_k^l(\omega)$	Frequency response of the decomposed *Q(n)* for k^{th} subband in the l^{th} level
QC_k^l	Quadrature-phase signal coefficients of the k^{th} subband in the l^{th} level
RC_k^l	Reverse signal coefficients of the k^{th} subband in the l^{th} level
$s(t)$	Time domain example signal, in real or quadrature format
sgn	Signum function
$s_f(n)$	Forward flow component in time domain
$s_r(n)$	Reverse flow component in time domain
$S(\omega)$	The quadrature signal in the frequency domain
$S_k^{l^+}(\omega)$	Forward signal component in the frequency domain for k^{th} subband in the l^{th} level
$S_k^{l^-}(\omega)$	Reverse signal component in the frequency domain for k^{th} subband in the l^{th} level
t	Time variable
w_i	The weight of the prediction of i^{th} network member in ensemble learning
$W_s(a,b)$	Wavelet transform of $s(t)$
$W_s(m,n)$	Discrete wavelet transform of $s(t)$
$\psi(t)$	Mother wavelet function
$\psi'(t)$	Hilbert transformed mother wavelet function in DTCWT
ω	Frequency variable

LIST OF ABBREVIATIONS

ADDT-CWPT	Asymmetrical Directional Dual Tree Complex Wavelet Packet Transform
ANN	Artificial Neural Network
Asym-PFT	Asymmetrical Phasing Filter Technique
BOSUF	Behavior Of Signals Upon Frequency
BOSUS	Behavior Of Signals Upon Scale
BOSUT	Behavior Of Signals Upon Time
CQFs	Conjugate Quadrature Filters
CWT	Continuous Wavelet Transform
DDT-RADWT	Directional Dual Tree Rational Dilation Wavelet Transform
DF	Delay Filter
DS	Doppler Speckle
DT-CWPT	Dual Tree Complex Wavelet Packet Transform
DTCWT	Dual Tree Complex Wavelet Transform
DT-RADWT	Dual Tree Rational Dilation Wavelet Transform
DWPT	Discrete Wavelet Packet Transform
DWT	Discrete Wavelet Transform
ES	Embolic Signal
FB	Filter Bank
FFT	Fast Fourier Transform
FIR	Finite Impulse Response
FT	Fourier Transform
HT	Hilbert Transform
k-NN	k-Nearest Neighbor
LDA	Linear Discriminant Analysis
MLP	Multi-layer Perceptron
MRA	Multi-resolution Analysis
PCA	Principal Component Analysis

PFT	Phasing Filter Technique
QPD	Quadrature Phase Detection
RADWT	Rational Dilation Wavelet Transform
SDDT-CWPT	Symmetrical Directional Dual Tree Complex Wavelet Packet Transform
STFT	Short Time Fourier Transform
SVM	Support Vector Machine
Sym-PFT	Symmetrical Phasing Filter Technique
TF	Time-frequency
TS	Time-scale
WFT	Windowed Fourier Transform
WGN	White Gaussian Noise
WT	Wavelet Transform

1. INTRODUCTION

As a biological system, human body is made up of many complex systems, which carry on many physiological processes. These physiological processes are accompanied by or manifest themselves as biomedical signals that reflect their nature and activities. Due to the inherent time-varying characteristics of biological systems, most biomedical signals are expected to have non-stationary character, independently of the time scale over which they are analyzed. Frequently, they consist of, high-frequency components closely spaced in time, accompanied by long-lasting, low-frequency components closely spaced in frequency. Any appropriate analysis method for dealing with them should therefore exhibit good frequency resolution along with fine time resolution - the first to localize the low-frequency components, and the second to resolve the high-frequency components.

Classical Fourier transform (FT), which assumes that the analyzed signal is stationary and does not give any time information, is not appropriate to analyze most of the biomedical signals. Short time Fourier transform (STFT) is the mostly used method in literature to describe how the spectral content of non-stationary signals are changing in time. However, a drawback of this transform is that it has a fixed time-frequency (TF) resolution. In contrast, the wavelet transform (WT) provides a time-scale (TS) representation of signals, which has good frequency resolution at low frequencies and good time resolution at high frequencies, resulting in an optimised TF resolution. Therefore, the WT plays a key role in the process of non-stationary biomedical signals.

1.1 Motivation Background and Objectives

Automatic computerized analysis of non-stationary biomedical signals has become an active research area due to the improvements in digital acquisition systems,

computer technology, and signal processing techniques in the last three decades. In this respect, in Chapters 2 and 3, wavelet based biomedical signal detection techniques, which can be used in automatic real-time diagnosis systems, are proposed. As biomedical signals, acoustic lung signals and blood flow signals are used. Certainly, detection of some anomalies in these two types of signals and understanding the TF behavior of them would critically impact the success of biomedical systems which use these signals.

In acoustic lung signals part, to detect pulmonary crackles; which are the indicators of airways diseases such as pneumonia, bronchiectasis, asthma or chronic obstructive pulmonary disease, an automated system, that is using time-frequency/scale based feature extraction and ensemble learning, is proposed.

In blood flow signals part, to detect asymptomatic embolic waveforms; which can be utilized in the diagnosis of stroke, an important illness that can cause paralysis or death, an automated system, that is using dual tree complex wavelet transform (DTCWT) as a feature extraction method and stacking as an ensemble learning method, is proposed.

The dyadic discrete wavelet transform (DWT), which provides an octave-band frequency decomposition, is a very effective tool for processing piecewise smooth signals. However, due to its poor frequency resolution and severe frequency aliasing drawbacks, the dyadic DWT is less effective in processing signals having more oscillatory behavior such as speech, biomedical signals like EEG, audio signals and etc. The embolic signals (ESs) have also oscillatory behavior. These signals are superimposed on normal directional blood flow, which must be obtained from quadrature format outputs of the Doppler ultrasound systems by using decoding techniques. To process ESs more efficiently, WTs that have better frequency resolution are needed. Discrete wavelet packet transform (DWPT) avoids this problem by iterating on the high-pass filters as well which results a full tree. However, neither the DWT nor the DWPT has shift-invariance property which is very important in processing ESs. Additionally, to process ESs with the DWT or DWPT, the forward and reverse blood flow signals must be obtained first. Only then these transforms can be applied. However, this increases

the computational complexity of whole process.

Therefore, in Chapters 4 and 5, with the aim of processing quadrature Doppler signals, in which the directional blood flow signals are encoded, a novel directional complex discrete wavelet packet transform and a novel directional complex rational dilation wavelet transform are proposed. In contrast to existing wavelet based methods, these proposed transforms can be directly applied to quadrature format signals and have the capability of extracting direction information during analysis. Hereby, the directional signal extraction stage is no more needed and the computational complexity of whole process is dramatically reduced. Besides, these proposed transforms are approximately shift-invariant, which is crucial in processing quadrature signals due to the phase relationship of their in-phase and quadrature-phase components. As a last advantage, these proposed transforms have adjustable TF resolution and this allows us to obtain optimum representation of ESs in scale domain.

1.2 Organization of the Thesis and Publications

Chapter 1 is an introduction with the description of the central theme of this research. A systematic organisation of thesis is also presented.

In Chapter 2, an automated detection algorithm for pulmonary crackles, which are used as indicators for the diagnosis of different pulmonary disorders in auscultation, is proposed. Crackles are very common adventitious transient sounds. From the characteristics of crackles such as timing and number of occurrences, the type and the severity of the pulmonary diseases may be assessed. In the proposed crackle detection algorithm, various feature sets are extracted from pulmonary signals using TF and TS analysis. In order to understand the effect of using different window and wavelet types in TF and TS analysis in detecting crackles, different windows such as Gaussian, Blackman, Hanning, Hamming, Bartlett, Triangular, Rectangular and wavelets such as Morlet, Mexican Hat, Paul are tested. The extracted feature sets, both individually and as an ensemble of networks, are fed into three different machine learning algo-

rithms: Support Vector Machines (SVMs), k-Nearest Neighbor (k-NN) and Multilayer Perceptron (MLP). Moreover, in order to improve the success of the model, prior to the TF and TS analysis, frequency bands containing no-crackle information are removed using DTCWT, which is a shift-invariant transform with limited redundancy compared to the conventional DWT. The comparative results of individual feature sets and ensemble of sets, which are extracted using different window and wavelet types, for both the pre-processed and the raw data with different machine learning algorithms, are extensively evaluated and compared. Some parts of this chapter have been published by the authors in [1, 2, 3, 4].

In Chapter 3, with the aim of building an accurate and robust automated emboli detection system, Doppler ultrasound signals including both forward and reverse blood flow information have been processed using Fast Fourier Transform (FFT), DWT, and DTCWT. After obtaining the coefficients, dimensionality of the extracted features from both the forward and the reverse blood flows are reduced using Principal Component Analysis, and then these features are fed to k-NN and SVMs classifiers. Unlike the artifacts, ESs are unidirectional. Therefore, we train the classifiers using the forward flow signals for predicting whether a signal is emboli, artifact or speckle, whereas we build up a model from the reverse signal for predicting whether a signal is an artifact or not. Considering that combination of these different representations belonging to the blood flow that carry different characteristics can explicitly results in a better identification and classification of emboli, artifact or speckle, we constitute an ensemble model with stacking. For this purpose, the probability estimates of the three-class forward signal SVMs are combined with those of the two-class reverse signal SVMs. We show that the features extracted using the DTCWT gives the highest accuracy and the highest emboli detection rates. It is also observed that combining forward SVMs with reverse SVMs using stacking ensemble method increases the emboli and artifact detection rates, and the general accuracy. Some of the methods presented in Chapter 3 have been published by the authors in [5], and have been submitted to [6].

Doppler ultrasound is a widely used non invasive diagnostic technique to evaluate cardiovascular disorders. The outputs of most Doppler ultrasound systems are in

quadrature format. In order to obtain directional blood flow information, the quadrature outputs have to be pre-processed using methods such as asymmetrical and symmetrical phasing filter techniques. These resultant directional signals can be employed to detect asymptomatic ESs caused by small emboli, which are indicators of possible future stroke in the cerebral circulation. ESs can be considered as narrow-band (or band-limited) signals. Therefore, various frequency based methods such as Fourier and wavelet transforms were frequently used for denoising and feature extraction in processing ESs. Unfortunately, most of the times the dyadic time-frequency tiling of DWT is not appropriate for the analysis of ESs due to their non-stationary TF behavior. Alternatively, DWPT, which is a generalization of the ordinary DWT allowing subband analysis without the constraint of dyadic decomposition, can be used to perform an adaptive decomposition of the TF axis. Hence, in Chapter 4, directional discrete wavelet packet transforms are introduced. They have the ability of mapping directional information while processing quadrature signals. Moreover they have less computational complexity than the existing wavelet packet based methods. The performances of the proposed methods are examined in detail using single frequency quadrature signal, synthetic narrow-band quadrature signal, and real quadrature embolic signals. Some parts of Chapter 4 have been published by the authors in [7, 8], and have been submitted to [9, 10].

In Chapter 5, we introduce a directional rational dilation wavelet transform which can be directly performed on quadrature signals. This transform's frequency resolution can be changed by tuning the Q-factor of its wavelets according to the behavior of the analyzed signal and an optimum representation of ESs can be achieved in the scale domain. Additionally, it is also a near shift-invariant transform which is very important in processing quadrature Doppler signals due to the phase relationship between their in-phase and the quadrature-phase components. A part of this chapter has been submitted to [11].

A summary of the main contributions and the main conclusions of this thesis have been presented in Chapter 6. Possible future works related to the proposed methods are also discussed in this chapter.

2. PULMONARY CRACKLE DETECTION USING TIME-FREQUENCY AND TIME-SCALE ANALYSIS

2.1 Introduction

Chest auscultation of pulmonary sounds by using a stethoscope is a commonly used, economic and noninvasive method for the evaluation of the respiratory disorders. However, due its inherent subjectivity and limited frequency response (the stethoscope attenuates frequencies above 120 Hz), the stethoscope is considered to be an inadequate diagnostic method for respiratory disorders. Over the last three decades, the analysis of pulmonary sound signals with computers has become an established research area with the improvements in digital acquisition systems and advanced digital signal processing techniques [12, 13, 14].

Although the exact mechanism is still a mystery, the pulmonary sounds are assumed to be produced in the lungs due to the air turbulence produced in their airways. Pulmonary sounds can be divided into two classes, vesicular sounds and adventitious sounds. Vesicular sounds are the normal respiratory sounds which can be heard over the chest wall. Vesicular sounds are synchronous with the air flow occurring in the airways. Adventitious sounds, on the other hand, are additional sounds which usually occur because of respiratory disorders [15].

Crackles are discontinuous, adventitious non-musical respiratory sounds, which are attributed to sudden bursts of air within bronchioles. Their duration is less than 20 ms and their frequency range is between 150 to 2000 Hz. Crackles frequently occur in pathological conditions and are superimposed on vesicular sounds. Their morphologic character is explosive and transient, and they occur frequently in respiratory diseases. The inherent properties of pulmonary crackles such as timing, epochs of occurrence, and pitch can be used in the diagnosis for various types of pulmonary diseases such as pneumonia, bronchiectasis, fibrosing alveolitis, and asbestosis [16, 17, 18, 19].

For an automatic computerized analysis of pulmonary diseases, proper detection of crackles is very important. In this chapter, a novel method is proposed for pulmonary crackle detection. For the analysis, a pulmonary dataset consisting of 3000 512-point crackle signals and 3000 512-point non-crackle signals are used. In order to facilitate detecting crackle signals, various feature sets, which contain frequency and scale information are extracted by using TF and TS analysis. With the aim of obtaining the best crackle detection performance, different window and wavelet types such as Gaussian, Blackman, Hanning, Hamming, Bartlett, Triangular and Rectangular for TF analysis and Morlet, Mexican Hat and Paul for TS analysis are tested for these 6000 signals. Eventually, as an end-product of these trials 20 different feature subsets are obtained.

In order to improve the generalization and crackle detection capability of the model, as a pre-processing stage, frequency components of processed signals containing no-information (below 150 Hz and above 2400 Hz) are removed using DTCWT, which is an improved version of DWT with better shift-invariance property. Then, the extracted feature subsets are fed into SVMs, k-NN and MLP classifiers as inputs both individually and as an ensemble of networks. Comparative results of the individual and the ensemble feature sets with pre-processed and raw data are presented and analyzed. An overall block diagram of the proposed method can be seen in Figure 2.1.

The remainder of the chapter is organized as follows: Section 2.2 describes the materials and the methods. Section 2.3 presents the experimental results on the pulmonary dataset. Section 2.4 provides the discussions and the conclusions.

2.2 Materials and Methods

2.2.1 Data Acquisition System

In the data acquisition system fourteen air-coupled electret microphones (Sony-ECM 44) are placed on the posterior chest, and airflow is recorded using Fleisch-

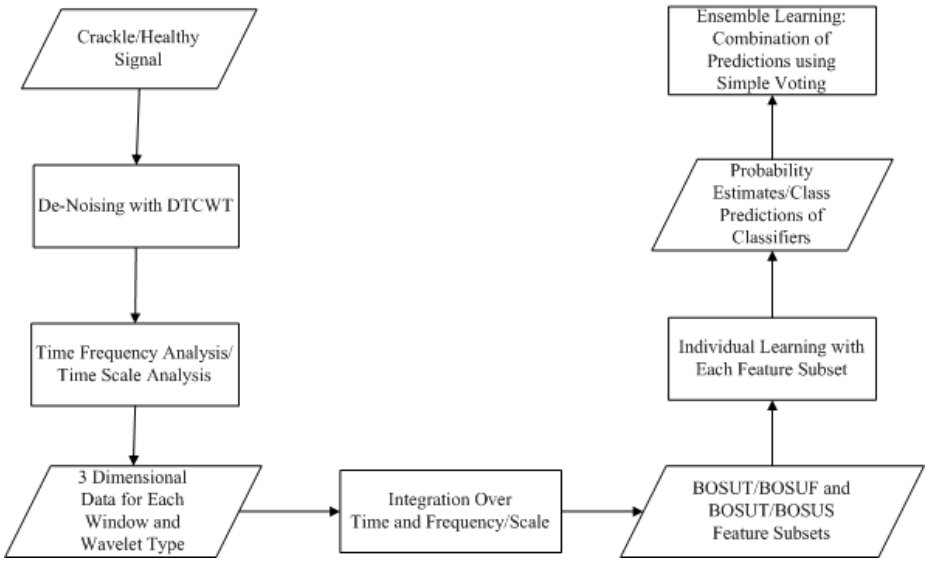

Figure 2.1 Overall block diagram of proposed method for one machine learning algorithm. (BOSUT is the abbreviation of "behavior of signals upon time", BOSUF and BOSUS are the abbreviations for "behavior of signals upon frequency" and "behavior of signals upon scale" respectively. A more detailed explanation of the abbreviations can be found in Section 2.2.2).

type flowmeter (Validyne CD379) to synchronize on the inspiration-expiration phases. A low-noise preamplifier, 8^{th} order Butterworth low-pass filters with 4 kHz cut-off frequency and 6^{th} order Bessel high-pass filters with 80 Hz cut-off frequency are used for minimizing frictional noise and heart sound interference. The low-pass filter also acts as an anti-aliasing filter. The amplified signals are digitized by a 12-bit ADC Card (NIDAQ500) at a sampling rate of 9.6 kHz and stored [20]. The details of the system are described in [21]. Figure 2.2 illustrates an example consisting of two 512-point crackle signals and two healthy signals.

2.2.2 Feature Extraction Using Time-Frequency and Time-Scale Analysis

The spectral characteristics of lung sounds show different behaviors according to the state and pathology of the lung. The pathological sounds appear in higher frequency bands, i.e. as crackles which are explosive and transient in time. For feature extraction, we use the frequency characteristics of crackles using TF and TS analysis for both the non-pre-processed and pre-processed signals. For pre-processing, we apply DTCWT with the aim of removing the frequency bands, which do not contain crackle

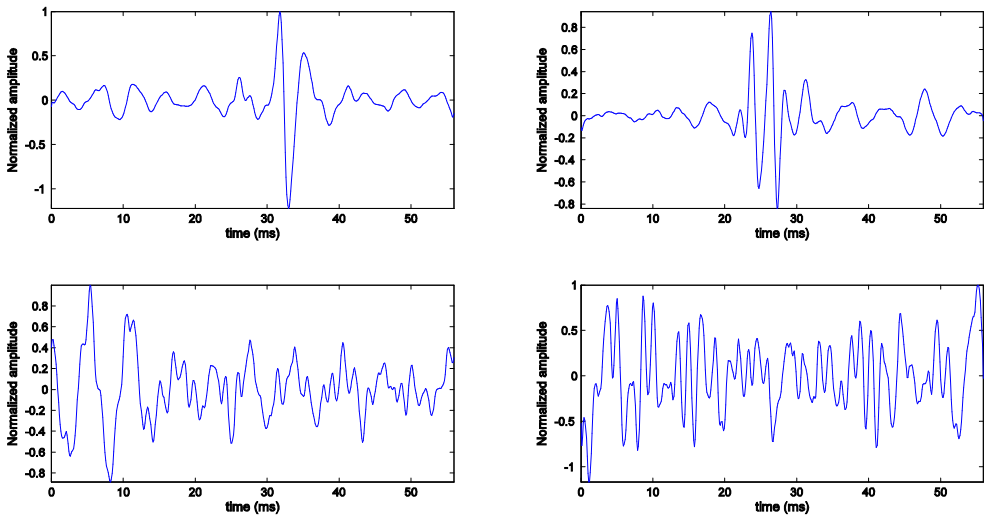

Figure 2.2 Examples of 512-point signals containing crackles (upper two) and healthy signals (lower two).

information.

The dataset consists of 6000 samples collected from 26 subjects (13 healthy, 13 pathological) are divided into two subsets; a crackle dataset containing 3000 crackle samples and a healthy dataset containing 3000 healthy samples, each consisting of 512 points. In the preparation of crackle dataset, 3000 crackles which were identified previously by physicians are randomly placed into 512-point frames. The frame size is chosen as 512 points because the duration of crackles is less than 20 ms and due to the sampling frequency of the data acquisition system, which is 9600 Hz, 512 points of the signal is equal to 53.34 ms which guarantees that one or more crackles are located in a frame. In the preparation of healthy dataset, 3000 512-point frames were randomly created from healthy subjects data.

To underscore frequency characteristics of crackles, TF and TS analysis are applied to both crackle signals and healthy signals with different windows in TF analysis and with different wavelets in TS analysis. In order to obtain the optimum frequency/scale resolution in the TF and TS analyses, 64-point FT with Gaussian, Blackman, Hanning, Hamming, Bartlett, Triangular and Rectangular windows and 64 scales

WT with Morlet, Paul and Mexican Hat wavelets are used, respectively.

The output of TF analysis gives information about the behavior of analyzed signals with respect to both time and frequency for each type of window. In order to obtain the behavior of signals with respect to time and frequency separately, for each window type, the outputs of TF analysis are integrated over frequency and the behavior of signals upon time (BOSUT) is obtained [22]. Similarly for each window type, the outputs of TF analysis are integrated over time, and the behavior of signals upon frequency (BOSUF) is obtained. This procedure is also carried out for TS analysis [23]. For forming feature sets with related wavelet type, the outputs of TS analysis are integrated over scale and time, and the behaviors of signal upon time and scale (BOSUS), respectively, are obtained. At the end of these integration operations, for each different TF analysis window and TS analysis wavelet type, two new feature subsets are obtained (for TF analysis BOSUT and BOSUF, for TS analysis BOSUT and BOSUS) from an original crackle/healthy signal. As a result, from a single crackle or healthy signal analysis, using 7 TF windows and 3 TS wavelets, $2 \times 10 = 20$ new feature subsets are obtained.

2.2.2.1 Time-Frequency Analysis. The FT expands a time-domain signal into sines and cosines, which are completely unlocalized in time. That is, the spectrum gives us information on the frequencies contained in the signal as well as their amplitudes and phases, but does not give any information at which times these frequencies occur. Thus, FT processes signals assuming that they are stationary. In reality, however, most natural signals, including pulmonary signals, are non-stationary. In order to characterize a non-stationary signal properly, it is necessary to observe the changes in the signal both in time and in frequency. The windowed Fourier transform (WFT) has been used widely in this regard as it partially fulfills these requirements. The WFT introduces time dependency in the FT by pre-windowing the signal $s(t)$ around a particular time t, and calculating its FFT, which is repeated for each time instant t.

The WFT of $s(t)$ is given by

$$F_s(t,f) = \int_{-\infty}^{+\infty} s(\tau) g(\tau - t) \mathrm{e}^{-2j\pi\tau} \, \mathrm{d}\tau \tag{2.1}$$

where $g(t)$ is a short time analysis window function. As multiplication by a relatively short window suppresses the signal outside a neighborhood around analysis time point $\tau = t$, the WFT is a local spectrum of the signal $s(t)$ around a particular t.

An important FFT parameter which may influence the crackle detection performance is window type of WFT. Multiplying the signal with a suitable window function highlights the information near the middle of the window and suppresses the information near the ends of the window. Many window functions have been proposed in the literature [24, 25].

In this study for the TF analyses, 64-point WFT with Gaussian, Blackman, Hanning, Hamming, Bartlett, Triangular and Rectangular windows are used. In WFT, shifting the analysis window by less than the window length results in an overlapped FFT of the analyzed signals [26]. Conventionally, the signals are processed sequentially by sliding the window less than the window size at each processing stage, most of the times sliding by 1 point. Consequently, overlapping FFT windows produces higher-dimensional WFTs. Some of the information in an overlapped WFT is redundant, and some of it is novel. In this study 15 points of window-sliding is used in the TF analyses for crackle detection which gives us a reduced computational complexity rather than conventional sliding factor 1 with approximately same detection performance. Then, the three dimensional outputs of TF analyses are integrated over frequency and over time in order to obtain the behavior of signals upon time and frequency separately.

2.2.2.2 Time-Scale Analysis. The WT decomposes a time dependent signal into TS space and allows exact localization of any abrupt change, or an exact time and duration to be attributed to a short signal, which may not be evidenced by conventional signal processing techniques. A complete WT analysis creates a two-dimensional de-

composition of a one-dimensional signal, typically with the horizontal axis as time and vertical axis corresponding to the wavelet scale. The third dimension is the amplitude of the WT coefficients. It is performed by projecting a signal $s(t)$ onto a family of zero-mean functions deduced from an elementary function $\psi(t)$ by translations and dilations, and given by

$$W_s(a,b) = \frac{1}{\sqrt{|a|}} \int_{-\infty}^{+\infty} s(t)\psi\Big(\frac{t-b}{a}\Big)\mathrm{d}t \tag{2.2}$$

where $\psi(t)$ is the analyzing wavelet.

In the TS analysis, in which the wavelet can be defined as a complex function, the variable $a(\neq 0)$ controls the scale of the wavelet. The variable b is the time translation and controls the position of the wavelet. The basic difference between the WT and the WFT is that when the scale factor a is changed, the duration and the bandwidth of the wavelet are both changed but its shape remains the same. The WT uses short windows at high frequencies and long windows at low frequencies in contrast to the FFT, which uses a single analysis window. This partially overcomes the TF resolution limitation of the WFT. In this study 64 scales of wavelet transform with Morlet, Paul and Mexican Hat wavelets are used in order to obtain new feature sets from original crackle and healthy datasets. Three-dimensional output of TS analysis for each wavelet type was integrated over scale and time, and the behaviors of signal upon time and scale, separately, are obtained. In Figure 2.3, a crackle signal (a) and a healthy signal (b) WFT analysis results with Gaussian window are depicted. The behavior of crackle upon time (c) and upon frequency (e) is distinctively different than the behavior of healthy signal upon time (d) and upon frequency (f).

2.2.3 Denoising Using Dual Tree Complex Wavelet Transform

Vesicular sounds mainly have frequency components between 0-200 Hz, rarely extending up to 600 Hz whereas the frequency components of crackles extend between 150-2000 Hz. In order to improve the performance of the proposed method, a pre-

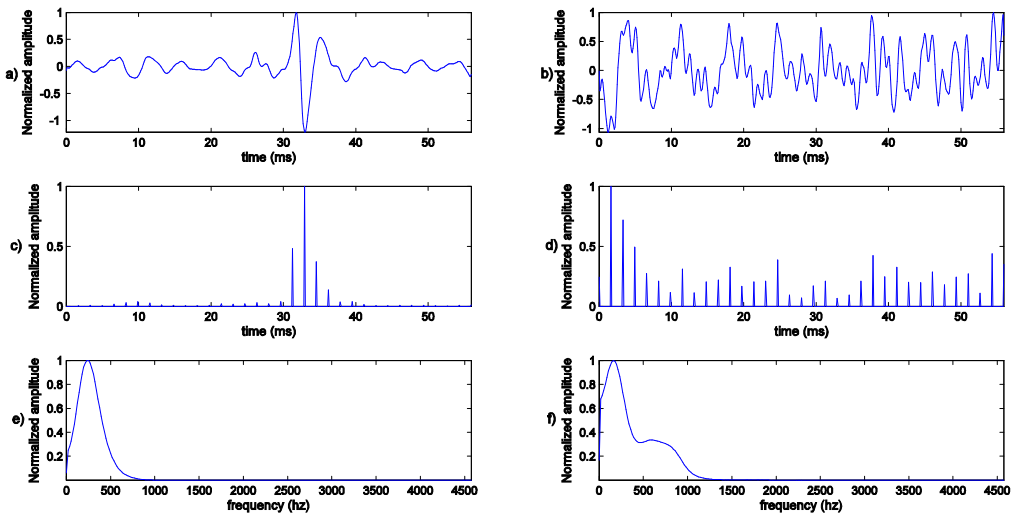

Figure 2.3 For the WFT analysis using Gaussian window. (a) Original crackle signal, (b) original healthy signal, (c) BOSUT for crackle sample, (d) BOSUT for healthy sample, (e) BOSUF for crackle sample, (f) BOSUF for healthy sample.

processing step which removes the frequency components with no-crackle information, is applied to the dataset before extracting the feature sets. For this task, a five-level DTCWT is applied on both crackle and healthy signals. The DTCWT is developed to overcome the lack of shift-invariance property of ordinary DWT. Moreover it has limited redundancy ($2^m : 1$ for m-dimensional signals, which is a very good ratio as compared with undecimated DWT). In the analysis of nonstationary crackles, which are transient signals, DTCWT removes undesirable signal components more successfully than DWT because of its shift-invariance property [27, 28]. With DTCWT, for each crackle and healthy sample in the dataset, the frequency bands below 150 Hz and above 2400 Hz are replaced with null vectors and then the processed signals are reconstructed. The details of DTCWT are given in [29, 30], whereas a block diagram of a two-level DTCWT which demonstrates both analysis and synthesis parts is depicted in Figure 2.4.

In order to visualize the effect of feature extraction and denoising, we reduce the dimensions of the original signal feature set and extracted feature sets, which are obtained at the end of WFT analysis with Gaussian window, using Principal Component Analysis (PCA). The projections of the original signal feature sets into two-dimensional

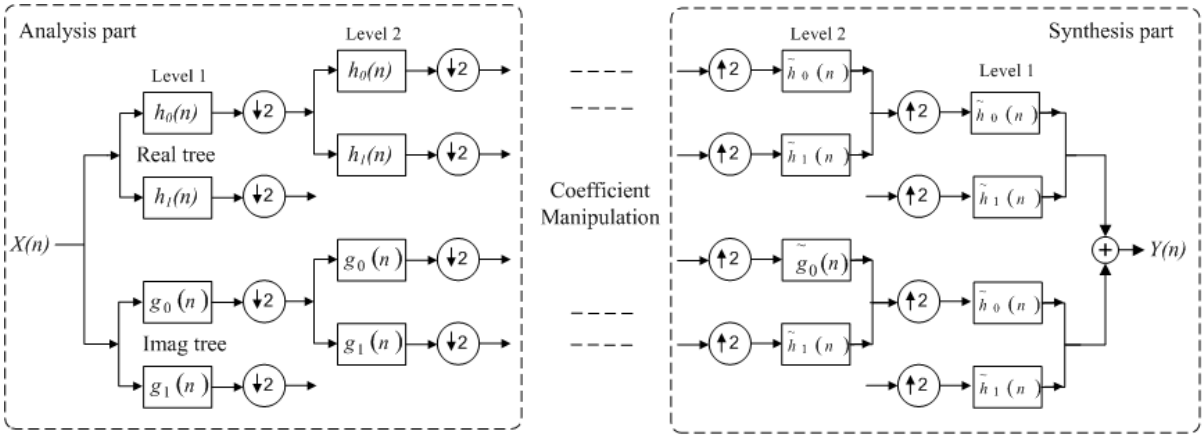

Figure 2.4 Block diagram for a 2-level DTCWT which demonstrates both analysis and synthesis parts. $X(n)$ is the input signal and $Y(n)$ is the processed signal.

space before and after denoising are shown in Figure 2.5(a) and (b). Additionally, the projections of the extracted feature sets, the output of time-frequency analysis upon time (TFAUT) and time-frequency analysis upon frequency (TFAUF), into two dimensional space before denoising and after denoising are shown in Figure 2.5(c)-(e) and (f). It is seen that extracting new features by WFT and denoising by DTCWT improves the discriminative capability of the crackle detection algorithm.

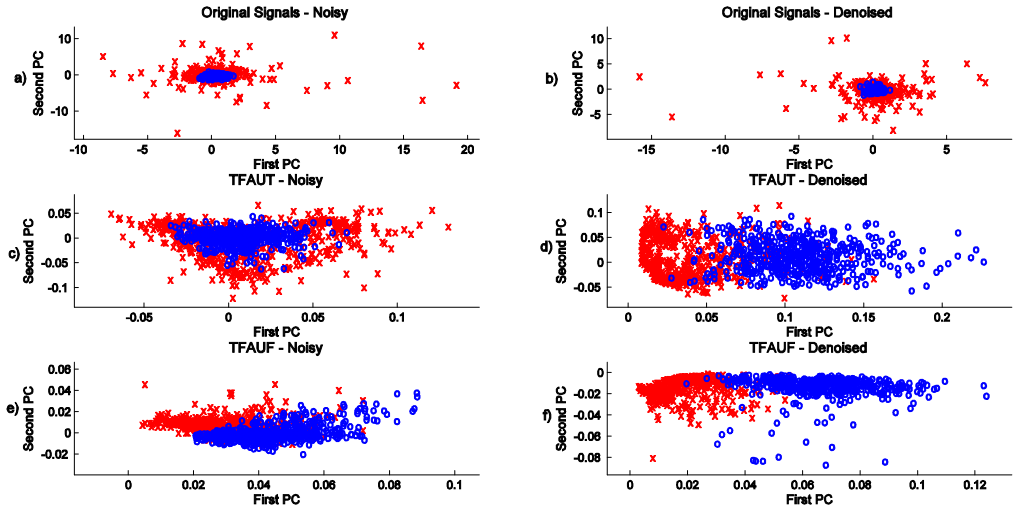

Figure 2.5 Projections of the original feature sets before (a), and after denoising (b). Projections of the outputs of time-frequency analysis upon time before (c), and after denoising (d) with Gaussian window. Projections of the outputs of time-frequency analysis upon frequency before (e), and after denoising (f) with Gaussian window ('x' represents crackle, and 'o' represents healthy signals).

2.2.4 Individual Learning with Feature Sets

In crackle detection method, the original crackle-healthy signals and extracted feature sets obtained by TF and TS analysis are fed individually into three classifiers: SVMs, MLP, and k-NN. The aim is to measure and compare the predictive power of the feature sets with various classifiers. The effect of denoising with DTCWT on the classifiers is also tested. The aim of each of the classifiers is to build a predictive model capable of distinguishing between the crackle and non-crackle signals. For this purpose, we divide the dataset into three groups with equal number of samples: 2000 samples for the training, 2000 for the validation, and 2000 for the test. The distribution of the samples to the datasets has been done such that each set contains 1000 samples from each class type.

SVMs is a very popular machine learning algorithm which aims to find the optimally placed hyperplanes to discriminate the classes from each other [31]. The closest samples to these hyperplanes are called support vectors, and the solution is defined in terms of this subset of samples which limits the complexity of the problem. Because the optimization problem has a unique solution, any iterative optimization procedure is not needed for convergence [32]. We use LIBSVM [33] implementation of SVMs. We train each feature subset using training set and test on validation set in order to find the most suitable kernel type among linear, polynomial and Gaussian. The parameter values of the SVMs, C (cost) and g (the spread parameter), are also optimized for each of the feature sets. The complexity of the solution is controlled by parameter C. Higher values of C may result in overfitting to the training set. After tuning the parameters on validation set, the optimized models are finally tested on the yet unseen test sets, and the unbiased success of each feature set is proposed.

We also use MLP to classify the pulmonary sounds which is the mostly used Artificial Neural Network (ANN) model for nonlinear modeling. MLP is a feed-forward ANN model consisting of an input layer, an output layer, and at least one hidden layer. MLP is included in this study for comparison purposes because it is capable of modeling complex non-linear problems with many interactions among the input variables [34].

The elements of the hidden and output layers are called neurons. Each neuron is a processing element with a non-linear activation function. Our MLP model is composed of an input, an output, and a hidden layer. The same training, validation, and test sets of SVMs model are used for MLP model. The parameters of the MLP model of each feature set such as number of neurons in the hidden layer (in the analysis hidden layer neuron number is chosen as 10), number of iterations and learning rate are fine tuned on the validation set, and the most suitable model is applied to the test set to propose the unbiased success of each feature set.

The third classifier we use for comparison purposes is k-NN classifier, which is based on non-parametric density estimation. The k-NN method requires an integer k, a set of labeled examples and a measure of "closeness", and assigns the input to the class having most examples among the k neighbors of the input [32]. Small values of k result in more sensitive classifiers to the undenoised observations. The k parameter is optimized on the validation set (in the analysis k parameter is chosen as 3 or 5 depending on the feature subset) and the accuracy of the optimized model on the unseen test set for each feature set is proposed. Type of closeness measure has big impact on determining which set of learning examples is closest to the new example. In our study, we use City-block distance as the k-NN closeness metric which is a special case of the Minkowski metric,

$$d(x_s, x_t) = \sqrt[p]{\sum_{i=1}^{n} |x_s^i - x_t^i|^p} \tag{2.3}$$

where $p = 1, d(x_s, x_t)$ is the distance between samples x_s and x_t, and n is the dimension of the feature space.

2.2.5 Ensemble Learning

We use the ensemble of feature subsets in order to improve the overall accuracy and generalization capability of the constructed model based on the proof of Hansen and Salamon [35]: if each member of the ensemble, i.e. feature subset, can get the right

answer more than half the time, and if the responses of members are independent, the likelihood of an error by a majority voting strategy will monotonically decrease with the increasing number of members. Learning from multiple sets of features, called ensemble learning, is based on employing separate classifiers on each feature subset and combining the predictions of the views using techniques such as voting and stacking [32, 36]. The final prediction, y, of an ensemble network is given by

$$y = \sum_{i=1}^{M} w_i d_i \tag{2.4}$$

satisfying

$$w_i \geq 0, \quad \forall i \quad \text{and} \quad \sum_{i=1}^{M} w_i = 1 \tag{2.5}$$

where w_i is the weight of the prediction of i^{th} network member, d_i is the prediction of i^{th} network member, and M is the total number of network members. The weight of the vote of each network member, i.e. w_i , is equal in the simple voting scheme ($w_i = 1/M$). The class with the maximum number of votes is the final prediction of the network. This voting strategy is called majority voting for two class classification problems. Besides, the information of how much confident the network member is for its prediction can be used to specify the final prediction. We use the class posterior probability estimates as the votes of the network members for SVMs case.

We train each of the 20 extracted feature sets and also the original signals individually on the training set. Then the individual predictions of the obtained models are used as a member of an ensemble network. Each ensemble network consists of three members: the two feature subsets which were obtained by the TF and TS analysis of each window/wavelet type resulting behavior of signals upon time/frequency and time/scale, respectively, and the original signals as themselves. For the SVMs case, the class posterior probability estimates of the network members are combined using simple voting. For the MLP and k-NN case, the hard label predictions of each individual subset are combined using simple voting, and the ensemble learning results are obtained for each undenoised and denoised case. The SVMs ensemble learning architecture with

Gaussian window type is depicted in Figure 2.6.

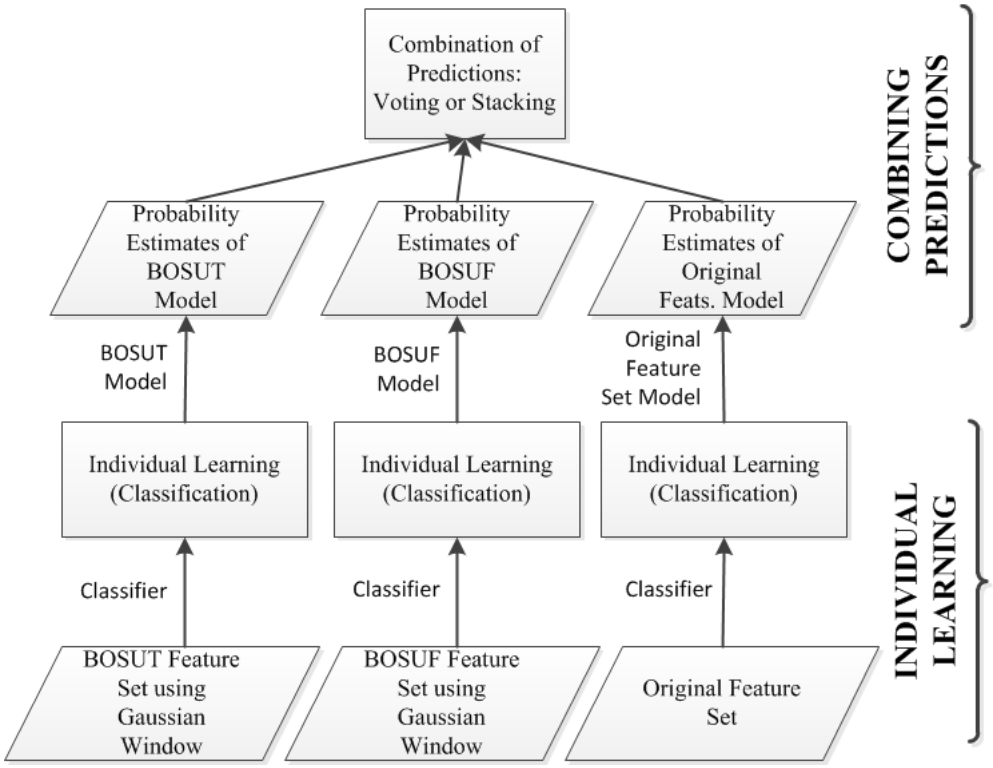

Figure 2.6 SVM ensemble learning architecture for Gaussian window type.

2.3 Experimental Results

The overall accuracy error rates for SVM, MLP and k-NN learning algorithms of 20 extracted feature subsets and the original signal subset individually can be seen in Figure 2.7. In this figure, the leftmost column set results belong to the original signal subset calculations. The following 14 column sets belong to the TF feature subset calculations. Final 6 column sets belong to the TS feature subset calculations. The feature set order is the same as the order in Table 1, column 1. From the figure it can be seen that MLP gives the worst performance for most of the feature subsets in both before denoising (16 of 21) and after denoising (18 of 21) cases. SVM gives the best performance for more than half of the feature subsets, both in undenoised (11 of 21) and after denoised (11 of 21) cases.

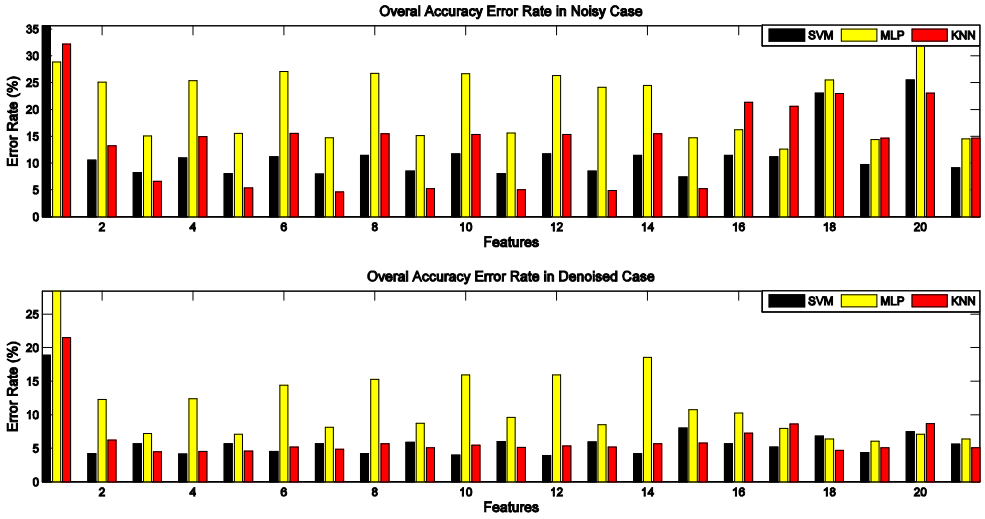

Figure 2.7 Overall accuracy error rate of individual feature sets with undenoised and denoised case for three learning algorithms. (The leftmost column set results belong to the original signal subset calculations. The following 14 column sets belong to the TF feature subset calculations. Final 6 column sets belong to the TS feature subset calculations.)

Figure 2.8 depicts the true positive error rates for the SVMs, MLP and k-NN learning algorithms of 20 extracted feature subsets and the original signal subset (feature set order is the same as Figure 2.7) individually. SVMs gives the best performance for more than half of the feature subsets, in both undenoised (13 of 21) and denoised (17 of 21) cases. MLP gives the worst performance for most of the feature subsets in both undenoised (15 of 21) and denoised (18 of 21) cases.

Figure 2.9 shows how denoising with DTCWT affects TP error rate of all feature subsets for SVM, MLP and k-NN learning algorithms individually. It can be seen from the figure that for all three methods, the TP error rate is decreased by denoising with the DTCWT. This indicates that denoising improves the success of the proposed method in detecting the crackle signals.

All individual and ensemble learning results for SVMs, MLP, and k-NN classifiers are listed in Tables 2.1, 2.2 and 2.3, respectively. It is seen that the highest overall accuracy (97.50) is obtained with our proposed method when a Gaussian window is used and DTCWT is applied as a pre-processing step, and the resulting feature sets are used as an ensemble of networks. Also the highest TP rate with 97.30 is obtained with

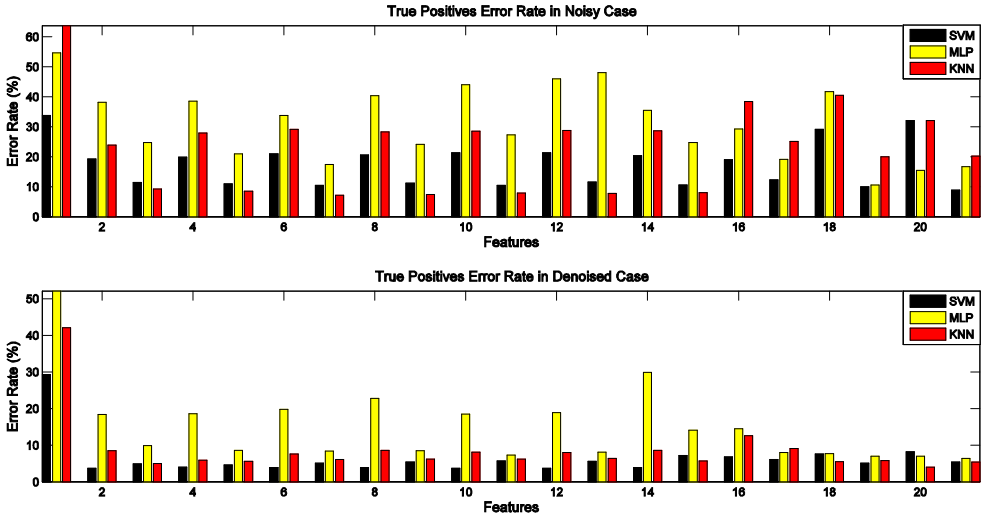

Figure 2.8 True positive error rate of individual feature sets with undenoised and denoised case for three learning algorithms. (The leftmost column set results belong to the original signal subset calculations. The following 14 column sets belong to the TF feature subset calculations. Final 6 column sets belong to the TS feature subset calculations.)

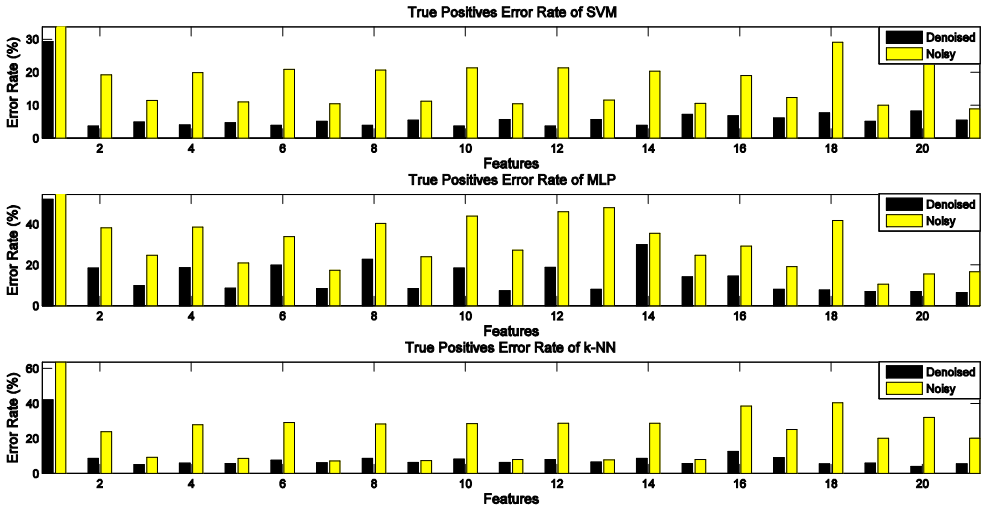

Figure 2.9 True positive error rate of three learning methods sets for undenoised and denoised case. (The leftmost column set results belong to the original signal subset calculations. The following 14 column sets belong to the TF feature subset calculations. Final 6 column sets belong to the TS feature subset calculations.)

the same procedure (with Gaussian window, DTCWT pre-processing, and ensemble of networks).

Table 2.1
Overall accuracies, true positive (TP), and true negative (TN) rates of the individual feature sets and their ensembles for SVMs case. (TFAUT and TFAUF indicate the feature subsets obtained by time-frequency analysis upon time and time-frequency analysis upon frequency respectively. Similarly, TSAUT and TSAUS indicate the feature subsets obtained by time-scale analysis upon time and by time-scale analysis upon scale respectively.)

	Denoised						Undenoised					
	Overall	TP	TN	Ensemble			Overall	TP	TN	Ensemble		
Original Signals	81.10	70.70	91.50	Overall	TP	TN	64.40	66.20	63.00	Overall	TP	TN
TFAUT-Gaussian	95.80	96.30	95.30	**97.50**	**97.30**	97.70	89.45	80.80	98.10	91.55	84.00	99.10
TFAUF-Gaussian	94.35	95.10	93.60				91.80	88.60	95.00			
TFAUT-Blackman	95.85	96.00	95.70	97.40	97.10	97.70	89.05	80.10	98.00	91.50	83.90	99.10
TFAUF-Blackman	94.35	95.40	93.30				91.95	89.00	94.90			
TFAUT-Hanning	95.45	96.10	94.80	97.30	96.90	97.70	88.80	79.10	98.30	91.05	83.00	99.10
TFAUF-Hanning	94.35	94.90	93.80				92.05	89.60	94.50			
TFAUT-Hamming	95.80	96.10	95.50	97.20	96.80	97.60	88.55	79.40	97.70	90.70	82.20	99.20
TFAUF-Hamming	94.10	94.60	93.60				91.50	88.80	94.20			
TFAUT-Bartlett	96.00	96.30	95.70	97.15	96.80	97.50	88.25	78.70	97.80	91.05	82.90	99.20
TFAUF-Bartlett	94.00	94.30	93.70				92.00	89.60	94.40			
TFAUT-Triang	96.05	96.30	95.80	97.15	96.80	97.50	88.25	78.70	97.80	90.70	82.30	99.10
TFAUF-Triang	94.05	94.40	93.70				91.50	88.50	94.50			
TFAUT-Rectang	95.80	96.10	95.50	97.05	96.10	98.00	88.55	79.70	97.70	90.55	82.40	98.70
TFAUF-Rectang	92.00	92.80	91.20				92.60	89.40	95.80			
TSAUT-Morlet	94.30	93.20	95.40	96.70	95.50	97.90	88.55	81.00	96.10	90.90	86.10	95.70
TSAUS-Morlet	92.00	92.80	91.20				92.60	89.40	95.80			
TSAUT-Paul	93.20	92.40	94.00	96.25	94.80	97.70	76.95	70.90	83.00	87.35	81.20	93.50
TSAUS-Paul	95.65	94.90	96.40				90.25	90.00	90.50			
TSAUT-Mexican	92.50	91.80	93.20	96.25	94.90	97.60	74.50	68.00	81.00	87.85	80.80	94.20
TSAUS-Mexican	94.40	94.60	94.20				90.85	91.10	90.60			

2.4 Discussion and Conclusions

The computerized analysis of pulmonary sound signals is a recent research area due to the improvements in digital recording systems and advanced digital signal processing techniques. In this chapter, a crackle detection method in which the DTCWT is used as a pre-processing step for removing the frequency bands containing no-crackle information, is proposed. In this method, various feature sets using TF and TS analysis are extracted and fed to the SVMs, MLP, and k-NN classifiers.

It is observed that the overall accuracy performances of the SVMs and the k-NN classifiers are very close to each other for both undenoised and denoised signals. However, the SVMs appears to be superior over the k-NN in detecting the crackle signals on both undenoised and denoised data observations. It must be noted that

Table 2.2
Overall accuracies, true positive (TP), and true negative (TN) rates of the individual feature sets and their ensembles for MLP case. (TFAUT and TFAUF indicate the feature subsets obtained by time-frequency analysis upon time and time-frequency analysis upon frequency respectively. Similarly, TSAUT and TSAUS indicate the feature subsets obtained by time-scale analysis upon time and by time-scale analysis upon scale respectively.)

	Denoised						Undenoised					
	Overall	TP	TN	Ensemble			Overall	TP	TN	Ensemble		
Original Signals	71.55	47.90	95.20	Overall	TP	TN	71.20	45.40	97.00	Overall	TP	TN
TFAUT-Gaussian	87.70	81.60	93.80	91.65	84.80	98.50	74.95	61.90	88.00	81.10	62.80	99.40
TFAUF-Gaussian	92.80	90.10	95.50				84.95	75.30	94.60			
TFAUT-Blackman	87.60	81.40	93.80	91.70	84.90	98.50	74.65	61.50	87.80	82.10	64.90	99.30
TFAUF-Blackman	92.90	91.40	94.40				84.45	79.10	89.80			
TFAUT-Hanning	85.60	80.20	91.00	91.50	84.90	98.10	72.95	66.20	79.70	83.95	68.80	99.10
TFAUF-Hanning	91.85	91.60	92.10				85.30	82.60	88.00			
TFAUT-Hamming	84.70	77.20	72.20	91.20	84.30	98.10	73.25	59.60	86.90	80.90	62.30	99.50
TFAUF-Hamming	91.25	91.50	91.00				84.90	75.90	93.90			
TFAUT-Bartlett	84.05	81.50	86.60	91.80	86.60	97.00	73.35	56.00	90.70	80.00	60.20	99.80
TFAUF-Bartlett	90.40	92.70	88.10				84.40	72.70	96.10			
TFAUT-Triang	84.05	81.10	87.00	91.80	86.20	97.40	73.70	54.00	93.40	75.00	50.00	100
TFAUF-Triang	91.50	91.90	91.10				73.85	51.90	99.80			
TFAUT-Rectang	81.45	70.10	92.80	87.45	76.20	98.70	75.50	64.50	86.50	81.20	63.00	99.40
TFAUF-Rectang	89.25	85.90	92.60				85.25	75.30	95.20			
TSAUT-Morlet	89.75	85.50	94.00	93.70	89.60	97.80	83.80	70.80	96.80	85.35	71.20	99.50
TSAUS-Morlet	92.05	92.00	92.10				87.40	80.90	93.90			
TSAUT-Paul	93.60	92.30	94.90	95.40	93.00	97.80	74.50	58.30	90.70	85.05	71.40	98.70
TSAUS-Paul	93.95	93.00	94.90				85.65	89.40	81.90			
TSAUT-Mexican	92.90	93.00	92.80	95.20	93.20	97.20	67.85	84.50	51.20	86.70	77.70	95.70
TSAUS-Mexican	93.60	93.60	93.60				85.50	83.30	87.70			

SVMs is successful at separating the class partitions when there are enough number of data observations as is the case with our dataset to determine the optimal value of cost parameter, C, which controls the complexity of the SVMs model. One of the advantages of SVMs is that the solution is defined in terms of support vectors consisting of a small subset of the data observations, which limits the complexity of the problem. On the other hand, k-NN does not have an explicit model training, so the computational load of the testing step is very high in contrast to SVMs since we need to compute the distance of the test instance to all training instances. Besides, k-NN is very sensitive to outliers and undenoised features because the algorithm does not reduce the effect of irrelevant features unless a feature selection as a pre-processing step is applied.

According to our results, it is concluded that ensemble of networks increases the overall and TP accuracy performances of SVMs classifier for all 10 ensemble results. In

Table 2.3
Overall accuracies, true positive (TP), and true negative (TN) rates of the individual feature sets and their ensembles for k-NN case. (TFAUT and TFAUF indicate the feature subsets obtained by time-frequency analysis upon time and time-frequency analysis upon frequency respectively. Similarly, TSAUT and TSAUS indicate the feature subsets obtained by time-scale analysis upon time and by time-scale analysis upon scale respectively.)

	Denoised						Undenoised					
	Overall	TP	TN	Ensemble			Overall	TP	TN	Ensemble		
Original Signals	78.50	58.00	99.00	Overall	TP	TN	67.80	36.30	99.30	Overall	TP	TN
TFAUT-Gaussian	93.80	91.50	96.10	95.70	93.10	98.30	86.80	76.10	97.50	87.85	76.10	99.60
TFAUF-Gaussian	95.50	95.00	96.00				93.40	90.70	96.10			
TFAUT-Blackman	95.45	94.10	96.80	96.10	94.00	98.20	85.05	72.10	98.00	86.15	72.40	99.90
TFAUF-Blackman	95.40	94.40	96.40				94.65	91.50	97.80			
TFAUT-Hanning	94.80	92.40	97.20	95.20	92.40	98.00	84.45	70.90	98.00	85.65	71.80	99.50
TFAUF-Hanning	95.15	93.90	96.40				95.40	92.80	98			
TFAUT-Hamming	94.30	91.40	97.20	95.05	91.60	98.50	84.55	71.70	97.70	85.80	72.00	99.60
TFAUF-Hamming	94.90	93.80	96.00				94.75	92.60	96.90			
TFAUT-Bartlett	94.55	91.90	97.20	95.00	91.70	98.30	84.65	71.50	97.80	85.65	71.70	99.60
TFAUF-Bartlett	90.40	92.70	88.10				84.40	72.70	96.10			
TFAUT-Triang	94.65	92.00	97.30	95.00	91.60	98.40	84.65	71.30	98.00	85.55	71.50	99.60
TFAUF-Triang	94.80	93.60	96.00				95.10	92.30	97.90			
TFAUT-Rectang	94.30	91.40	97.20	94.95	91.60	98.30	84.55	71.40	97.70	85.80	72.00	99.60
TFAUF-Rectang	94.20	94.30	94.10				94.80	92.00	97.60			
TSAUT-Morlet	92.75	87.40	98.10	93.50	88.50	98.50	78.65	61.60	95.70	79.40	60.60	98.20
TSAUS-Morlet	91.40	90.90	91.90				79.45	74.90	84.00			
TSAUT-Paul	95.30	94.50	96.10	96.15	94.50	97.80	77.05	59.50	94.60	79.55	60.70	98.40
TSAUS-Paul	94.95	94.20	95.70				85.35	80.00	90.70			
TSAUT-Mexican	91.30	96.00	86.60	96.00	95.70	96.30	76.95	67.90	86.00	82.00	67.10	96.90
TSAUS-Mexican	94.90	94.60	95.20				85.35	79.80	90.90			

contrast, for k-NN and MLP classifiers ensemble of networks is not as efficient as SVMs case, which originates from the fact that the individual learning accuracy of original signals with SVMs (overall accuracy rate = 81.10, TP rate = 70.70 in denoised case) is higher than MLP (overall accuracy rate = 71.55, TP rate = 47.90 in denoised case) and k-NN (overall accuracy rate = 78.50, TP rate = 58.00 in denoised case) cases.

The MLP classifier provided the worst performance for most of the feature sets. There are two main reasons for this. First, neural networks are prone to overfitting unless some build-in mechanisms like weight decay are applied. We observed that in contrast to test set accuracies, best performance on training set is obtained with MLP. Second, neural networks require a very careful pre-processing step. The signal-to-noise ratio must be increased by eliminating the undenoised or irrelevant features in the dataset by applying feature selection methods.

As a conclusion we can say that using DTCWT as a preprocessing step, extracting features instead of using the original signals and combining the feature sets as an ensemble of networks improve the crackle detection capability of the proposed model. It should also be noted that combining the SVMs models with different feature sets as an ensemble improves the overall accuracy and TP rate of the proposed method more than k-NN and MLP classifiers. In the future, it will be a challenge to implement the proposed method in real time as an online crackle detection system.

3. AN EMBOLI DETECTION SYSTEM BASED ON THE DUAL TREE COMPLEX WAVELET TRANSFORM AND ENSEMBLE LEARNING

3.1 Introduction

The transcranial Doppler ultrasound, which enables monitoring the middle cerebral artery, is a commonly used method to detect asymptomatic embolic signals (ESs) in the cerebral circulation [37]. In certain conditions, such as carotid artery stenosis, cardiac valvular disease and atrial fibrillation, asymptomatic ESs are used for the identification of active embolic sources in stroke-prone individuals and the selection of high-risk patients for appropriate treatment [38]. Therefore, for these patients, accurate detection of asymptomatic ESs has a significant clinical importance.

Traditionally, for detecting ESs, visual detection by using individual spectral recordings and acoustic detection by hearing the Doppler shift sound by human experts are the gold standards. These types of detection are time consuming (recordings of the patients may last for one hour or more) and subject to observer's experience. As a consequence of these drawbacks, an automated system is required for a reliable and clinically useful emboli detection technique.

A Doppler ultrasound signal detected by the transcranial Doppler ultrasound system contains two more signal types other than the ESs. These signals are the Doppler speckle (DS) (signals caused by red blood cell aggregates) and the artifacts (signals caused by tissue movement, probe tapping, speaking, and any other environmental effects). ESs are the results of the reflection of transmitted Doppler ultrasound signals from emboli, which are bigger than red blood cells. Therefore, ESs have some distinctive characteristics when compared to DS and artifacts. ESs appear as increasing and then decreasing in intensity for a short duration, usually less than 300 ms and their bandwidth is usually much narrower than that of DS. Therefore, ESs can be

considered as narrow-band signals relative to DS [39].

The outputs of a Doppler ultrasound system employing quadrature detection are in-phase and quadrature-phase components. The information concerning blood flow direction is encoded in the phase relationship between these two components and forward and reverse blood flow signals are obtained by using various methods [40, 41]. Unlike the artifacts, ESs and DS are unidirectional.

Generally, the aim of automated emboli detection systems is to distinguish ESs from artifacts and DS using Doppler ultrasound. For this purpose, an automated system is aimed to be built up by extracting features from these signals using various methods followed with classification. After the feature extraction step, any dimensionality reduction method such as principal component analysis (PCA) or linear discrimination analysis (LDA) can be applied to deal with the curse of dimensionality problem [42]. A preferred method is to obtain the spectra of audio recordings via complex discrete Fourier transform (FT) and use PCA to make it easy for a classifier such as support vector machines (SVMs) to identify whether the signal contains ES or not [43].

Considering the narrow-band assumption, frequency analysis based methods are frequently used as feature extraction step in ES detection systems [44]. In [45] a spectrogram analysis based detection method is proposed. Along with these techniques, fast Fourier transform (FFT) is also commonly used in feature extraction. However, continuous wavelet transform (CWT) based methods perform better than FFT in describing ESs [46]. In [47], an automated system using DWT to derive several parameters for detecting ESs was proposed. In [47], Doppler ultrasound signals were decomposed into an optimum number of frequency bands and then these bands were reconstructed. From these reconstructed bands several parameters were obtained and used in detection algorithm.

Dual tree complex wavelet transform (DTCWT), which is an improved version of ordinary DWT with limited redundancy, can also be used in the analysis of ESs. The DTCWT was developed to overcome the lack of shift-invariance property

of ordinary DWT [29, 30]. This property of DTCWT can be very important when the wavelet coefficients are used as features in machine learning algorithms to detect emboli, because the emboli information is encoded in the phase relationship of the in-phase and quadrature-phase components and any phase-distortion during the analysis steps can reduce the discriminative power of wavelet features. In literature, the success of DTCWT in the analysis of nonstationary signals was proved in [1].

In our study, a Doppler ultrasound dataset consisting of 100 samples from each embolic, DS and artifact 1024-point signal pairs - forward and reverse direction - is used. Exemplary time-domain representations of ESs, artifact and DS in both forward and reverse directions can be seen in Figure 3.1. FFT, DWT and DTCWT are applied to these 300 signal pairs in order to extract features. Thereafter, the dimensionality (1024 in this case) of resulted coefficients is reduced with a dimensionality reduction method for removing signal components that do not carry useful information. Dimensionality reduction is a critical pre-processing step in machine learning problems especially when the dimensionality of the dataset is high when compared with the number of samples such as the Doppler ultrasound dataset dealt with in this paper [48]. The dimensionality reduction techniques can be categorized into two groups: (1) unsupervised techniques that do not utilize the class labels (PCA), (2) supervised techniques (linear discriminant analysis - LDA) that incorporate the class labels into their frameworks [49]. Even though mainly the PCA is used in this work, the LDA is also used to visualize the samples according to their classes.

Ensuing the feature extraction and dimensionality reduction phases, the features acquired from forward flow direction of the blood are fed into k-NN and SVMs. Additionally, in order to increase the classification accuracy, the information extracted from the features acquired from reverse flow direction of the blood are also used. However, these features are not combined in a conventional way. First, the features from forward and reverse directional signals are fed to classifiers separately since forward signals are suitable for three-class classification whereas the reverse signals are for two-class classification. Then, the outputs of these two classifiers are combined using the stacking ensemble combination technique. The obtained individual and combined results are

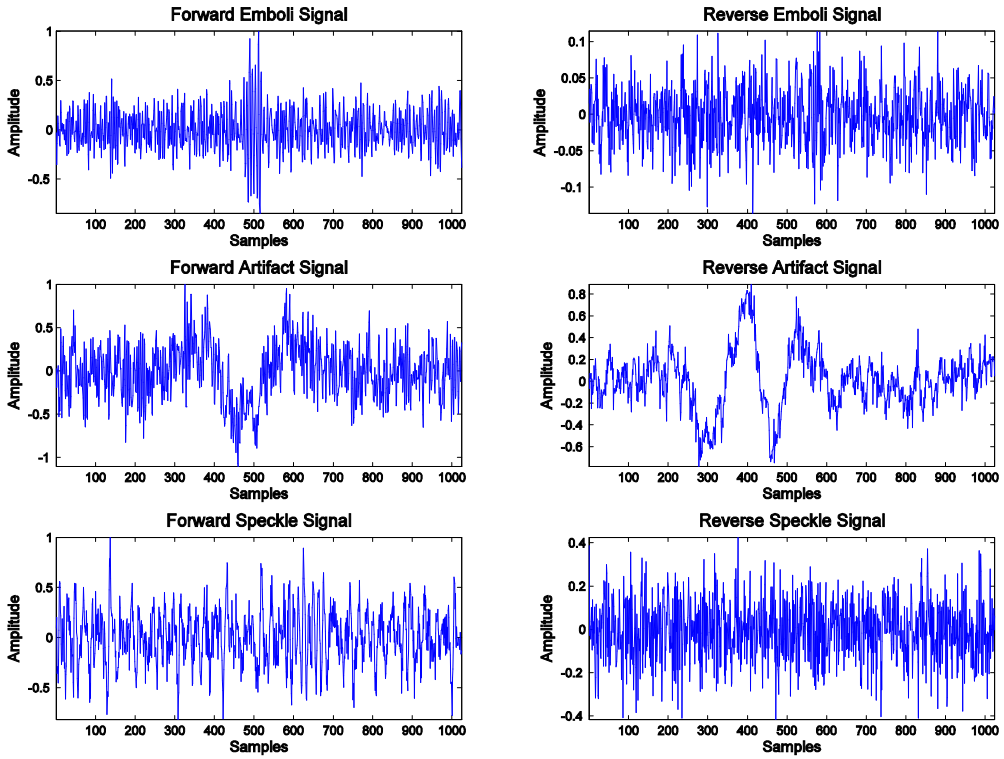

Figure 3.1 Time domain representation of an ES, an artifact and a DS.

presented and compared for each feature extraction method in detail.

The remaining of the chapter is organized as follows: Section 3.2 gives the description of the Doppler ultrasound dataset, presents the theory of signal processing methods used, and declares brief information about feature extraction and dimensionality reduction methods. Additionally, in section 3.2 proposed individual and combined emboli detection systems are explained. Section 3.3 provides the experimental results on the Doppler ultrasound dataset. Lastly, section 3.4 is the discussions and conclusions.

3.2 Materials and Methods

3.2.1 Doppler Ultrasound Dataset Description

Doppler ultrasound signals were recorded using a transcranial Doppler system (EME Pioneer TC4040 which is manufactured by Nicolet Biomedical, Madison, USA) with the sampling frequency of 7150 Hz and the data length of 1024 points. Patients with symptomatic carotid stenosis were the subjects and the recordings were taken from ipsilateral middle cerebral artery. 100 embolic, 100 Doppler speckles and 100 artifact signal pairs were created to constitute a Doppler ultrasound dataset. Tapping the probe, speech or coughing created the artifacts artificially during patient recordings and natural artifacts occurred during patient movement, speech, or coughing during routine patient recordings [47].

3.2.2 Signal Processing Methods

The normal Doppler ultrasound blood flow signals are formed by the signals scattered from red blood aggregate and usually assumed as a random distribution [50]. However, the Doppler ultrasound signal produced by an embolus has more certain characteristics because of two following reasons. Firstly, since an embolus can be assumed as a single scatterer, the velocity of an embolus is relatively stationary and this results a more located signal in the frequency spectrum. Secondly, in Doppler ultrasound the scattered power from a point scatterer is related to its sectional area [51]. The embolus has a much bigger volume than an ordinary red blood cell and this usually causes the ESs to be more powerful than the signal of the normal blood flow. So, when the frequency characteristics of the ESs are considered, they can be accepted as more located signals in frequency spectrum with high power compared to Doppler speckle and artifacts. Therefore, to make use of these characteristics of the blood flowing normally and with emboli for ES detection, frequency based features are extracted by using FFT, DWT, and DTCWT.

3.2.2.1 Fourier Transform. In the separation process of the ESs from the speckles and the artifacts, to reveal and enhance the narrowband frequency characteristics of ESs, Doppler ultrasound signals can be analyzed (decomposed) with classical FT, which is extensively used in many signal processing applications. It expands a time-domain signal onto orthogonal basis functions (sine and cosine waves) to reveal the frequency contents of the signal. But the classical FT cannot localize the frequency components in time and it assumes that the analyzed signal is stationary. However, due to the inherent time-varying characteristics of cardiovascular system, Doppler ultrasound signals are expected to have non-stationary character, independent of the time scale over which they are analyzed. In this study, the FFT, which is a fast algorithm to implement classical FT in real time, is used for extracting FT coefficients that used in detection algorithm.

3.2.2.2 Discrete Wavelet Transform. Doppler ultrasound signals obtained from blood flow have highly complex time-frequency characteristics (non-stationary characteristics). Therefore, any appropriate analysis method which deals with them should have adjustable time-frequency resolution. Wavelet transform [52, 53] (WT) is known as a good tool for the analysis of non-stationary signals having transient behavior such as embolic signals. The WT can be thought as an extended version of the classic FT. Unlike FT, WT works on a multi-scale basis.

In the WT, a signal can be represented in terms of simple building blocks, named as wavelets. These building blocks are actually a family of functions which are derived from a single generating function called the mother wavelet by translation (shifting) and dilation (scaling) operations. The WT can be categorized into continuous and discrete. Continuous wavelet transform (CWT) of a signal $s(t)$ is defined by

$$W_s(a,b) = \frac{1}{\sqrt{|a|}} \int_{-\infty}^{+\infty} s(t)\psi\Big(\frac{t-b}{a}\Big)\mathrm{d}t \tag{3.1}$$

where a is the scale, b is the translation, and $\psi_{a,b}$ is the mother wavelet. Scaling either dilates (expands) or compresses a signal. Large scales (low frequencies) expand

the signal and provide global information about the signal, while small scales (high frequencies) compress the signal and provide the detailed information hidden in the signal.

In the CWT, the scale and translation parameters change continuously, and this results in a huge computation complexity and a vast amount of data. Therefore, in real-time applications, in order to reduce memory requirements and increase the computation speed of the analysis, discrete wavelet transform (DWT), in which the scale and translation parameters are discretized, is commonly used.

In the DWT, a countable set of coefficients are obtained at the end of the transform and these coefficients correspond to the points on a two-dimensional grid of discrete points in the time-scale domain. The formula of the DWT can be defined as

$$W_s(m,n) = \frac{1}{\sqrt{|a_0^m|}} \int_{-\infty}^{+\infty} s(t)\psi\Big(\frac{t - nb_0a_0^m}{a_0^m}\Big)\mathrm{d}t \tag{3.2}$$

where m and n are discrete scale and translation steps. When compared with CWT, a and b are replaced by a_0^m and $nb_0a_0^m$ respectively, where a_0 and b_0 are discrete scale and translation step sizes.

In practice, the DWT can be implemented by using multi-resolution analysis (MRA) approach [54, 55], which is computationally more efficient. In MRA, the dyadic DWT employs two set of functions named as scaling functions and wavelet functions, which are associated with the low-pass filters and high-pass filters (a pair of quadrature mirror filters) respectively. To decompose a time-domain signal into different frequency bands, these high-pass and low-pass filters must be applied to that signal and the resultant signal of each filter must be down-sampled by a factor of two. At the end of these processes, the time-domain signal is split into two components, and each of these two components has half-size of the original signal length. One of these components contains the low-frequency (coarse) information and the other one contains high-frequency (detail) information. If these computations are performed for one level of decomposition, for the first level, the decomposition is expressed mathematically as

follows

$$D_1[k] = y_{high}[k] = \sum x[n]h[2k-n] \tag{3.3}$$

$$A_1[k] = y_{low}[k] = \sum x[n]g[2k-n] \tag{3.4}$$

where $h[n]$ and $g[n]$ are the high-pass and low-pass filters, $y_{high}[k]$ and $y_{low}[k]$ are the resultant coefficients of high-pass and low-pass filters respectively. High-pass and low-pass coefficients are also named as detail ($D_1[k]$) and approximation ($A_1[k]$) coefficients of the first level. This procedure, which can be applied with a binary tree, is usually performed for the second level of analyses using the coarse part of the first level as a new input to the second one, and this process can be iterated up to a certain number of levels for further decomposition (ultimately until a single sample is left). The structure of the DWT can be seen in Figure 3.2.a. At the end of all levels, the dyadic DWT consists of the set of detail coefficients generated at each level of the transform, together with the approximation coefficients generated at the last level of the transform.

3.2.2.3 Dual Tree Complex Wavelet Transform. In literature, the DWT has been widely used in various medical application areas such as denoising, feature extraction, etc. [56, 57, 58]. Despite of all its useful time-frequency resolution and fast computation advantages, the DWT has some very important drawbacks such as alising, lack of directionality, and shift-variance [29]. In processing ES, due to the transient time behavior of ES, shift-variance problem of the DWT arising from the use of down-sampling operator becomes crucial. As a consequence of this shift-variance limitation, which means that any small shift in the input sequence greatly distorts the wavelet coefficients and changes their energy in each sub-band, the DWT based features that are fed into a machine learning algorithm to detect emboli, are badly affected. Therefore, in order to obtain more robust wavelet based features, the DTCWT having near shift-invariant property is more appropriate than the ordinary DWT.

DTCWT [29, 30], which utilizes two real DWTs operating in parallel on an input

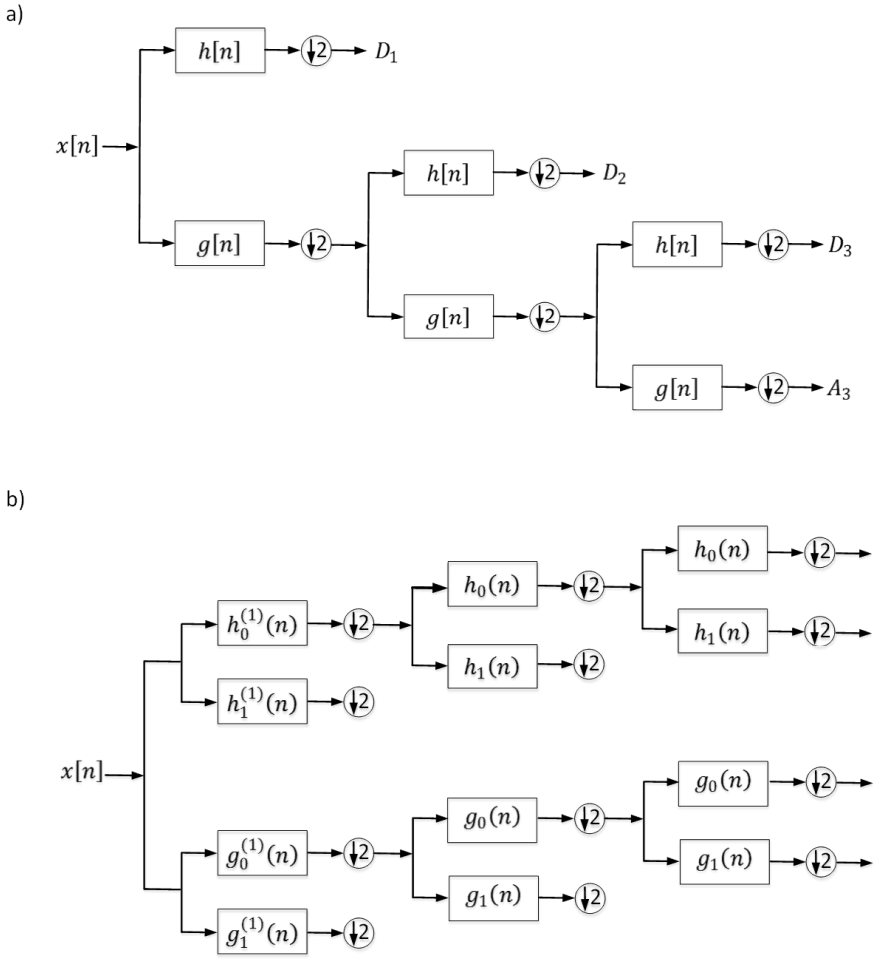

Figure 3.2 a) A 3 level binary tree implementation, only the analysis part, of the DWT. D_1, D_2 and D_3 are the detail coefficients and A_3 is the approximation coefficients. b) Structure of the analysis part of the DTCWT for 3 levels. $h_0^{(1)}(n)$ is the low-pass filter of real tree and $g_0^{(1)}(n)$ is the low-pass filter of imaginary tree in the first band. $h_0(n)$ and $h_1(n)$ are the low-pass and high-pass filters of the real tree for following bands. $g_0(n)$ and $g_1(n)$ are the low-pass and high-pass filters of the imaginary tree for following bands.

signal, is a recent enhancement to the ordinary dyadic DWT and it is approximately shift-invariant. In the DTCWT, the first DWT stands for the real part of the transform while the second DWT stands for the imaginary part. The analysis part of the DTCWT for 3 levels can be seen in Figure 3.2.b.

In order to attain perfect shift-invariance property in the DTCWT, the second tree's (imaginary tree) wavelet function ($\psi'(t)$) must be the Hilbert transformed version

of the first DWT's wavelet function ($\psi(t)$) as shown below,

$$\psi'(t) = \mathbf{H}[\psi(t)] \tag{3.5}$$

where $\mathbf{H}[\ \ ]$ stands for the Hilbert transform (HT) and this relation is named as HT pair condition.

In [59, 60], it is stated that if the low-pass filter of second tree ($g_0(n)$) is equal to the half sample delayed version of the low-pass filter of first tree ($h_0(n)$), then the wavelet functions of DTCWT satisfy HT pair condition and this condition can be shown as below in time domain.

$$g_0(n) \approx h_0(n - 0.5) \Rightarrow \psi_g(t) \approx \mathbf{H}[\psi_h(t)] \tag{3.6}$$

In frequency domain, this can be interpreted as

$$G_0(\omega) = e^{-j0.5\omega} H_0(\omega)\ for\ |\omega| < \pi \tag{3.7}$$

Finite impulse response (FIR) filters can never satisfy half sample delay condition and hence the resulting wavelet function pairs can never be perfectly analytic. Therefore, it is necessary to make an approximation [59]. To overcome this condition, instead of using a half sample delay system, in the first stage different filters from the following stages can be employed. For the first stage any orthonormal perfect reconstruction filter pair which satisfies the following equation can be used

$$g_0^{(1)}(n) = h_0^{(1)}(n - 1) \tag{3.8}$$

where $h_0^{(1)}(n)$ is the low-pass filter of real tree and $g_0^{(1)}(n)$ is the low-pass filter of imaginary tree in the first band. If these conditions can be satisfied, then an approximately analytic DTCWT at every stage excluding the first can be obtained. For the inverse DTCWT case, to invert the transform the real tree and the imaginary tree should be inverted separately and then the outputs should be summed.

3.2.3 Feature Extraction and Dimensionality Reduction Methods

3.2.3.1 Feature Extraction. Features are extracted from the forward and reverse directional signals in three different ways. First one is the FFT. The absolute values of the FFT coefficients are found and used as features. Secondly, forward and reverse directional Doppler ultrasound signals are decomposed into 5 scales in DWT and DTCWT feature extraction phase. In the DWT, the filter coefficients given in [61] and for the DTCWT the filter coefficients given in [30] are used. As the FFT, also for both the DWT and the DTCWT absolute values of coefficients are given to the dimensionality reduction algorithm. Usually, an ES exists only in the forward direction [47]. In FFT features emboli shows itself as a narrow-band signal pattern [44]. In DWT and DTCWT features emboli patterns are seen in second and third scales [47].

3.2.3.2 Dimensionality Reduction. Large input dimensionalities make a classification model more complex and more samples should be fed to the classifiers to deal with the curse of dimensionality problem [62]. Dimensionality reduction is a stage of machine learning to avoid high dimensionality small sample size problem which is very common especially in the field of biomedical applications [63]. Therefore, in order to reduce the dimension of the feature set obtained by FFT, DWT, and DTCWT, the PCA, which is an unsupervised dimensionality reduction technique, is used with different proportions of variance [64] since not all eigenvalues contribute to the variance substantially [65]. Dimensionality of the forward directional signal dataset is reduced by preserving the 90% of the data variance. Similarly 90% of the data variance is kept for the ensemble method initially, then 95% and 99% of the data variance are used to observe the change in accuracy of the classifiers.

Additionally, for visualization and comparison of feature extraction methods, LDA is employed as a supervised dimensionality reduction technique. As known, LDA has the limitation of less than number of classes' orthogonal projective directions due to the rank deficiency of the between-class scatter matrix [32]. Therefore, as the emboli dataset includes three classes, the dimension of the datasets is reduced to two by using

LDA.

3.2.4 Overall Structure of the Emboli Detection System

The collected Doppler ultrasound signals are transformed with FFT, DWT, and DTCWT methods to obtain transform coefficients. The obtained datasets consists of 1024 features (transform coefficients) and 300 samples. In order to overcome the curse of dimensionality problem, before feeding the features to the classifiers, the dimension of the datasets are reduced by applying linear dimensionality reduction techniques. Also the number of samples in the training set (90 or 150 samples) and the proportion of variance values of the dimensionality reduction method is changed to view if there is a significant difference in accuracy when the number of training instances or the proportion of variance varies. Finally, the obtained reduced dimensionality feature sets are fed to SVMs with linear kernel and k-NN classifiers. The classification process consists of two phases: using forward directional signals separately and the ensemble of forward - reverse directional signals as the inputs.

3.2.4.1 Individual Emboli Detection System. The features extracted from the forward directional signals (according to the blood flow) are used to make predictions to estimate emboli, artifact or speckle. For the individual emboli detection system, primarily the features obtained from forward directional signals are used. Considering that a signal can be identified as emboli, artifact or speckle from the forward directional signals, the next stage is a three-class classification with the preferred classifiers. The flow chart of the proposed individual method can be seen in Figure 3.3.

3.2.4.2 Ensemble of Forward and Reverse Directional Signals. Using different representations of the same input or object can end up with an explicit identification [32]. Consequently, features extracted from the reverse directional signals, which can estimate if there is an artifact or not, are also used for prediction. Then

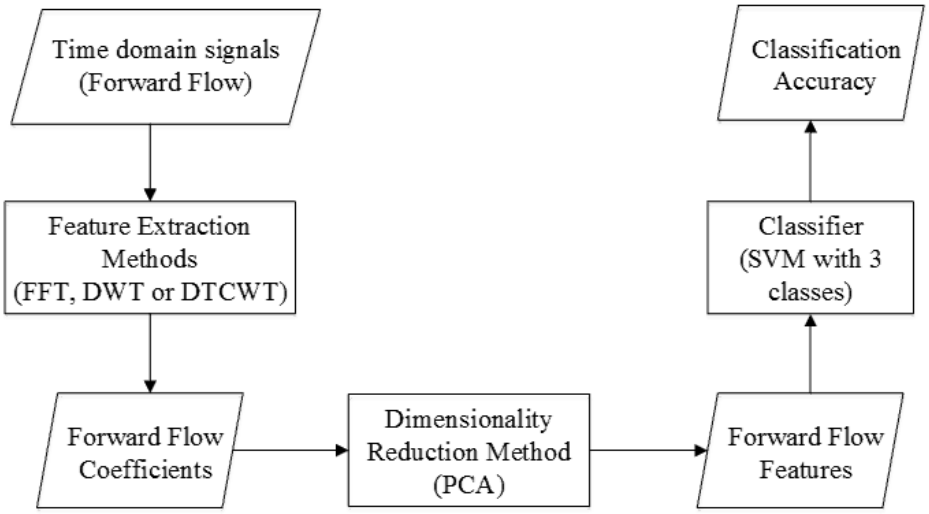

Figure 3.3 Proposed Individual Emboli Detection System.

these predictions are combined to come up with our final ensemble model. In this way, we utilize the information contained in both forward and reverse flow directional signals to discriminate the emboli signals from artifacts and speckles.

In our ensemble emboli detection system, firstly only the features from the forward directional signals, which can set off a three class problem to discriminate ESs, DS and artifacts, are fed into SVMs. Secondly, a two class classification problem to identify if a signal is artifact or not using the features from the reverse directional signals is solved with SVMs. As a result of these processes two sets of probability estimates are obtained: the first set has the information extracted from the forward directional signals and the second has the reverse. Lastly, these two sets are merged into a final dataset consisting of probability estimates of the individual forward and reverse SVMs models. This dataset is used to build a final model, which is a three class problem to classify ESs, DS and artifacts. In this model, the three resultant probability estimate values of forward model and two probability estimate values of reverse model are combined into a row vector and constituted a dataset with five features. Later, this dataset consisting of five element row vectors is fed to the final SVMs. The flow chart of the proposed ensemble method is illustrated in Figure 3.4.

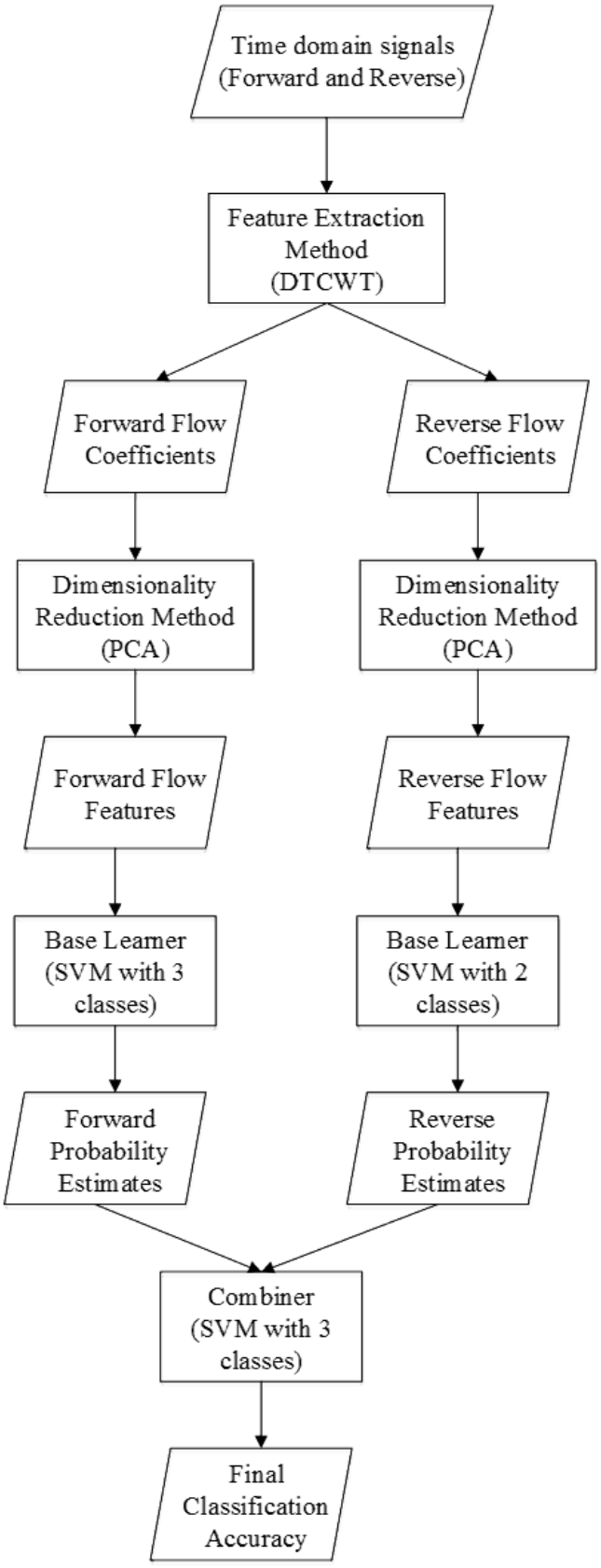

Figure 3.4 Proposed Ensemble Emboli Detection System.

3.3 Experimental Results

Features extracted by FFT, DWT, and DTCWT using the forward directional signals are fed to SVMs and k-NN classifiers with training sets including 150 and 90 samples and different PCA variance proportions. As mentioned before, dataset includes 100 samples from each of the speckle, artifact and emboli classes. First, the half of the forward direction samples (50 samples) from each class is selected randomly for the training set and the left samples are used for the test set. The train-test splits are repeated 10 times for statistical significance and the average accuracies along with class detection rates are reported. For k-NN classifier, Euclidean distance metric and k parameter of 3 are used. For SVMs application, LIBSVM [33] package is used with a linear kernel along with cost value (C) parameter of one.

The overall SVM and k-NN general accuracy and detection rates of emboli, artifact, and speckle classes with half of the samples selected as the training instances after dimensionality reduction with PCA alongside 90% of variance kept of are presented in Table 3.1. As seen in Table 3.1, the highest general accuracy with the highest detection rates of emboli, artifact, and speckle classes is obtained with DTCWT features for both SVMs and k-NN classifiers. Additionally, higher accuracies are obtained with DWT than FFT. As to compare the classifiers, SVMs performed much better than k-NN since SVMs is more robust to both noise and irrelevant features.

Subsequently, to observe the change in accuracy with the variation in the number of the training instances, the training set size is decreased. For this purpose, 30 samples from each class are used to constitute the training set, and the others are used for test phase. The reason to decrease the number of training samples is to observe the behaviors of the feature extraction methods, classifiers, and ensemble model with small training sample size. In other words, we aim to examine if our method still learns a generalizable model with less number of training samples or overfits to the noisy samples and outliers. Once again the data splitting for the training and test sets are repeated for 10 times. The results attained by the small size training set are also shown in Table 3.1. Parallel to the results of 150 training samples, the highest accuracies are produced

Table 3.1
General accuracy (%) and detection rates (%) of each class obtained with SVMs and k-NN using 150 and 90 training samples.

150 Training Samples						
Feature Extraction	**DTCWT**		**DWT**		**FFT**	
Classifier	***k*-NN**	**SVM**	***k*-NN**	**SVM**	***k*-NN**	**SVM**
General Accuracy	75.73	**92.47**	69.73	**89.20**	71.20	**80.53**
Emboli Detection Rate	90.40	88.20	89.00	80.40	80.80	71.20
Artifact Detection Rate	93.80	94.80	93.80	92.80	89.40	90.40
Speckle Detection Rate	43.00	94.40	26.40	94.40	43.40	80.00
90 Training Samples						
Feature Extraction	**DTCWT**		**DWT**		**FFT**	
Classifier	***k*-NN**	**SVM**	***k*-NN**	**SVM**	***k*-NN**	**SVM**
General Accuracy	76.71	**89.86**	69.76	**87.76**	73.10	**80.33**
Emboli Detection Rate	93.29	85.86	93.43	83.14	81.00	72.14
Artifact Detection Rate	90.29	91.86	90.43	90.14	89.14	89.00
Speckle Detection Rate	46.57	91.86	25.43	90.00	49.14	79.86

by the DTCWT features fed to SVMs classifiers.

Thereafter gathering the results with forward directional signals, additionally reverse directional signals are used to build up the ensemble model. For the proposed ensemble model, SVMs is used as the classifier since it yielded higher accuracies and 90 training samples are used since the accuracy is not significantly affected from the decrease of the number of the training samples. The information acquired from the reverse directional signals cannot be used to classify the signal as emboli, artifact or speckle but only as artifact or not. Even so it is still important to take this information into account. Accordingly, first the forward and reverse directional signals are fed to the SVMs classifiers individually and the resultant probability estimates are combined and fed to another SVMs classifier as an input. In other words, with this technique called the stacked generalization, the outputs of the classifiers (SVMs) used with the individual forward and reverse directional signals are fed to a combiner learner, which

is also SVMs. The results obtained with the forward directional signal individually and the ensemble of forward and reverse directional signals (combined signals) are given in Table 3.2 for comparison. As shown, using stacking to combine the forward and reverse directional signal estimates increases the accuracy approximately 1.5% by using all the feature extraction methods. This ratio might seem low but such low accuracy differences are vital in biomedical decision support systems. Yet, the highest accuracy is again reached by DTCWT features. Likewise the emboli and artifact detection are also better discriminated and the speckle detection rate is nearly the same. The DTCWT features are once more superior to the DWT and the FFT.

Table 3.2
General accuracy (%) and detection rates (%) of each class with SVMs using the forward directional signal individually and the combined signals.

Feature Extraction	**DTCWT**		**DWT**		**FFT**	
Model Type	**Forward**	**Combined**	**Forward**	**Combined**	**Forward**	**Combined**
General Accuracy	89.86	**91.38**	87.76	**88.14**	80.33	**82.81**
Emboli Detection Rate	85.86	88.14	83.14	85.00	72.14	74.14
Artifact Detection Rate	91.86	94.29	90.14	92.29	89.00	93.71
Speckle Detection Rate	91.86	91.71	90.00	87.14	79.86	80.57

Last but not least, the SVMs classification using DTCWT features is done again with repeating the PCA dimensionality reduction with different proportion of variance. Even though all eigenvalues might be greater than 0, not all of them contribute to the variance substantially. Hence usually different percentages of the eigenvalues are selected after sorting them in descending order. Selected percentage will be smaller if the dimensions are more correlated.

In our case, 90%, 95% and 99% of the variance are selected to inspect whether there is a significant difference in the general accuracy and emboli, artifact and speckle detection rates. 90%, 95% and 99% of the variance does not change the classification rates much (91.38%, 90.90% and 92.38% respectively) as shown in Table 3.3. Once more the combined system yields better results. Although increasing the proportion of the variance increases the general accuracy slightly and artifact detection rate significantly,

it is better to use less proportion of the variance, because there is no gain in using PCA as the proportion of the variance increases.

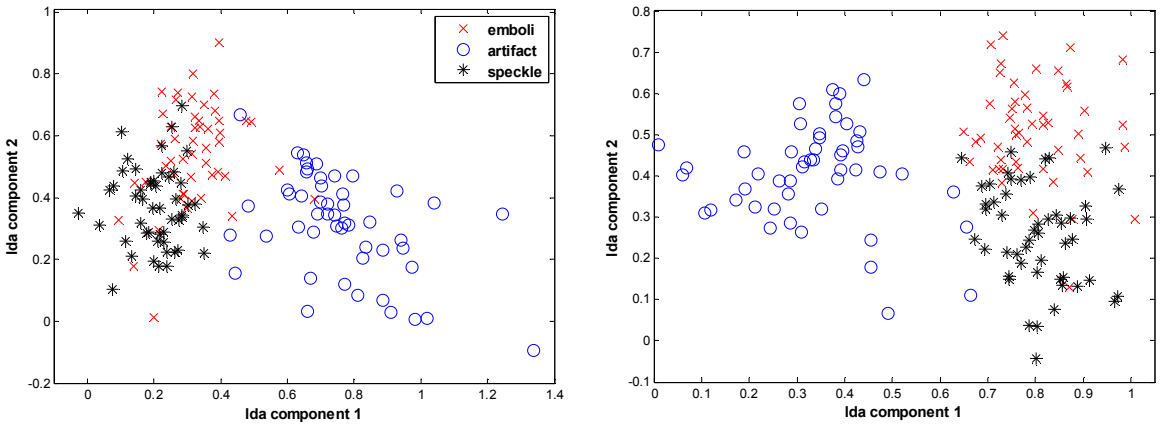

Figure 3.5 Projections on the LDA components extracted from **(left)** FFT and **(right)** DTCWT data of forward flow view.

Table 3.3
General accuracy (%) and detection rates (%) of each class with SVMs using the DTCWT features forward directional signal individually and the combined signals with different proportion of PCA variance.

	DTCWT					
	PCA 0.90		**PCA 0.95**		**PCA 0.99**	
Model Type	**Forward**	**Combined**	**Forward**	**Combined**	**Forward**	**Combined**
General Accuracy	89.86	**91.38**	89.81	**90.90**	91.38	**92.38**
Emboli Detection Rate	85.86	88.14	89.14	90.71	87.00	87.43
Artifact Detection Rate	91.86	94.29	91.57	94.14	95.14	**98.14**
Speckle Detection Rate	91.86	91.71	88.71	87.86	92.00	91.57

As seen from the results, using DTCWT features increases the classification accuracy notably. To visualize this difference, the projections of the FFT and the DTCWT feature sets on the LDA components of the forward view are shown in Figure 3.5. The reason to choose LDA for this visualization is the usage of class labels in LDA. Artifact samples are well discriminated from the other two classes using both FFT and DTCWT features. Some emboli samples are intermixed with artifact samples with FFT features but not with DTCWT. Besides emboli and speckle samples are discriminated better by DTCWT features.

3.4 Discussion and Conclusions

As analysis and detection of ESs visually by experts are very time-consuming and also subjective to observer's experience, development of computer-based decision support systems that aim to discriminate ESs from artifacts and noisy samples is very important and also popular in the field of biomedical engineering. In this chapter, an ensemble emboli detection system is proposed. Within this system, first forward and reverse signals obtained by Doppler ultrasound are transformed by using FFT, DWT and DTCWT. Then PCA is applied to both signals to reduce the dimensionality and the resultant features of the forward directional signal are fed to SVMs and k-NN classifiers with different training set sizes and proportion of variance values. After proving that the best results are yielded by SVMs, the probability distributions obtained by running distinct SVMs on forward and reverse directional signals separately are concatenated and used as a single input to the ensemble system. The success of DTCWT features are compared with those of FFT and DWT by stacking. First of all, we must note that SVMs based detection methods are superior to k-NN based methods for all the dimensionality reduction methods due to the known generalization and sensitivity to noisy samples and irrelevant feature problems of k-NN classifier especially on high-dimensional datasets. The DTCWT is superior to the other coefficient transformation techniques due to its shift-invariance property. Also, changing the proportion of variance in PCA does not affect the classification accuracy much, showing that using all eigenvalues obtained from PCA is not necessary. Using stacking as an ensemble method to take different representations of the data into consideration, namely forward and reverse directional signals, boosts the accuracy rate of the classification.

Therefore, we can conclude that in the ensemble emboli detection using the reverse directional signals increases the classification accuracy since they also include significant discriminative information. Additionally, wavelet transform based extracted features give higher overall classification and emboli detection accuracies than the FFT based features in individual and ensemble SVMs based classification systems due to their well localization property in both time and frequency. The results show that a better time-scale representation of Doppler ultrasound signals having good frequency

resolution at low frequencies, and also good time resolution at high frequencies can be provided by the DTCWT. In the future, it will be a challenge to implement the proposed method in real time as an online emboli detection system.

4. DIRECTIONAL DUAL TREE COMPLEX WAVELET PACKET TRANSFORMS FOR PROCESSING QUADRATURE SIGNALS

4.1 Introduction

Quadrature signals containing in-phase and quadrature-phase components are used in many signal processing applications in every field of science and engineering, such as communication, radar, sonar, diagnostic ultrasound, and MR imaging [66]. As an example, Doppler ultrasound systems used in blood flow analysis also result in quadrature format signals. In most of the Doppler ultrasound systems, the Doppler frequency shifted signals, which are generated in the transducer by the returning ultrasonic signals, are demodulated by using quadrature phase detection (QPD) method [67]. At the end of QPD, the in-phase and the quadrature-phase components, which are within the audio frequency range and have 90 degrees phase difference between, are obtained. In order to derive directional information from these two signals, the in-phase and the quadrature-phase signals must be decoded into the forward and reverse direction components of flow [40].

A number of techniques in literature are described to obtain totally separated directional signals from the quadrature Doppler signals such as phasing filter technique (PFT), extended weaver receiver technique, complex fast Fourier transform method, frequency domain Hilbert transform method and spectral translocation method [41]. The PFT, which has symmetrical and asymmetrical implementations, is the most widely used method in literature [68]. Traditionally, after obtaining directional signals, Fourier domain and wavelet domain processing methods are applied to these directional signals for extracting further information.

In the scale domain, a complex continuous wavelet transform algorithm which maps the directional information, while performing the analysis, was introduced in

[69]. However, for the discrete wavelet transform (DWT) case, an algorithm, which can be applied directly to the in-phase and the quadrature-phase components and has the capability of mapping directional signals in the scale domain during analysis does not exist.

Traditional DWT represents discrete-time signals in dyadic subband decomposition but for specific discrete-time signals such as non-stationary biomedical signals, the frequency decomposition provided by the DWT might not be optimal. Generalization of the DWT in the discrete wavelet packet transform (DWPT) allows subband analysis without the constraint of dyadic decomposition. The DWPT can perform an adaptive decomposition, which fits the varying signal statistics, of the frequency axis. The DWPT represents a signal in many possible bases and a best decomposition (pruned wavelet packet tree) can be selected from this dictionary according to an optimization criterion [70]. At the end of these procedures, analyzed signals can be represented by as few and large coefficients as possible [71, 72]. This adaptive and sparse decomposition was used previously in a wide range of problems such as signal analysis, filtering or compression [70, 73, 74, 75].

In contrast to the wide application areas, the DWT lacks of being shift-invariant and does not provide a geometrically oriented decomposition in multiple dimensions. These drawbacks are also valid for the DWPT because it uses same high-pass/low-pass filter pair in the analysis and synthesis part of the transform. In the full DWPT, in addition to DWT both low-pass and high-pass outputs are iterated.

Dual tree complex wavelet transform (DTCWT) was proposed as an alternative for the DWT. When compared with DWT, the DTCWT has better shift-invariance property and provides better directional selectivity in M dimensions ($M \geq 2$) [30, 76]. The DTCWT employs two real DWTs; the first DWT can be thought as the real part of the transform while the second DWT as the imaginary part of the transform. In DTCWT, wavelet filter banks (FBs) used in the second tree are designed according to a certain criterion in order to provide near shift-invariance property. Specifically, wavelet FBs in the imaginary tree are designed so that their impulse responses are

approximately the discrete Hilbert transforms (HTs) of wavelet FBs in the real tree. In [77], a dual tree complex wavelet packet transform (analytic DT-CWPT) having the same shift-invariance and good directional selectivity properties was described.

In order to use DWPT or DT-CWPT in the analysis of quadrature Doppler signals, first directional signals (forward and reverse signals) must be obtained by using the PFT (symmetrical or asymmetrical implementation) and then DWPT or DT-CWPT is applied to those signals as illustrated in Figure 4.1. This procedure increases the computational cost of the processing system. However, it is possible to reduce the computational cost of the processing system by utilizing the HT property of the analysis and synthesis filters of analytic DT-CWPT. In this study, two novel directional complex wavelet packet methods, which can be applied directly to quadrature Doppler signals and have the capability of extracting directional information during analysis, are proposed. These methods are named as symmetrical directional dual tree complex wavelet packet transform (SDDT-CWPT) and asymmetrical directional dual tree complex wavelet packet transform (ADDT-CWPT).

With SDDT-CWPT and ADDT-CWPT, the HT filtering steps of symmetrical PFT (Sym-PFT) and asymmetrical PFT (Asym-PFT) are eliminated. 90 degrees phase shift normally provided by HT filter in the PFT is now performed by the wavelet FBs of imaginary tree of analytic DT-CWPT. With the proposed methods, obtained

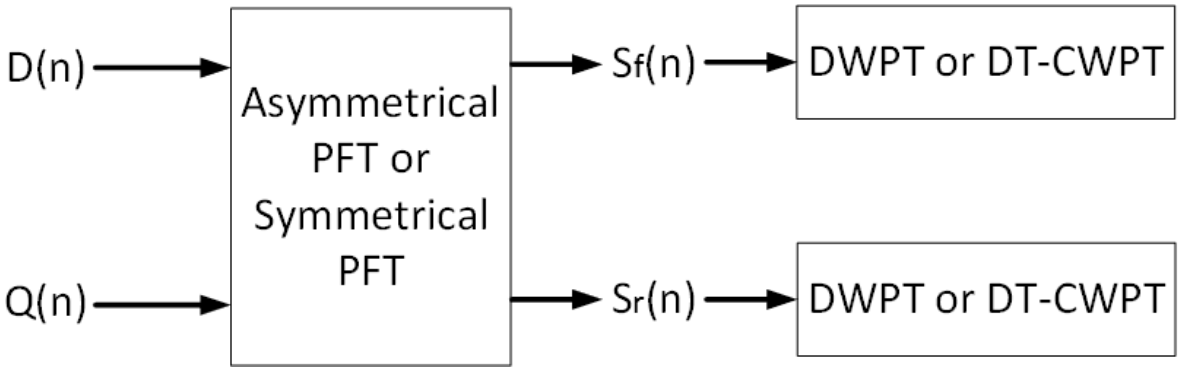

Figure 4.1 Process of quadrature signals with traditional methods. *D(n)* is the in-phase component and *Q(n)* is the quadrature component. $S_f(n)$ is the forward flow signal and $S_r(n)$ is the reverse flow signal.

directional coefficients during the analysis part of wavelet packet transform and also directional signals at the end of the synthesis part are almost identical to the outputs of analyzing the same signals with asymmetrical and symmetrical versions of the PFT followed by two DWPTs or DT-CWPTs.

In order to prove the proposed methods, three different sets of signals in quadrature format are used. In the first set, synthetic single frequency quadrature signals simulated as sines and cosines, are employed. In the second set, a band-limited quadrature signal created by using white Gaussian noise is utilized. Lastly for a real life application, quadrature signals obtained from a Doppler ultrasound system are used. For all the sets, signal-difference-ratios between the reference methods and the proposed methods are calculated in detail. For the real signals, the coefficients obtained with proposed methods at the end of analysis part are compared with the coefficients obtained by traditional methods and the shift-invariance properties of the proposed methods are demonstrated. Additionally, for the real signals case, a detailed time comparison of the proposed methods with traditional methods is given.

The remaining of the chapter is organized as follows: Section 4.2 gives the description of the quadrature signals and the classical PFT methods for directional information extraction. Section 4.3 explains existing wavelet based techniques for quadrature signal processing. Section 4.4 presents the proposed directional wavelet packet transforms and declares their properties. Section 4.5 provides the experimental results using synthetic and real quadrature signals. Lastly, the discussions and conclusions are given in section 4.6.

4.2 Quadrature Signals

In order to understand the proposed methods precisely, the nature of the quadrature Doppler ultrasound signals must be examined in detail. A quadrature Doppler signal can mathematically be assumed as a complex signal, in which the real and imaginary parts can be represented as the HT of each other. The HT is a widely used linear

frequency-domain operator that shifts the phase of positive frequency components of a signal by -90° and negative frequency components by +90°. Mathematically, a discrete quadrature Doppler signal can be modelled as

$$s(n) = Q(n) + jD(n) \tag{4.1}$$

where *D(n)* is in-phase and *Q(n)* is quadrature-phase components of the signal.

In quadrature Doppler signals the directional information is encoded in the phase relationship between *D(n)* and *Q(n)* components. In this respect, *D(n)* and *Q(n)* can also be represented in terms of the directional signals as

$$D(n) = s_f(n) + \mathbf{H}[s_r(n)] \tag{4.2}$$

$$Q(n) = \mathbf{H}[s_f(n)] + s_r(n) \tag{4.3}$$

where $s_f(n)$ and $s_r(n)$ represent the forward and reverse flow components respectively and $\mathbf{H}[\ \ ]$ stands for the HT.

4.2.1 Phasing Filter Techniques

The PFT, which is based on HT, is the most widely used method in real-time applications for extracting directional signals from the quadrature signals. The reason of using PFT is that it is more suitable for fixed point processors since it employs finite impulse response (FIR) type filters. It also requires less memory to record quadrature Doppler signals [41].

4.2.1.1 Asymmetrical Implementation of the Phasing Filter Technique.

In the Asym-PFT, which is seen in Figure 4.2, two types of filters are used. The first filter is the HT filter and the second one is delay filter (DF) introducing a time delay that equals to the time delay introduced by the FIR type HT filter.

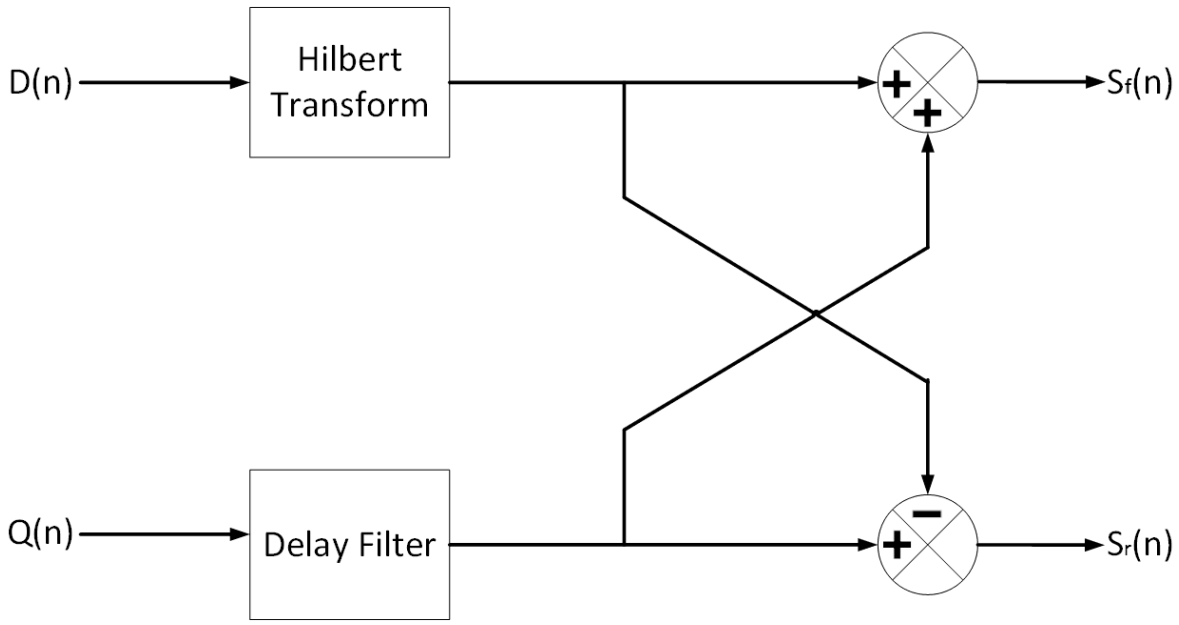

Figure 4.2 Asymmetrical implementation of the PFT.

If the $D(n)$ and $Q(n)$ components are fed into Asym-PFT as inputs, the following results are obtained as the output of the algorithm:

Ignoring the time delays introduced by the digital filters, the HT of $D(n)$ is

$$\mathbf{H}[D(n)] = \mathbf{H}\Big[s_f(n) + \mathbf{H}[s_r(n)]\Big] = \mathbf{H}[s_f(n)] + \mathbf{H}\Big[\mathbf{H}[s_r(n)]\Big] = \mathbf{H}[s_f(n)] - s_r(n) \quad (4.4)$$

According to the algorithm in Figure 4.2, the separated outputs (forward and reverse channel signals) can be obtained by addition and subtraction of equations (4.3) and (4.4) respectively:

$$y_f(n) = Q(n) + \mathbf{H}[D(n)] = \mathbf{H}[s_f(n)] + s_r(n) + \mathbf{H}[s_f(n)] - s_r(n) = 2\mathbf{H}[s_f(n)] \quad (4.5)$$

where the output contains only the 90 degrees phase shifted forward signal.

$$y_r(n) = Q(n) - \mathbf{H}[D(n)] = \mathbf{H}[s_f(n)] + s_r(n) - \mathbf{H}[s_f(n)] + s_r(n) = 2s_r(n) \quad (4.6)$$

where the output contains only the reverse signal.

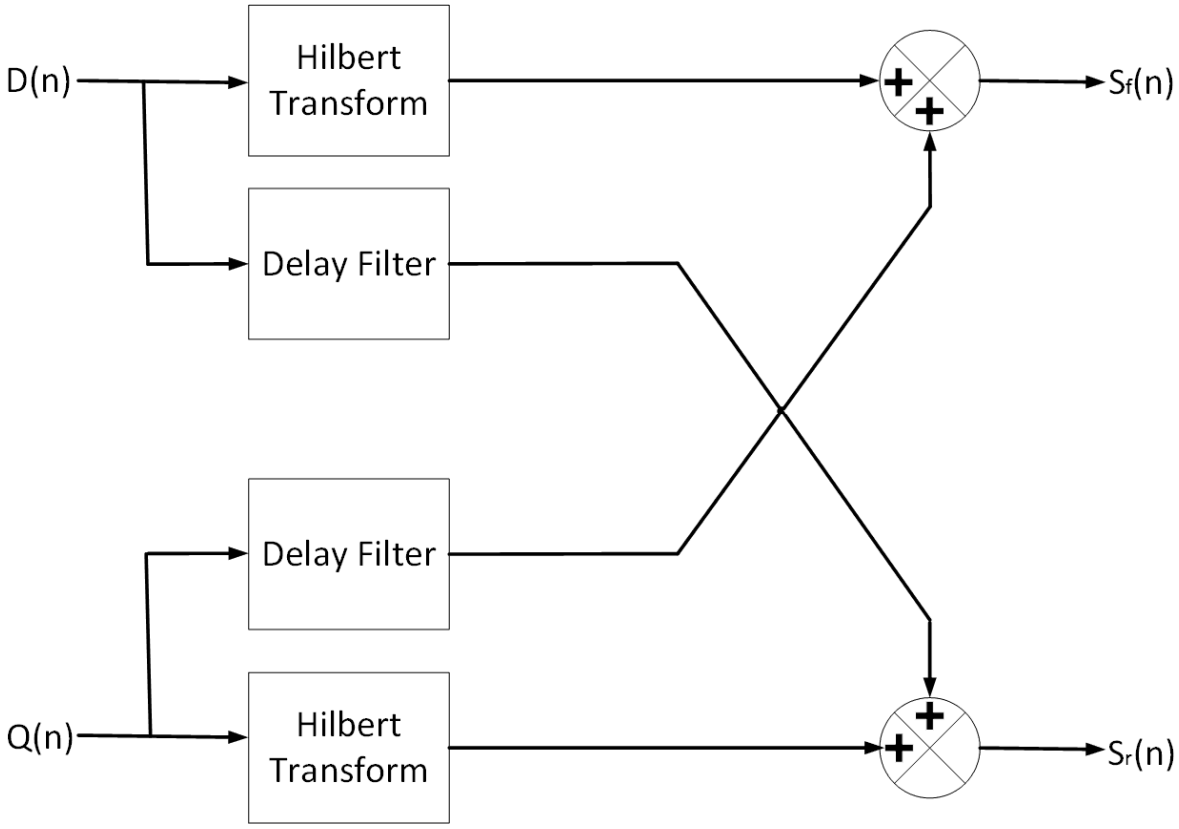

Figure 4.3 Symmetrical implementation of the PFT.

4.2.1.2 Symmetrical Implementation of the Phasing Filter Technique.

In the Sym-PFT, which is illustrated in Figure 4.3, the HT is applied to both *D(n)* and *Q(n)* components. In practical implementation, two delay filters must also be used to compensate the time delays introduced by the HT filters. The outputs of the HT and delay filters constitute a Hilbert pair for each channel [41]. If the *D(n)* and *Q(n)* components are fed into Sym-PFT as inputs, the following results are obtained as the output of the algorithm:

Ignoring the time delays introduced by the digital filters, the HT of *D(n)* is

$$\mathbf{H}[D(n)] = \mathbf{H}\Big[s_f(n) + \mathbf{H}[s_r(n)]\Big] = \mathbf{H}[s_f(n)] + \mathbf{H}\Big[\mathbf{H}[s_r(n)]\Big] = \mathbf{H}[s_f(n)] - s_r(n) \quad (4.7)$$

HT of *Q(n)* is

$$\mathbf{H}[Q(n)] = \mathbf{H}\Big[\mathbf{H}[s_f(n)] + s_r(n)\Big] = \mathbf{H}\Big[\mathbf{H}[s_f(n)]\Big] + \mathbf{H}[s_r(n)] = -s_f(n) + \mathbf{H}[s_r(n)] \quad (4.8)$$

Adding *D(n)* and H[*Q(n)*], and *Q(n)* and H[*D(n)*] yield

$$y_f(n) = Q(n) + \mathbf{H}[D(n)] = \mathbf{H}[s_f(n)] + s_r(n) + \mathbf{H}[s_f(n)] - s_r(n) = 2\mathbf{H}[s_f(n)] \quad (4.9)$$

$$y_r(n) = D(n) + \mathbf{H}[Q(n)] = s_f(n) + \mathbf{H}[s_r(n)] - s_f(n) + \mathbf{H}[s_r(n)] = 2\mathbf{H}[s_r(n)] \quad (4.10)$$

By implementing subtraction instead of addition, the unshifted separated time domain outputs can be obtained.

$$y_f(n) = D(n) - \mathbf{H}[Q(n)] = s_f(n) + \mathbf{H}[s_r(n)] + s_f(n) - \mathbf{H}[s_r(n)] = 2s_f(n) \quad (4.11)$$

$$y_r(n) = Q(n) - \mathbf{H}[D(n)] = \mathbf{H}[s_f(n)] + s_r(n) - \mathbf{H}[s_f(n)] + s_r(n) = 2s_r(n) \quad (4.12)$$

It is obvious that the fundamental concept in the PFT is to shift the phase of in-phase and/or quadrature components by 90 degrees. The phase shifting operation is performed by the HT filter. In the proposed methods (ADDT-CWPT and SDDT-CWPT) the phase shifting operation is attained by the wavelet filters utilised in the imaginary tree in analytic DT-CWPT. This eliminates the HT and delay filter stages in the PFT and reduces the computational complexity of analyzing quadrature signals with complex wavelet packet transform.

4.3 Complex Wavelet Transforms

4.3.1 Dual Tree Complex Wavelet Transform

DTCWT illustrated in Figure 4.4 is a modified version of ordinary DWT. It employs two real DWTs operating in parallel on an input signal [30]. The first DWT represents the real part of the transform and the second DWT represents the imaginary part of the transform, resulting a complex transform in total.

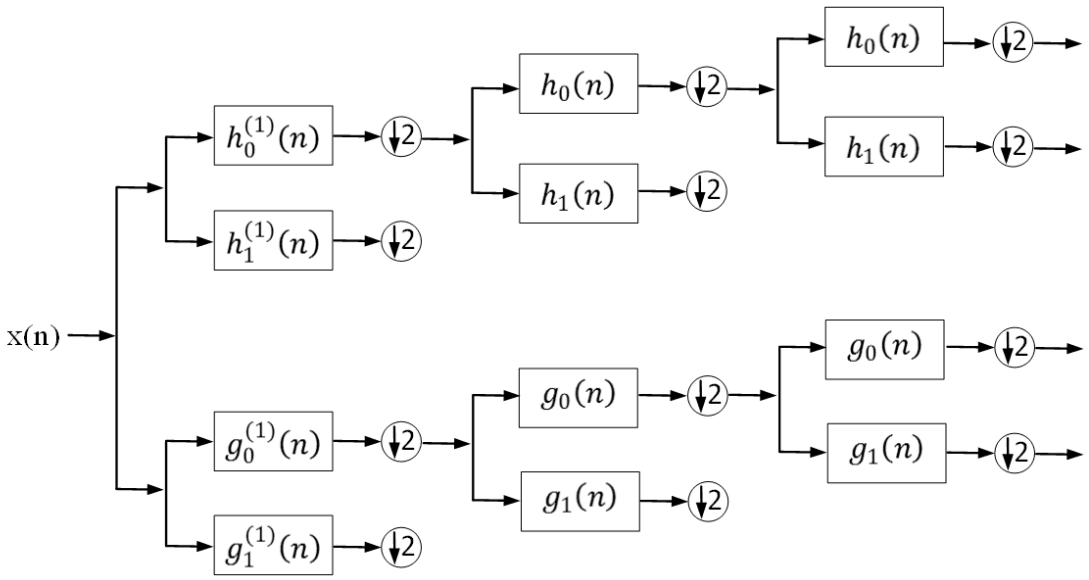

Figure 4.4 Analysis part of Dual Tree Complex Wavelet Transform.

The DTCWT comes up with solutions to: "lack of being shift-invariant" and "lack of being directionally selective in two and higher dimensions" drawbacks of ordinary DWT [76]. In order to posses its desirable properties, the DTCWT benefits from a second DWT tree (imaginary tree), designed according to a certain criterion. For the ideal DTCWT, if $\psi(t)$ is defined as the wavelet function of real part, the wavelet function of imaginary part ($\psi'(t)$) must be the HT of $\psi(t)$. This condition can be shown as,

$$\psi'(t) = \mathbf{H}[\psi(t)] \tag{4.13}$$

The wavelet function of real tree can be defined as

$$\psi(t) = \sqrt{2}\sum_{n} h_1(n)\phi(2t-n) \tag{4.14}$$

where $\phi(t)$ is the scaling function and defined as

$$\phi(t) = \sqrt{2}\sum_{n} h_0(n)\phi(2t-n) \tag{4.15}$$

In (4.14) and (4.15), $h_1(n)$ and $h_0(n)$ are the high-pass and low-pass FIR conjugate quadrature filters (CQFs) respectively. In the imaginary tree, the second wavelet, $\psi'(t)$, is defined similarly in terms of a different set of filters ($g_1(n)$ and $g_0(n)$). As it can be seen from the equations (4.14) and (4.15), wavelet functions depend on the scaling functions and scaling functions depend on the filters. Therefore, the design of wavelet function satisfying desired properties defined by (4.13) is equivalent to the design of filters satisfying specific properties [30]. In [59, 60, 78], it is stated that if the low-pass filter $g_0(n)$ is equal to the half sample delayed version of $h_0(n)$, then the wavelet functions of DTCWT will satisfy (4.13) and this condition can be shown as below in time domain.

$$g_0(n) \approx h_0(n-0.5) \Rightarrow \psi_g(t) \approx \mathbf{H}[\psi_h(t)] \tag{4.16}$$

In frequency domain, this can be interpreted as

$$G_0(\omega) = e^{-j0.5\omega}H_0(\omega) \quad \text{for} \quad |\omega| < \pi \tag{4.17}$$

For CQF we know that low-pass and high-pass filters have the following relation

$$h_1(n) = (-1)^n h_0(d-n) \quad \text{where } 'd' \text{ is an odd integer} \tag{4.18}$$

So, for an ideal DTCWT, the high pass filters must satisfy

$$G_1(\omega) = -jsgn(\omega)e^{j0.5\omega}H_1(\omega) \quad \text{for} \quad |\omega| < \pi \tag{4.19}$$

where "sgn" is the signum function.

This half sample delay property was proved by using the infinite product formula [59], which calculates the scaling function from an infinite number of filter stages. However, in real case there will be finite number of stages, so FIR filters can never satisfy half sample delay condition (half-sample delay condition requires an infinite impulse response system) and hence the resulting wavelet function pairs can never be perfectly analytic. Therefore it is necessary to make an approximation.

In order to overcome the constrain of the situation mentioned above, instead of using a half sample delay system, the first stage filters of the transform must be allowed to be different from the following stages. For the first stage, any orthonormal perfect reconstruction filter pair, which satisfies following equation for low pass filters of real tree and imaginary tree of the transform, can be used.

$$g_0^{(1)}(n) = h_0^{(1)}(n-1) \tag{4.20}$$

where $h_0^{(1)}(n)$ is the low pass filter of real tree and $g_0^{(1)}(n)$ is the low pass filter of imaginary tree in the first stage.

If the first stage of the DTCWT is chosen in this way and the remaining stages satisfy (4.17) approximately, then the DTCWT will be approximately analytic at every stage except the first stage. The detailed prove of these conditions can be found in [77].

For the inverse DTCWT case, in order to invert the transform, the real tree and the imaginary tree should be inverted separately and then the outputs should be summed. If the coefficients are not altered during the analysis part, the outputs of both real and imaginary trees will be approximately same with original signal at the

end of the synthesis stage.

4.3.2 Dual Tree Complex Wavelet Packet Transform

In order to extend the DTCWT into DT-CWPT, the most straight-forward way is to iterate both its low-pass and high-pass PR FBs' outputs using the same set of filters. This approach is proposed previously in [79, 80, 81, 82]. However, the resulting basis functions are far from being analytic and there are significant energy leakages into their negative frequency bands. Therefore this approach does not fully show desired HT property in PR filters. In order to overcome the shortfall of the straightforward construction, in [77] a new analytic DT-CWPT, which has better analytic subband responses, was developed. Similar to DTCWT, this analytic DT-CWPT is approximately shift-invariant and directionally selective in two and higher dimensions.

In this new analytic DT-CWPT, each of the subbands of DTCWT should be iteratively decomposed using low-pass and high-pass PR FBs. The PR FBs should be chosen so that the response of each branch of the imaginary tree FB is the discrete HT of the corresponding branch of the real tree FB. If this requirement is satisfied, then each subband of the analytic DT-CWPT will be analytic and this requirement can be fulfilled by using the simple rule of HT.

If a given filter $x(n)$ is the discrete Hilbert transform of some other filter $h(n)$, then

$$X(\omega) = jsgn(\omega)H(\omega) \quad \text{for} \quad |\omega| < \pi \tag{4.21}$$

When $x(n)$ is convolved with an another sequence $y(n)$, we obtain,

$$X(\omega)Y(\omega) = jsgn(\omega)H(\omega)Y(\omega) \quad \text{for} \quad |\omega| < \pi \tag{4.22}$$

As it can be seen from this equation, if $x(n)$ and $h(n)$ is a discrete HT pair, then $x(n) * y(n)$ and $h(n) * y(n)$ must also be a discrete HT pair because of the linear time-invariance property of discrete HT [83].

Assuming that specific filters $f_i(n)$ for real tree and $f_i'(n)$ for imaginary tree are needed, resulting DT-CWPT using these filters in the k^{th} $(k > 2)$ level shall be analytic. It was proved in [77] that to hold this property, it is necessary and sufficient that

$$f_i(n) = f_i'(n) \tag{4.23}$$

As it was proved in (4.21) and (4.22), if the subbands before $f_i(n)$ and $f_i'(n)$ are HT pairs then the convolution with $f_i(n)$ and $f_i'(n)$ will not violate HT pair property. Hence, if we decompose the k^{th} (where $k > 2$) stage high pass subband of the DT-CWT using some 2-channel PR FBs and the HT pair property has already been satisfied by previous bands, then the following filters for real tree and for imaginary tree must be equal for protecting HT pair property of related subbands. This procedure produces an analytic DT-CWPT consisting of two wavelet packet FBs operating in parallel, where some filters in the second wavelet packet FB are the same as those in the first wavelet packet FB. Details of the new DT-CWPT can be found in [77] and the structure can be seen in Figure 4.5.

As a result, in new analytic DT-CWPT, three types of filters are used. In the first level, for imaginary tree both low pass and high pass filters are one sample delayed version of the corresponding filters in the real tree and satisfies the following equations

$$g_0^{(1)}(n) = h_0^{(1)}(n-1) \tag{4.24}$$

and

$$g_1^{(1)}(n) = h_1^{(1)}(n-1) \tag{4.25}$$

where $g_0^{(1)}(n)$ and $h_0^{(1)}(n)$ represents the low pass filters of imaginary tree and real tree

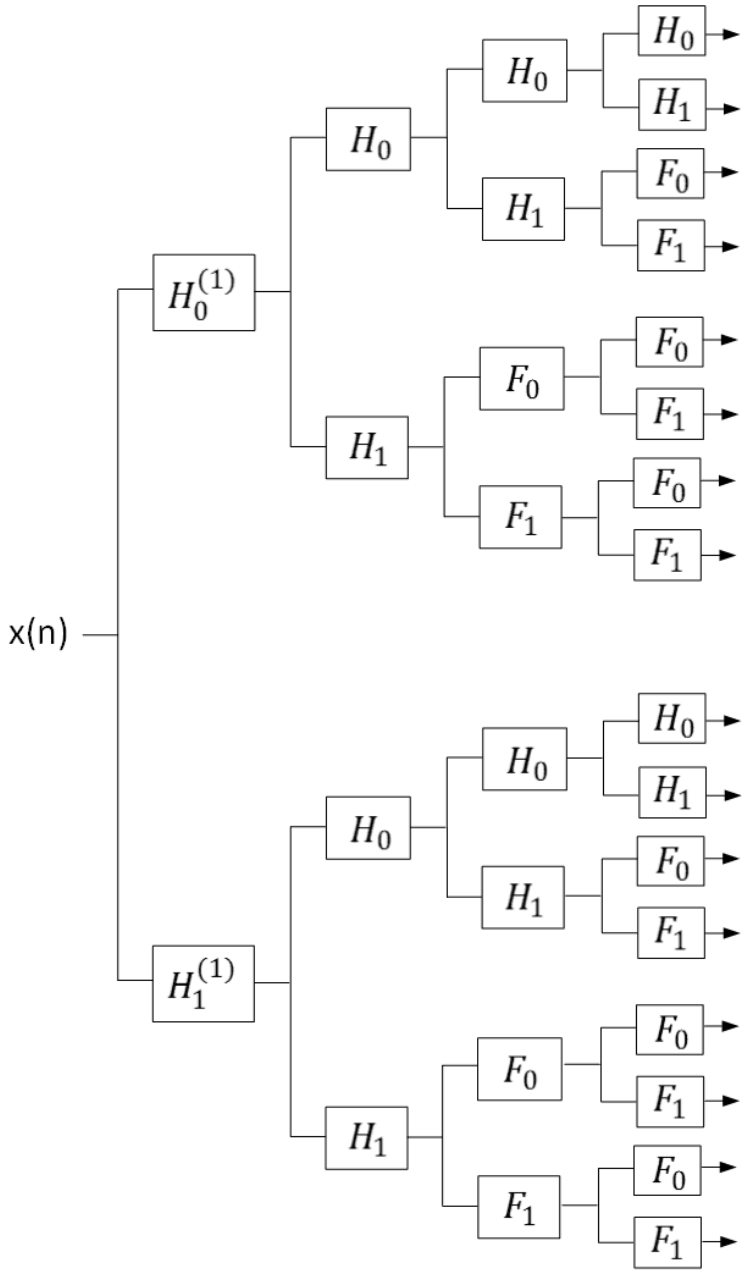

Figure 4.5 Real tree of four levels DT-CWPT. For the imaginary tree, the filters $h_i^{(1)}(n)$ must be replaced by $h_i^{(1)}(n-1)$ and $h_i(n)$ filters must be replaced by $g_i(n)$. In both real and imaginary trees, same $f_i(n)$ filters are used for $i \in 0, 1$.

respectively, and $g_1^{(1)}(n)$ and $h_1^{(1)}(n)$ represents the high pass filters of imaginary tree and real tree respectively. For the second type filters, $h_i(n)$ and $g_i(n)$ for $i \in 0, 1$, which approximately satisfy (4.17) and (4.19), are used. Finally, for the third type, $f_i(n)$ and $f_i'(n)$ extension filters satisfying (4.23) are used for both real and imaginary trees. In the selection of extension filters, $f_i(n)$, there is no restriction as long as same

filter pairs in both FBs of real tree and imaginary tree are used in order to preserve the HT property which is obtained before. Hence, the same criteria for the selection of a CQF pair to extend a regular DWT can be used for the selection of $f_i(n)$ [54].

4.4 Directional Dual Tree Complex Wavelet Packet Transforms

Doppler ultrasound is an important technique for detecting and measuring the velocity of moving structures. In medicine it is mostly used as a non-invasive method for measuring the velocity of blood. The output of a Doppler system is in quadrature format and in order to extract directional signals from this quadrature signals PFT is the most widely used method. As mentioned in section 4.2, in a real-time application of PFT while extracting flow signals from quadrature signals, HT filters and delay filters must be employed. Then, these obtained directional signals can be processed with various digital signal processing techniques for further applications. For example in blood flow detection systems, the DWT is used for emboli detection [47, 84]. But as mentioned before, DWT does not map directional signals in the scale domain during wavelet analysis. DTCWT can be thought as a solution to this problem but it does not provide directional signal decoding during analysis because of its unwanted energy leaks into the opposite frequency bands (the positive frequency band leaks into the negative one, the negative frequency band leaks into the positive one). To overcome this drawback a modified DTCWT was proposed, but it still uses HT filters and delay filters [85, 86, 87, 88, 89, 90, 91].

The main motivation of this study is to develope discrete wavelet packet transforms, which eliminates the use of the asymmetrical and symmetrical PFT steps during analysis and also provides an optimum frequency band representation of a signal of interest. Hence, symmetrical and asymmetrical Directional Dual Tree Complex Wavelet Packet Transforms, which use the HT pair property between real tree and imaginary tree of DT-CWPT, are proposed.

4.4.1 Asymmetrical Implementation of the Directional Dual Tree Complex Wavelet Packet Transform

As explained in section 4.3, specifically, filters of DT-CWPT's imaginary wavelet tree that their impulse responses are approximately the discrete HTs of those of the real wavelet tree's filters are designed. This property is the starting point of proposed method. If the imaginary tree's filters' impulse responses are approximately the discrete HTs of those of the real wavelet tree's filters, then we can derive the following equations.

In the frequency domain, for the DT-CWPT if we suppose $G_k^l(\omega)$ is the frequency response of the imaginary tree's k^{th} subband in the l^{th} level, where the HT pair property has already been satisfied (except the first and last subbands) and $H_k^l(\omega)$ is the frequency response of real tree in the same subband, then we know that

$$G_k^l(\omega) = \mathbf{H}\Big[H_k^l(\omega)\Big] \tag{4.26}$$

where $\mathbf{H}[\quad]$ represents the HT.

As mentioned in section 4.3, in frequency domain, this is equal to

$$G_k^l(\omega) = jsgn(\omega)H_k^l(\omega) \quad \text{for} \quad |\omega| < \pi \tag{4.27}$$

If a real signal $x(n)$ is applied to the both trees as an input, we obtain

$$G_k^l(\omega)X(\omega) = \mathbf{H}\Big[H_k^l(\omega)X(\omega)\Big] \tag{4.28}$$

By using linearity property of the HT, it is possible to restate (4.28) as follows

$$G_k^l(\omega)X(\omega) = jsgn(\omega)H_k^l(\omega)X(\omega) \quad \text{for} \quad |\omega| < \pi \tag{4.29}$$

$$G_k^l(\omega)X(\omega) = H_k^l(\omega)\Big[jsgn(\omega)X(\omega)\Big] \quad \text{for} \quad |\omega| < \pi \tag{4.30}$$

$$G_k^l(\omega)X(\omega) = H_k^l(\omega)\mathbf{H}\Big[X(\omega)\Big] \tag{4.31}$$

(4.31) shows that if we use the FB pairs in decomposition, the process done in the imaginary tree is the same as decomposing by the same filter in real tree plus taking the HT of input signal. Hence, the Hilbert Transformed coefficients are obtained in the output of imaginary tree FBs.

On the other hand, if the input is a quadrature signal pair and *D(n)* is applied to the imaginary tree and *Q(n)* to the real tree, for the imaginary tree the following derivations can be made

$$\mathbf{H}\Big[H_k^l(\omega)\Big]D_k^l(\omega) = jsgn(\omega)H_k^l(\omega)D_k^l(\omega) \quad \text{for} \quad |\omega| < \pi \tag{4.32}$$

$$H_k^l(\omega)\Big[jsgn(\omega)D_k^l(\omega)\Big] = H_k^l(\omega)\mathbf{H}\Big[D_k^l(\omega)\Big] \tag{4.33}$$

where $D_k^l(\omega)$ is the frequency response of the decomposed *D(n)* for the related subband.

According to (4.32) and (4.33), if the frequency response of a real tree filter for the k^{th} subband in the l^{th} level (where the HT pair has already been obtained) is $H_k^l(\omega)$, then the frequency response of the imaginary-tree filter for the same subband will be equivalent to decomposing and taking the HT of the *D(n)* for the k^{th} subband in the l^{th} level.

On the other hand, for the same subband, the frequency response of the real tree will be

$$H_k^l(\omega)Q_k^l(\omega) \tag{4.34}$$

It is possible to demonstrate that the concepts mentioned above can also be used to obtain directional information encoded in quadrature signals. Assuming that the quadrature signal given in (4.1) is decomposed by using the proposed transform.

HT of *s(n)* in frequency domain can be given as

$$\mathbf{H}\Big[S(\omega)\Big] = -jS(\omega) \quad \text{for} \quad 0 \leq \omega \leq \pi \tag{4.35}$$

$$\mathbf{H}\Big[S(\omega)\Big] = +jS(\omega) \quad \text{for} \quad -\pi \leq \omega < 0 \tag{4.36}$$

It is known that the Fourier transform (FT) of a quadrature signal maps directional information in the frequency domain [41]. Assuming that the positive frequencies represent forward flow signal $s_f(n)$ and the negative frequencies represent the reverse flow signal $s_r(n)$, the following frequency domain definitions can be made.

$$\mathbf{F}\Big[s_f(n)\Big] = S^+(\omega) \quad \text{for} \quad 0 \leq \omega \leq \pi \tag{4.37}$$

$$\mathbf{F}\Big[s_r(n)\Big] = S^-(\omega) \quad \text{for} \quad -\pi \leq \omega < 0 \tag{4.38}$$

Taking the HT of $s_f(n)$ and $s_r(n)$ results in

$$\mathbf{H}\Big[\mathbf{F}\Big[s_f(n)\Big]\Big] = -jS^+(\omega) \quad \text{for} \quad 0 \leq \omega \leq \pi \tag{4.39}$$

$$\mathbf{H}\Big[\mathbf{F}\Big[s_r(n)\Big]\Big] = +jS^-(\omega) \quad \text{for} \quad -\pi \leq \omega < 0 \tag{4.40}$$

where $\mathbf{F}[\quad]$ stands for the Fourier transform.

If we take FT of equations (4.2) and (4.3), we obtain

$$\mathbf{F}\Big[D(n)\Big] = +S^+(\omega) + jS^-(\omega) = D(\omega) \tag{4.41}$$

$$\mathbf{F}\Big[Q(n)\Big] = -jS^+(\omega) + S^-(\omega) = Q(\omega) \tag{4.42}$$

Applying HT to (4.41) results in

$$\mathbf{H}\Big[D(\omega)\Big] = -jS^{+}(\omega) - S^{-}(\omega) \tag{4.43}$$

Combining equations (4.33) and (4.43) for a certain subband (for the k^{th} subband in the l^{th} level) in the imaginary tree results in

$$H_k^l(\omega)\mathbf{H}\Big[D_k^l(\omega)\Big] = H_k^l(\omega)\Big[-jS_k^{l^+}(\omega) - S_k^{l^-}(\omega)\Big] = -jH_k^l(\omega)S_k^{l^+}(\omega) - H_k^l(\omega)S_k^{l^-}(\omega) \tag{4.44}$$

where $H_k^l(\omega)$ is the frequency response of the filter, $S_k^{l^+}(\omega)$ is the forward signal component in the frequency domain, and $S_k^{l^-}(\omega)$ is the reverse signal component in the frequency domain.

For the real tree, combining equations (4.34) and (4.42) results in

$$H_k^l(\omega)Q_k^l(\omega) = H_k^l(\omega)\Big[-jS_k^{l^+}(\omega) + S_k^{l^-}(\omega)\Big] = -jH_k^l(\omega)S_k^{l^+}(\omega) + H_k^l(\omega)S_k^{l^-}(\omega) \tag{4.45}$$

(4.44) and (4.45) are the frequency responses of subbands in DT-CWPT. Adding/subtracting (4.44) and (4.45) yields the following frequency response of the forward/reverse signal.

$$\begin{aligned} H_k^l(\omega)\mathbf{H}\Big[D_k^l(\omega)\Big] + H_k^l(\omega)Q_k^l(\omega) &= -jH_k^l(\omega)S_k^{l^+}(\omega) - H_k^l(\omega)S_k^{l^-}(\omega) - jH_k^l(\omega)S_k^{l^+}(\omega) \\ &\quad + H_k^l(\omega)S_k^{l^-}(\omega) = -2jH_k^l(\omega)S_k^{l^+}(\omega) \end{aligned} \tag{4.46}$$

$$\begin{aligned} H_k^l(\omega)Q_k^l(\omega) - H_k^l(\omega)\mathbf{H}\Big[D_k^l(\omega)\Big] &= -jH_k^l(\omega)S_k^{l^+}(\omega) + H_k^l(\omega)S_k^{l^-}(\omega) + jH_k^l(\omega)S_k^{l^+}(\omega) \\ &\quad + H_k^l(\omega)S_k^{l^-}(\omega) = 2H_k^l(\omega)S_k^{l^-}(\omega) \end{aligned} \tag{4.47}$$

At the end of these calculations the frequency response of negative frequencies (reverse signal coefficients) and 90 degree phase shifted version of the frequency response of positive frequencies (forward signal coefficients) are obtained for the related subband. It must be emphasized that the addition/subtraction procedure must be performed at the end of the analysis stage for all subbands for obtaining all directional coefficients (except the lowest and highest subbands, as they have no analyticity property).

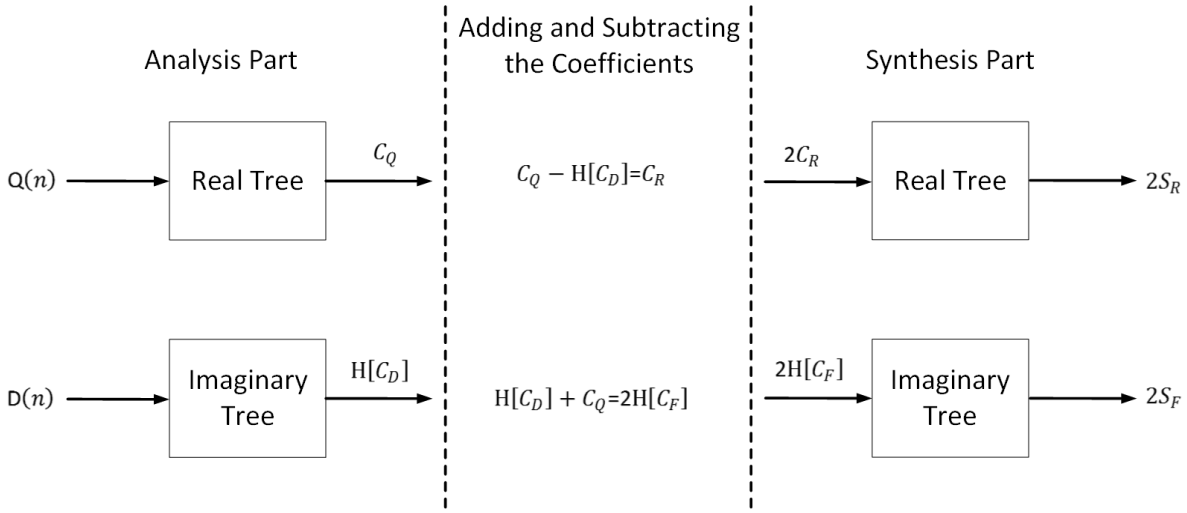

Figure 4.6 Asymmetrical Implementation of DDT-CWPT.

In the synthesis part of DT-CWPT, inverse FBs of analysis part are used. It should be noted that the inverse FBs in imaginary tree also exhibit HT property. Therefore, unlike Asym-PFT, instead of $\mathbf{H}[s_f(n)]$, $s_f(n)$ is obtained at the end of synthesis part of ADDT-CWPT. The structure of the ADDT-CWPT is illustrated in Figure 4.6.

4.4.2 Symmetrical Implementation of the Directional Dual Tree Complex Wavelet Packet Transform

In symmetrical implementation of the DDT-CWPT (SDDT-CWPT) illustrated in Figure 4.7, two DT-CWPTs must be used. *Q(n)* and *D(n)* are applied to the each DT-CWPTs respectively. Consequently, the coefficients and their Hilbert transformed versions for a specific subband (except the first and last subbands) are obtained for each DT-CWPT channels. The frequency responses of these Hilbert pairs for the related subbands can be seen below when the same approach is used as in section 4.4.1.

In the first DT-CWPT, when *D(n)* is given as input, for the k^{th} subband in the l^{th} level, equations (4.48) and (4.49) are obtained for the real and imaginary trees

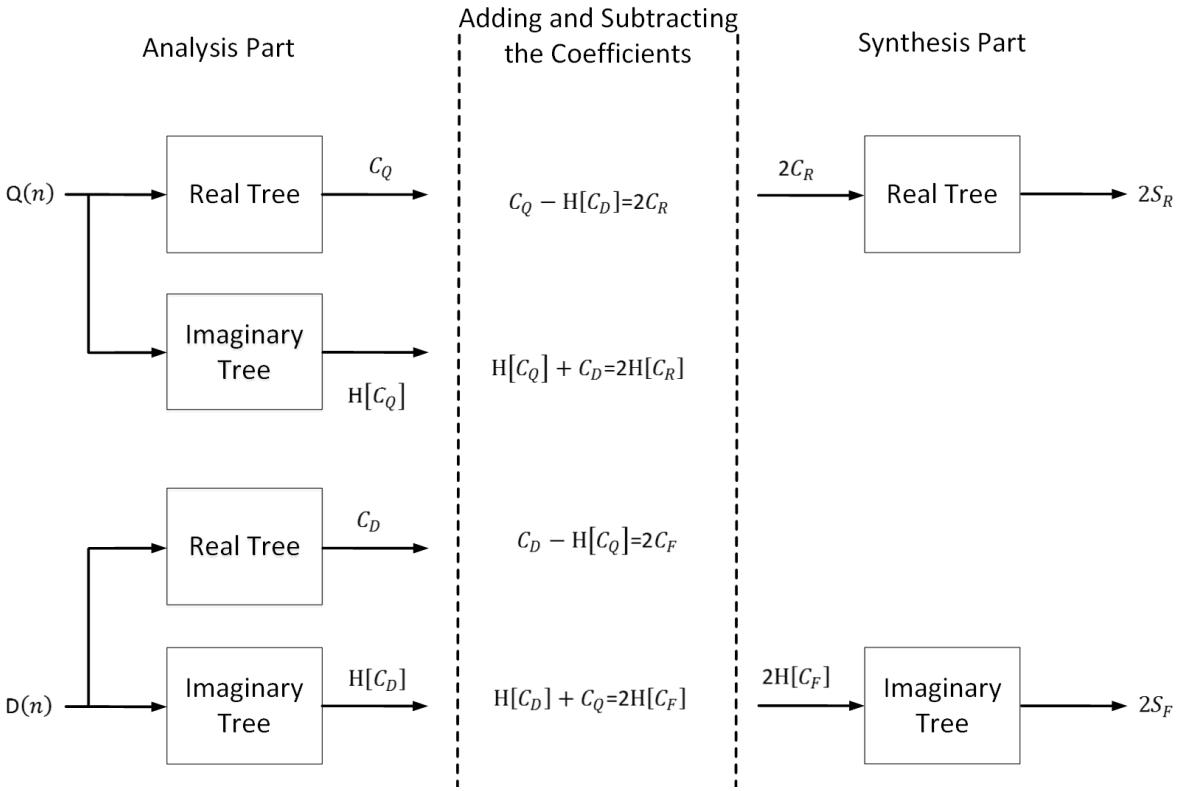

Figure 4.7 Symmetrical Implementation of DDT-CWPT. C_Q and C_D are the coefficients of *Q(n)* and *D(n)* in the related subband respectively, C_F and C_R are the coefficients of forward and reverse directional signals in the related subband respectively. H[ ] stands for the HT.

respectively.

$$H_k^l(\omega)D_k^l(\omega) = H_k^l(\omega)S_k^{l^+}(\omega) + jH_k^l(\omega)S_k^{l^-}(\omega) \tag{4.48}$$

$$H_k^l(\omega)\mathbf{H}\Big[D_k^l(\omega)\Big] = -jH_k^l(\omega)S_k^{l^+}(\omega) - H_k^l(\omega)S_k^{l^-}(\omega) \tag{4.49}$$

In the second DT-CWPT, for the same subband, when *Q(n)* is given as input, equations (4.50) and (4.51) are obtained for the real and imaginary trees respectively.

$$H_k^l(\omega)Q_k^l(\omega) = -jH_k^l(\omega)S_k^{l^+}(\omega) + H_k^l(\omega)S_k^{l^-}(\omega) \tag{4.50}$$

$$H_k^l(\omega)\mathbf{H}\Big[Q_k^l(\omega)\Big] = -H_k^l(\omega)S_k^{l^+}(\omega) + jH_k^l(\omega)S_k^{l^-}(\omega) \tag{4.51}$$

These are the frequency responses of each analytic subband at the end of analysis part (except the first and last).

If the first DT-CWPT's real tree coefficients for each subband and the imaginary tree coefficients of the second DT-CWPT are added, the phase shifted frequency response of negative frequencies (reverse directional coefficients)

$$H_k^l(\omega)D_k^l(\omega) + H_k^l(\omega)\mathbf{H}\Big[Q_k^l(\omega)\Big] = H_k^l(\omega)S_k^{l^+}(\omega) + jH_k^l(\omega)S_k^{l^-}(\omega) - H_k^l(\omega)S_k^{l^+}(\omega) \\ +jH_k^l(\omega)S_k^{l^-}(\omega) = 2jH_k^l(\omega)S_k^{l^-}(\omega) \tag{4.52}$$

If the first DT-CWPT's imaginary tree coefficients for each subband and the real tree coefficients of the second DT-CWPT are added, the phase shifted frequency response of positive frequencies (forward directional coefficients) are obtained.

$$H_k^l(\omega)Q_k^l(\omega) + H_k^l(\omega)\mathbf{H}\Big[D_k^l(\omega)\Big] = -jH_k^l(\omega)S_k^{l^+}(\omega) + H_k^l(\omega)S_k^{l^-}(\omega) - jH_k^l(\omega)S_k^{l^+}(\omega) \\ -H_k^l(\omega)S_k^{l^-}(\omega) = -2jH_k^l(\omega)S_k^{l^+}(\omega) \tag{4.53}$$

If the first DT-CWPT's imaginary tree coefficients for each subband are subtracted from the real tree coefficients of the second DT-CWPT, the frequency response of negative frequencies (reverse directional coefficients) are obtained.

$$H_k^l(\omega)Q_k^l(\omega) - H_k^l(\omega)\mathbf{H}\Big[D_k^l(\omega)\Big] = -jH_k^l(\omega)S_k^{l^+}(\omega) + H_k^l(\omega)S_k^{l^-}(\omega) + jH_k^l(\omega)S_k^{l^+}(\omega) \\ +H_k^l(\omega)S_k^{l^-}(\omega) = 2H_k^l(\omega)S_k^{l^-}(\omega) \tag{4.54}$$

If the second DT-CWPT's imaginary tree coefficients for each subband are subtracted from the real tree coefficients of the first DT-CWPT, the frequency response of positive frequencies (forward directional coefficients) are obtained.

$$H_k^l(\omega)D_k^l(\omega) - H_k^l(\omega)\mathbf{H}\Big[Q_k^l(\omega)\Big] = H_k^l(\omega)S_k^{l^+}(\omega) + jH_k^l(\omega)S_k^{l^-}(\omega) + H_k^l(\omega)S_k^{l^+}(\omega) \\ -jH_k^l(\omega)S_k^{l^-}(\omega) = 2H_k^l(\omega)S_k^{l^+}(\omega) \tag{4.55}$$

4.4.3 Shift-Invariance Property of the Proposed Methods

Shift-invariance is an important property that any transform should posses. However, the DWT and the DWPT do not posses this property [28]. In DWT and

DWPT, when the input signal is shifted by an arbitrary number of samples, the energy in each subband of transform is not preserved. The lack of shift-invariance property is a result of the aliasing caused by the down-sampling employed in the DWT and DWPT. DTCWT and DT-CWPT algorithms both have approximately analytic subbands due to usage of real and imaginary trees [28]. In these transforms, complex FB pairs are used. Therefore, the frequency response of each subband in the transform is approximately one sided. The near shift-invariance property of DT-CWPT comes from the reduction in aliasing, and is achieved by the approximately analytic band-pass response characteristics of each branch [76].

When the proposed symmetrical and asymmetrical implementations of DDT-CWPT are considered, in order to posses near shift-invariance property, a HT pair of forward and reverse coefficients at the end of decomposition stage has to be obtained. Necessary HT pair conditions can be given as $FC_k^l - \mathbf{H}[FC_k^l]$ and $RC_k^l - \mathbf{H}[RC_k^l]$, where FC_k^l represents the forward signal coefficients of the k^{th} subband in the l^{th} level and RC_k^l represents the reverse signal coefficients of the same analytic subband and $\mathbf{H}[\ \ ]$ is the HT operator.

By using proposed ADDT-CWPT, it is not possible to obtain a HT pair of forward and reverse coefficients at the end of decomposition stage. For ADDT-CWPT, the relation between the forward and reverse direction coefficients can be given as below,

For the k^{th} subband in the l^{th} level, at the end of decomposition stage, we obtain

$$QC_k^l = \mathbf{H}[FC_k^l] + RC_k^l \tag{4.56}$$

$$\mathbf{H}[DC_k^l] = \mathbf{H}[FC_k^l] - RC_k^l \tag{4.57}$$

Where QC_k^l is the quadrature phase signal coefficients of the k^{th} subband in the l^{th} level, and $\mathbf{H}[DC_k^l]$ is the Hilbert transformed in-phase signal coefficients of same subband.

When we add and subtract these coefficients, we obtain

$$\mathbf{H}[FC_k^l] + RC_k^l + \mathbf{H}[FC_k^l] - RC_k^l = 2\mathbf{H}[FC_k^l] \tag{4.58}$$

$$\mathbf{H}[FC_k^l] + RC_k^l - \mathbf{H}[FC_k^l] + RC_k^l = 2RC_k^l \tag{4.59}$$

Only, the Hilbert transformed forward coefficients and reverse coefficients can be obtained for the related subbands. Therefore, for the ADDT-CWPT, near shift-invariance property can not be achieved.

However, in the SDDT-CWPT, two DT-CWPTs are employed and therefore near shift-invariance property can be achieved. By using SDDT-CWPT, for the k^{th} subband in the l^{th} level, at the end of decomposition stage, we obtain

$$QC_k^l = \mathbf{H}[FC_k^l] + RC_k^l \quad \text{and} \quad \mathbf{H}[QC_k^l] = -FC_k^l + \mathbf{H}[RC_k^l] \tag{4.60}$$

$$DC_k^l = FC_k^l + \mathbf{H}[RC_k^l] \quad \text{and} \quad \mathbf{H}[DC_k^l] = \mathbf{H}[FC_k^l] - RC_k^l \tag{4.61}$$

Where, $\mathbf{H}[QC_k^l]$ is the Hilbert transformed quadrature phase signal coefficients of k^{th} subband in the l^{th} level, and DC_k^l is the in-phase signal coefficients of same subband.

When QC_k^l is added to $\mathbf{H}[DC_k^l]$, we obtain

$$\mathbf{H}[FC_k^l] + RC_k^l + \mathbf{H}[FC_k^l] - RC_k^l = 2\mathbf{H}[FC_k^l] \tag{4.62}$$

When $\mathbf{H}[QC_k^l]$ is added to DC_k^l, we obtain

$$-FC_k^l + \mathbf{H}[RC_k^l] + FC_k^l + \mathbf{H}[RC_k^l] = 2\mathbf{H}[RC_k^l] \tag{4.63}$$

When $\mathbf{H}[DC_k^l]$ is subtracted from QC_k^l, we obtain

$$\mathbf{H}[FC_k^l] + RC_k^l - \mathbf{H}[FC_k^l] + RC_k^l = 2RC_k^l \tag{4.64}$$

When $\mathbf{H}[QC_k^l]$ is subtracted from DC_k^l, we obtain

$$FC_k^l + \mathbf{H}[RC_k^l] + FC_k^l - \mathbf{H}[RC_k^l] = 2FC_k^l \tag{4.65}$$

Hence, it can be seen that by using above addition/subtraction operations, $2\Big(FC_k^l - \mathbf{H}[FC_k^l]\Big)$ and $2\Big(RC_k^l - \mathbf{H}[RC_k^l]\Big)$ HT pairs of both forward and reverse coefficients can be obtained. This shows us that the proposed SDDT-CWPT has the near shift-invariance property.

4.4.4 The Effect of Non-Analytic Subbands and Energy Leakages in Opposite Frequencies

In theory, both with symmetrical and asymmetrical implementations of DDT-CWPT, at the end of synthesis, directional signals must be reconstructed perfectly. In reality, an ideal HT pair property between the frequency responses of real and imaginary tree FBs cannot be achieved because of the energy leakages in opposite frequency bands of DT-CWPT. However, the effect of these energy leakages in the ADDT-CWPT and the SDDT-CWPT is very small.

Additionally, for an analysis with DT-CWPT for l levels, we know that the lowest and highest subbands have no analyticity property [28, 92]. This is due to the fact that they are processed by low-pass filters and high-pass filters only. But low-pass filters or high-pass filters alone can never achieve a flat phase response difference which is necessary for approximating the HT phase response.

Due to the two main reasons mentioned above ADDT-CWPT and SDDT-

CWPT have no perfect reconstruction property, but the differences between the ideal cases and proposed methods outputs are very small and have a very limited effect on the whole transform. Therefore, in the real signal case, as an additional study, pass-band performances of proposed methods were also compared with the PFT+DWPT and the PFT+DT-CWPT when the non-analytic first and last subband coefficents are removed while processing quadrature signals. By doing so, the amount of the distortion caused by the first and the last subbands, which is insignificant in processing embolic signals, can be accurately quantified.

4.5 Simulations and Results

Doppler devices function by transmitting a beam of ultrasound into a medium (in a cardiovascular system, the middle cerebral artery for example), and collecting and analyzing the returning signals reflected by the object. Main concern in Doppler devices is the frequency of the returning echoes and whether there has been a Doppler shift as a result of interaction with a moving target (for example red blood cells and embolic particles can be thought as moving particles for the detection of embolic signals). The Doppler shift signal is obtained by quadrature demodulation resulting in a band-pass signal in kHz range, such as narrow-band embolic signals [44]. Therefore, in the first two parts of our simulations, synthetic signals in kHz ranges are used. In the first part, a single frequency quadrature signal constructed by using sines and cosines is employed. In the second part, two synthetic quadrature signals in different frequency bands were created by using white Gaussian noise. In the last part, 100 quadrature embolic Doppler ultrasound signals recorded from patients [47] are employed.

4.5.1 Single Frequency Quadrature Signal Simulations

Quadrature signals can be simulated by using sines and cosines. In this section, as a substitute of the $s_f(n)$ and $s_r(n)$ signals (directional signals), we use cosines and

sines respectively in the following manner.

$$D(n) = A\cos(2 \times \pi \times n \times \frac{f_A}{f_s}) + B\sin(2 \times \pi \times n \times \frac{f_B}{f_s}) \tag{4.66}$$

$$Q(n) = A\sin(2 \times \pi \times n \times \frac{f_A}{f_s}) + B\cos(2 \times \pi \times n \times \frac{f_B}{f_s}) \tag{4.67}$$

For the synthetic signal, A is chosen to be equal to B, f_A and f_B are chosen to be 400 and 1200 Hz respectively, the sampling frequency is chosen to be 10kHz. Both *D(n)* and *Q(n)* sizes are 4096 samples. Assuming the signal is discrete, n is the sample index.

In order to evaluate proposed method's reconstruction performance and also the ability to extract directional information, synthetic quadrature signal in the above format is analyzed and then synthesized with both symmetrical and asymmetrical implementations of DDT-CWPT without doing any alteration on coefficients. The obtained directional signals by using ADDT-CWPT and the directional signals obtained by Asym-PFT when the signal is decomposed and reconstructed for 6 levels can be seen in Figure 4.8. For the sake of clarity only the first 256 samples are shown.

As it can be seen from the figure, by using the ADDT-CWPT, directional signals can be obtained accurately at the end of the transform. But still three are small differences due to the non-analytic subbands and energy leakages in opposite frequencies. In order to quantify amount of the difference between the output of the proposed methods and the conventional ones, first, the absolute value of difference and absolute value of directional signals, and then the difference-ratio are found. In order to point out the performance of ADDT-CWPT and SDDT-CWPT, algorithm is tested for various decomposition levels (5, 6, 7, 8) and for each different level, forward and reverse signal difference-ratios between proposed method's outputs and PFT's outputs are calculated. The following formula is used for calculating difference-ratio and the

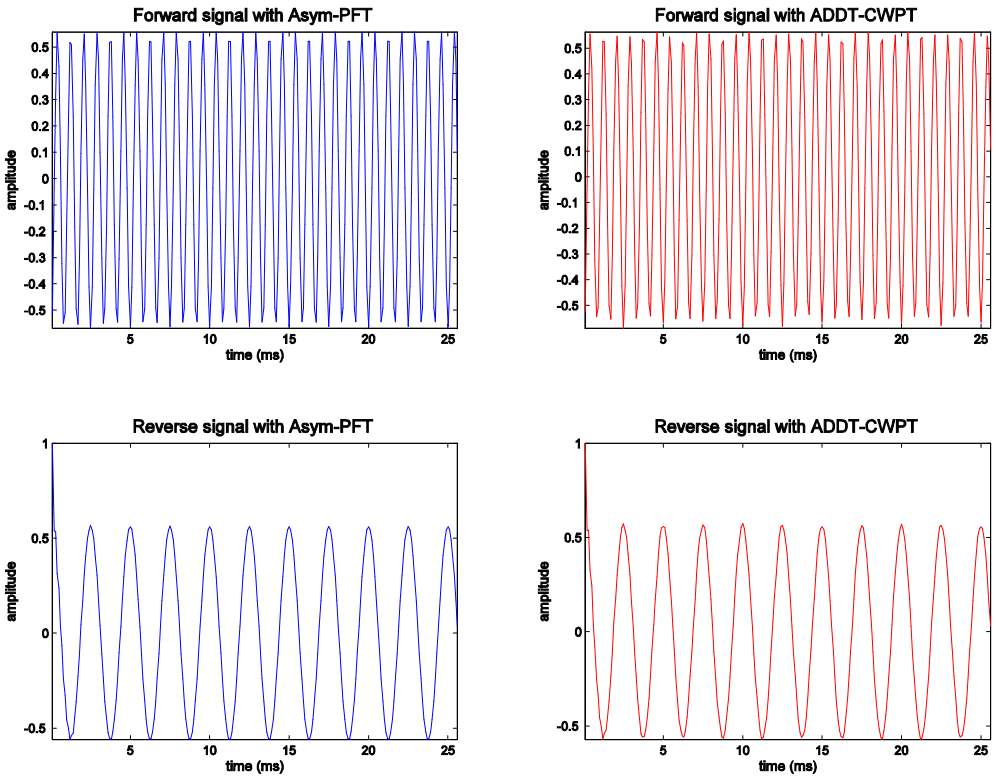

Figure 4.8 The first 256 points of reconstructed signals with ADDD-CWPT and Asym-PFT.

results are denoted in Table 4.1.

$$\text{Difference Ratio} = \frac{\sum |X_{PFT} - X_{DDT-CWPT}|}{\sum |X_{PFT}|} \times 100 \tag{4.68}$$

X_{PFT} is the directional signal obtained with PFT versions and $X_{DDT-CWPT}$ is the directional signal obtained with proposed methods.

As it can be seen from the table, with proposed methods for the levels 5, 6, 7 and 8 the signal difference-ratio for both reverse and forward signals is very small. However, because the effect of non-analytic subbands is more significant, difference-ratio for levels 3 and 4 is higher. The effect of non-analyticity depends on the number of levels. If a small number of levels are utilised, the band-width of the lowest and highest subbands become relatively larger, resulting in more distortion.

Table 4.1
Difference-Ratios of Forward and Reverse Signals for decomposition with different levels.

	ADDT-CWPT		SDDT-CWPT	
Level number:	**Forward Signal Difference-Ratio**	**Reverse Signal Difference-Ratio**	**Forward Signal Difference-Ratio**	**Reverse Signal Difference-Ratio**
3	%27.701	%27.579	%27.701	%27.690
4	%5.445	%5.368	%5.450	%5.456
5	%1.633	%1.667	%1.634	%1.640
6	%1.571	%1.602	%1.572	%1.575
7	%1.561	%1.603	%1.561	%1.564
8	%1.560	%1.602	%1.560	%1.563

4.5.2 Band-Limited Quadrature Signal Simulations

In this section, a synthetic quadrature signal is constructed by using band-limited synthetic directional signals. Band-limited directional signals are created by using "wgn" function of MatLab software. Firstly, by using this function 4096 samples long white Gaussian noise (WGN) is created. WGN is a special noise type which has all the frequency components in its spectrum and all samples of it are statistically independent. Later this WGN signal is filtered by two elliptic band-pass filters for obtaining synthetic directional signals with different cut-off frequencies. For the first filter, pass-band and stop-band cut-off frequencies are chosen as 1000 Hz and 2000 Hz respectively. For the second filter, pass-band and stop-band cut-off frequencies are chosen as 3000 Hz and 4000 Hz respectively. The pass-band ripple and stop-band attenuation values are chosen as 1 dB and 150 dB respectively. The filtered signals resulting synthetic forward and reverse signals can be seen in Figure 4.9.

In order to construct the quadrature signal, HT of both synthetic directional signals is taken and later HT of reverse signal is added to forward signal resulting *D(n)*. Besides the HT of forward signal is added to reverse signal resulting *Q(n)*. The simulated band-limited in-phase and quadrature-phase signals can be seen in Figure 4.10.

Later, this simulated quadrature signal is decomposed using both symmetrical

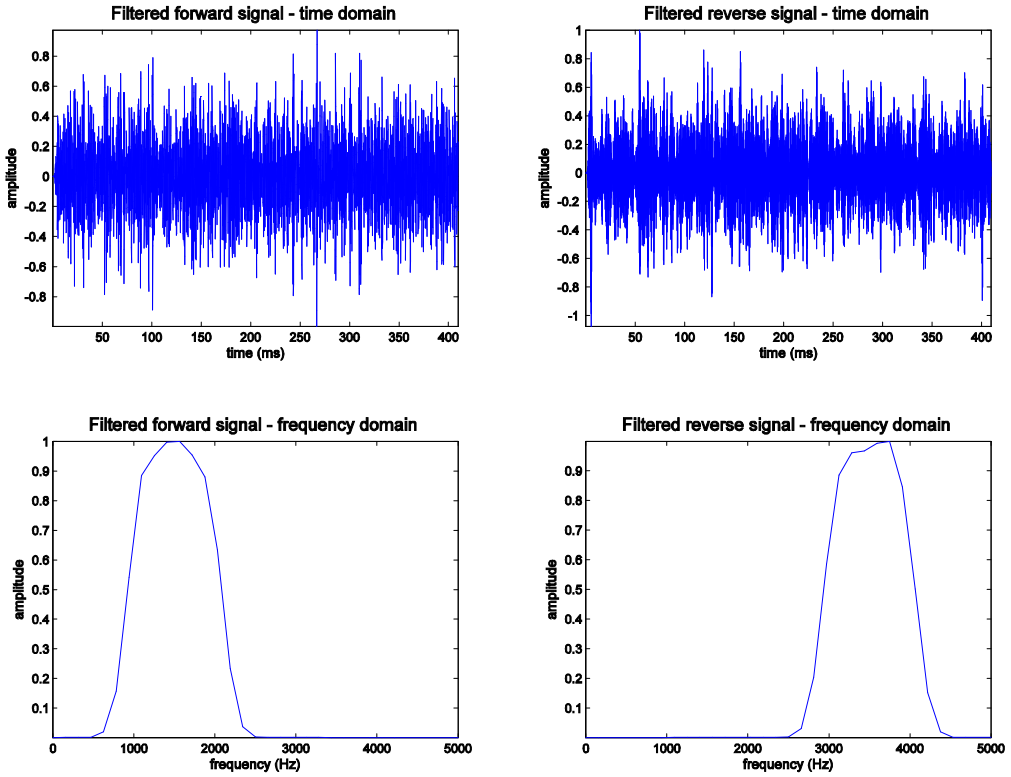

Figure 4.9 Time domain and frequency domain representations of filtered signals.

and asymmetrical DDT-CWPTs for six levels and then reconstructed without any alteration to the coefficients. As a consequence of this process the directional signals are obtained as an output. For the sake of clarity, the first 256 samples of the outputs with Asym-PFT and ADDT-CWPT can be seen in the Figure 4.11. As one can see from the figure, output of the ADDT-CWPT is almost the same as the asymmetrical PFT output.

However, still there is a small difference between the methods due to the non-analytic subbands and energy leakages in the opposite frequencies. In order to quantify the difference, the signal-difference ratio were calculated for various analysis levels (3,4,5,6,7,8) for both the ADDT-CWPT and the SDDT-CWPT. The results are reported in the Table 4.2, in which the signal-difference ratio is very low for all levels. Unlike the Table 4.1, the signal-difference ratio in the Table 4.2 is very low for the levels 3 and 4. This is due to use of a band-limited directional signal, in which there is

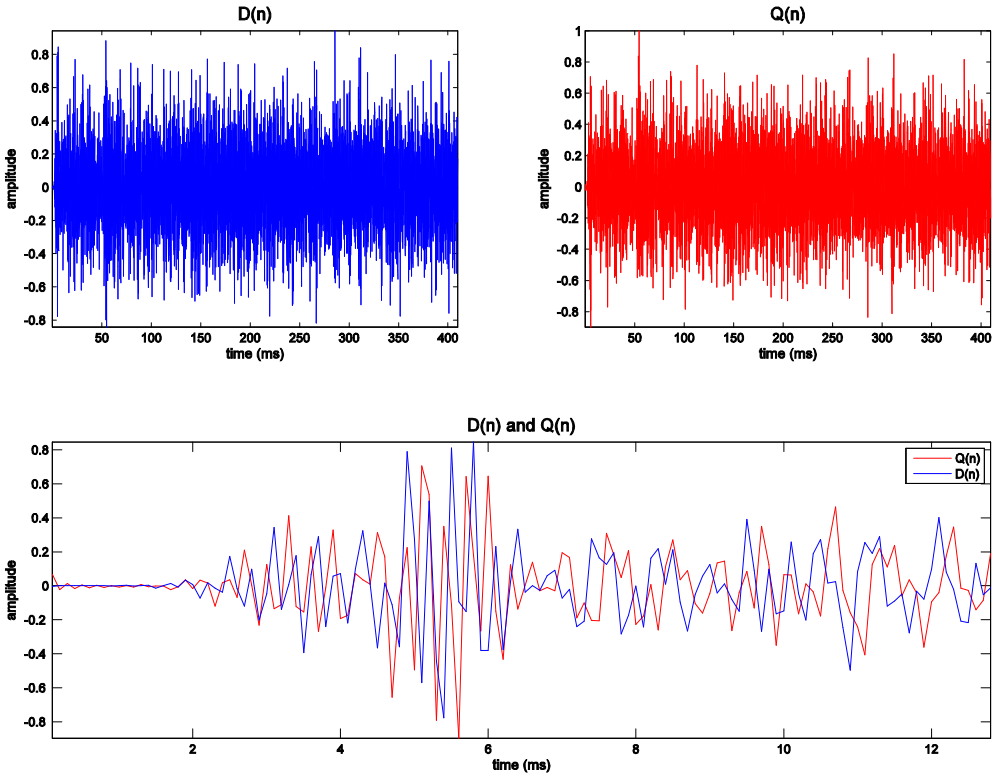

Figure 4.10 *D(n)* and *Q(n)* in time domain.

no signal component at the non-analytic frequency bands covering the levels 3 and 4. This proves that the proposed methods work well for band-limited directional signals.

Table 4.2
Signal-Difference Ratios of Forward and Reverse Signals for decomposition with different levels.

	ADDT-CWPT		SDDT-CWPT	
Level number:	Forward Signal Difference-Ratio	Reverse Signal Difference-Ratio	Forward Signal Difference-Ratio	Reverse Signal Difference-Ratio
3	%1.806	%1.792	%1.807	%1.790
4	%1.551	%1.546	%1.551	%1.567
5	%1.315	%1.301	%1.315	%1.316
6	%1.284	%1.265	%1.284	%1.287
7	%1.282	%1.262	%1.282	%1.285
8	%1.281	%1.262	%1.281	%1.283

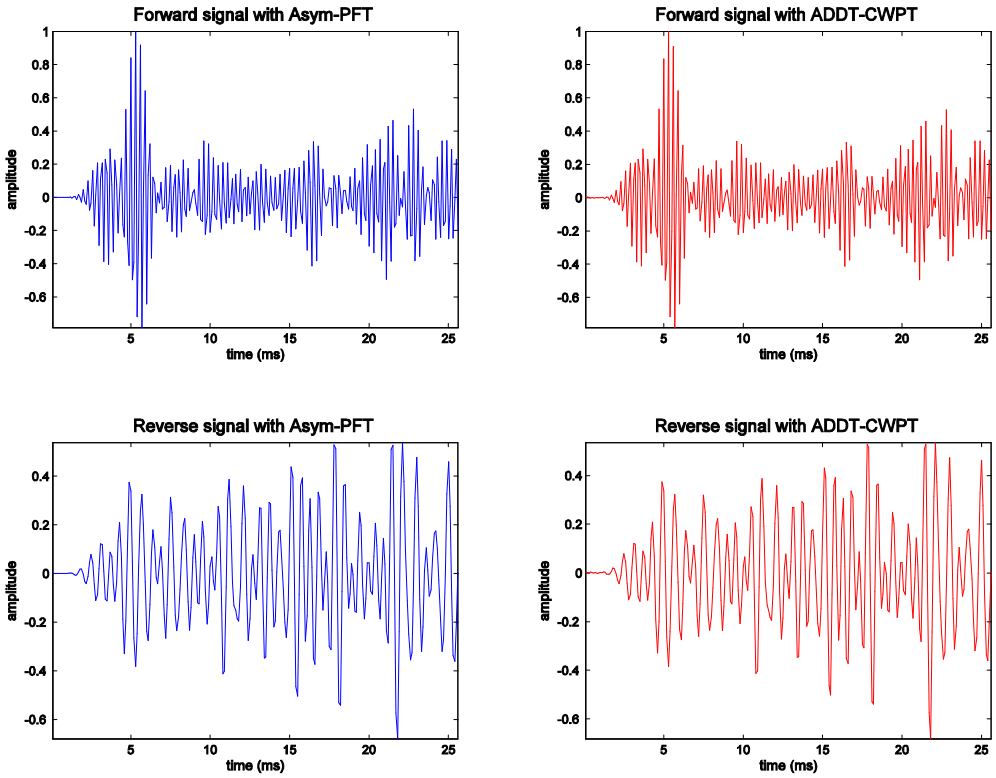

Figure 4.11 Output of ADDT-CWPT and Asym-PFT for synthetic quadrature signal.

4.5.3 Processing Real Quadrature Blood Flow Signals

In this part, as a real life application, embolic quadrature Doppler signals, which are used in detection of asymptomatic circulating cerebral emboli, are examined. The ESs used for this study were recorded using a commercially available transcranial Doppler system (EME Pioneer TC4040) with a 2-MHz transducer. The recordings were made from the ipsilateral middle cerebral artery of a patient with symptomatic carotid stenosis [47].

In order to show the performance of the proposed methods for real signals, first a quadrature embolic signal is decomposed by using ADDT-CWPT for 6 levels, and then the subbands are reconstructed without altering its coefficients. At the end of this process, directional signals almost the same as the ones obtained by the classical Asym-PFT are obtained. The resultant signals for both the Asym-PFT and the ADDT-

CWPT are illustrated in Fig 4.12.

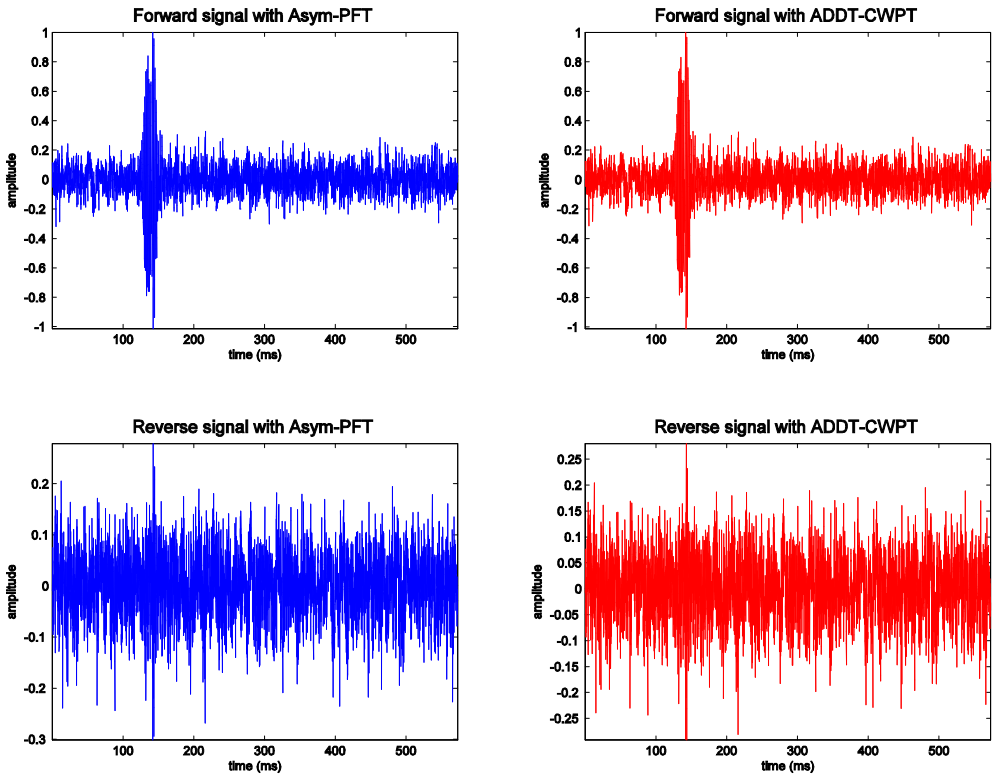

Figure 4.12 Output of ADDT-CWPT and Asym-PFT for quadrature embolic signal.

Additionally to compare the resulted coefficients of classical (Asym-PFT + DWPT) and proposed ADDT-CWPT and see the non-analytic subbands' effect, coefficients of 4 randomly chosen subbands and the coefficients of the first (lowest) and the last (highest) subbands in forward and reverse direction, are presented in Figure 4.13 and Figure 4.14. For comparison, as the DWPT, the real part of DT-CWPT is used. As it can be seen from the figures, the first and last subbands' coefficients obtained with ADDT-CWPT are different from the result of traditional method due to the non-analyticity drawback of DT-CWPT, on the other hand in the remaining subbands the resulted coefficients are very similar. As mentioned before, ESs have band-limited frequency character, that's why in the analysis of these signals, subband coefficients except the first and last can be trustfully used.

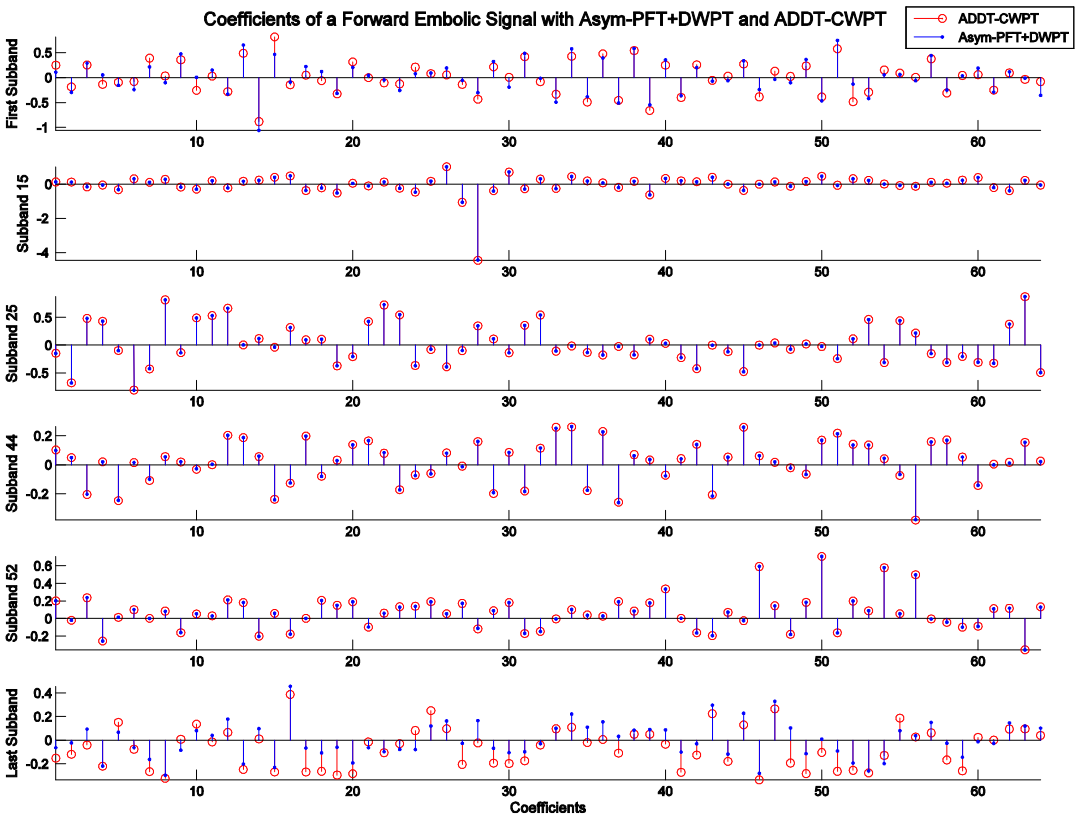

Figure 4.13 Coefficients of a forward emboli signal obtained with ADDT-CWPT and traditional method.

Time-frequency (TF) representations of Doppler ultrasound signals are used for emboli detection [93]. In TF based detection systems, first DWT or DWPT are used for de-noising as pre-processing stage. Therefore, in order to understand behavior of non-analytic subbands, the effect of proposed methods on the TF representations must be investigated in detail. In Figure 4.15, a TF representation of an embolic signal obtained by using the Asym-PFT and a TF representation of the same signal decomposed and reconstructed by using the ADDT-CWPT are illustrated. In the wavelet analysis part, forward and reverse signals are decomposed for 6 levels (decomposed into 2^6 subbands) and the resultant coefficients are reconstructed without any processing. In the forward direction, in both the Asym-PFT and the ADDT-CWPT cases, embolic signal can easily be identified. This shows us that using proposed methods in processing Doppler ultrasound signals has no negative effect on the frequency bands, in which the embolic signal exists. This result also verifies that ESs can be assumed as narrow band signals

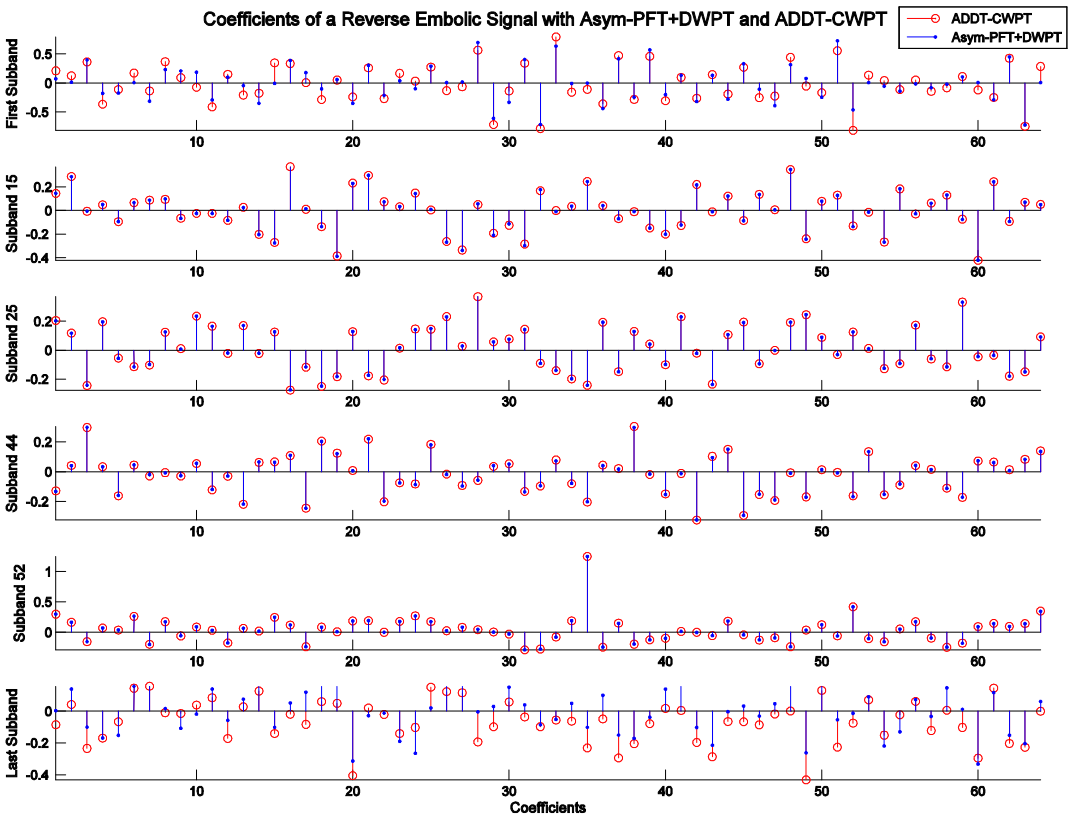

Figure 4.14 Coefficients of a reverse emboli signal obtained with ADDT-CWPT and traditional method.

[44]. Since the validity of the SDDT-CWPT has already been proven by using the simulated signals above, the study of the SDDT-CWPT for the real signal case was omitted for the brevity.

4.5.4 Shift-Invariance Property of Proposed Symmetrical Implementation

In part 4.4.3, it is proven that to have the near shift-invariance property, at the end of analysis part of wavelet packet transform, HT pairs of both forward and reverse coefficients have to be obtained. This situation can only be satisfied in symmetrical implementation of DDT-CWPT.

In order to prove this property, firstly, a real quadrature Doppler ultrasound signal is processed with classical Sym-PFT and the directional signals are obtained.

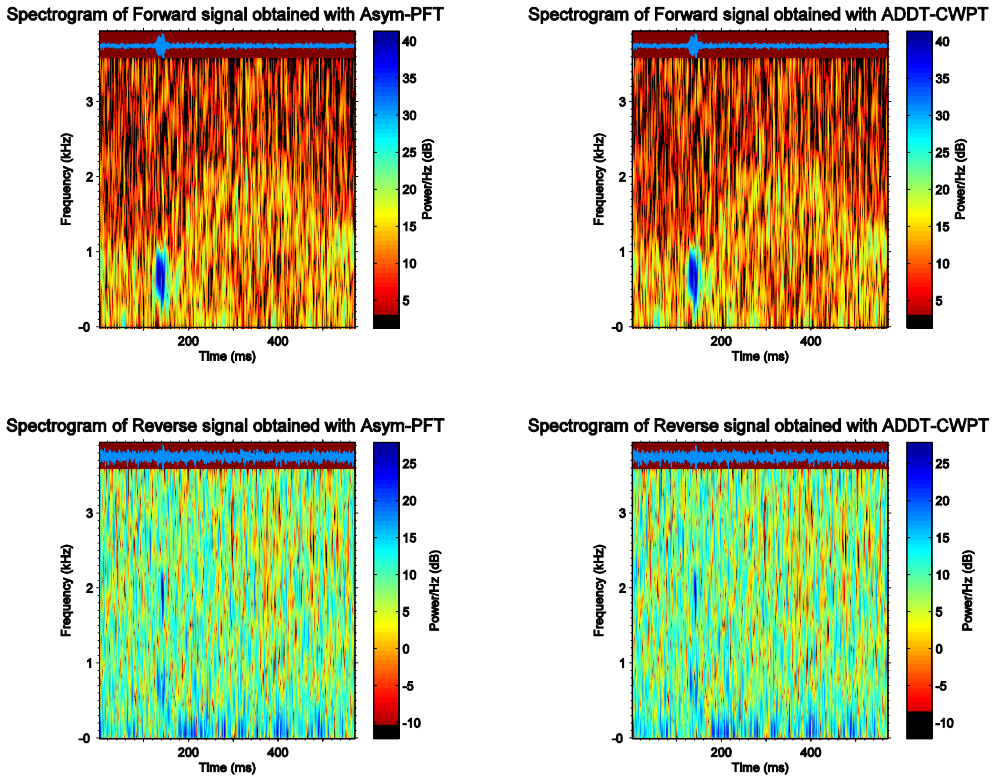

Figure 4.15 Spectrogram of an embolic signal in both directions.

Later the forward and reverse directional signals are decomposed with two analytic DT-CWPTs [77] for 6 levels. As an output of these two DT-CWPTs' real and imaginary tree analysis FBs, the coefficients of forward and reverse directional signals are obtained as illustrated in Figure 4.16. Secondly, same quadrature signal is given directly to SDDT-CWPT and at the end of analysis stage, the directional coefficients are obtained. In Figures 4.17, 4.18, 4.19, 4.20, in order to present the near shift-invariance property of proposed SDDT-CWPT, for both classical processing method and SDDT-CWPT, coefficients of 4 randomly chosen subbands plus the coefficients of the first (lowest) and the last (highest) subbands are presented. The obtained coefficients of forward signal in real tree and imaginary tree (Hilbert transformed coefficients) by using both traditional method and proposed SDDT-CWPT can be seen for 6 subbands including the first and last subband in Figures 4.17 and 4.18 respectively. Likewise, the obtained coefficients of reverse signal in real tree and imaginary tree (Hilbert transformed coefficients) by using both traditional method and proposed SDDT-CWPT can be seen in Figures 4.19

and 4.20 respectively. As expected for the first and last subband, the coefficients are different. But for the remaining subbands, the obtained coefficients by using SDDT-CWPT are approximately same with the coefficients obtained with traditional method. This proves us that in processing quadrature signals, for the subbands except the first and last, the proposed SDDT-CWPT has the same near shift-invariance property of DT-CWPT.

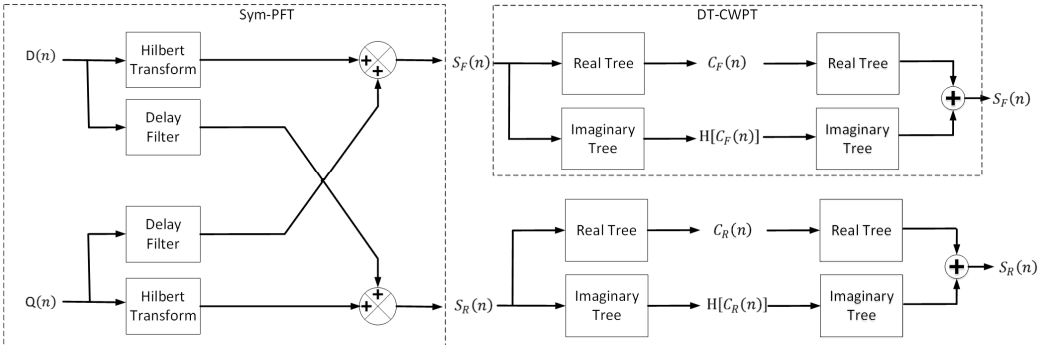

Figure 4.16 Traditional quadrature signal processing system with DT-CWPT.

4.5.5 The Effect of Non-Analytic Bands

In this section, in order to see the effect of non-analytic subbands of DT-CWPT, 100 Embolic Doppler ultrasound signals (4096 sample points each, with a sampling frequency of 7150 Hz) were used. First, the quadrature signals are processed by using classical Asym-PFT and the forward and reverse signals are obtained. Then, the same quadrature signals are decomposed and reconstructed by using the ADDT-CWPT resulting in the directional signals. Due to the non analytical first and last subbands and energy leakages in opposite frequencies, a little difference between the PFT outputs and the ADDT-CWPT outputs occurs. These differences are calculated for each forward and reverse directional signal and a signal-difference ratio is obtained. The average and standard deviation of these difference-ratios can be seen in Table 4.3 (left side, when all the bands are used). Later, in order to investigate the weight of non-analytic subbands in this difference, same 100 Asym-PFT outputs are firstly decomposed by using only the real part of DT-CWPT (as a DWPT) and coefficients of the first and

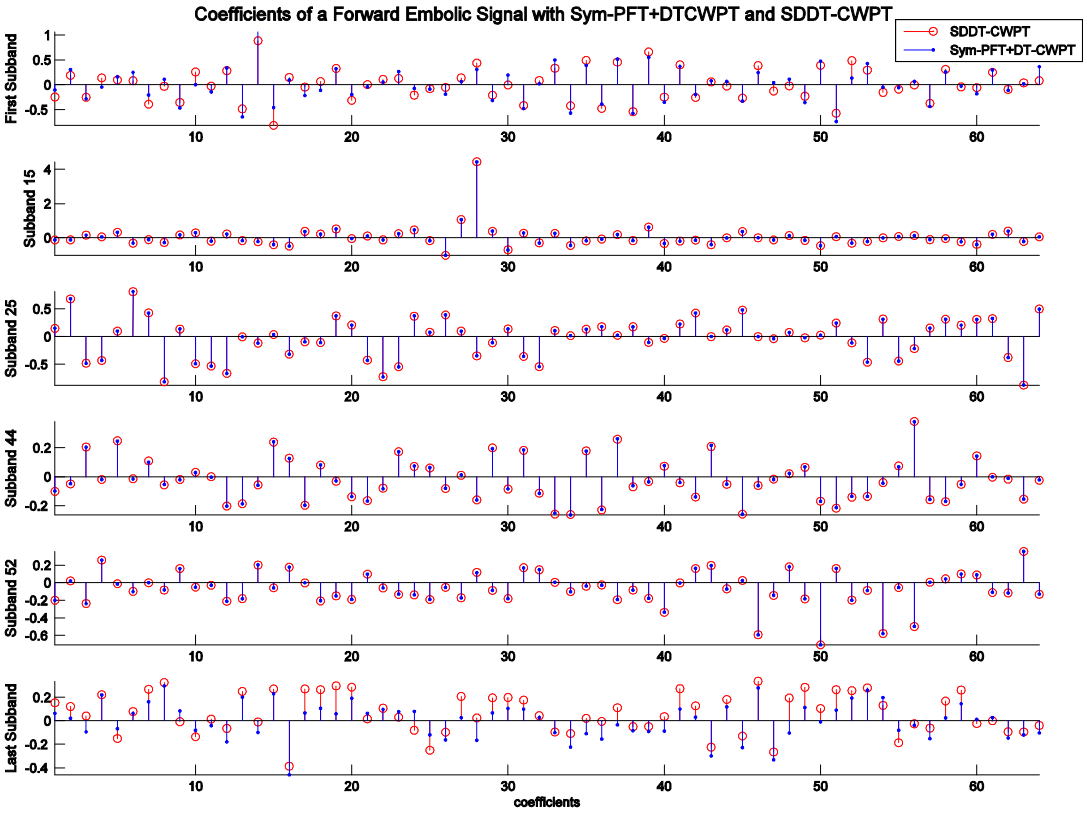

Figure 4.17 Coefficients of a forward emboli signal obtained with proposed SDDT-CWPT and traditional method.

last subbands are set to zero, then the subbands are reconstructed resulting the 100 quadrature signals whose first and last subbands are removed. Secondly, the same 100 quadrature signals decomposed by using ADDT-CWPT and coefficients of the first and the last subbands are set to zero. Then the subbands are reconstructed. At the end of these steps, the signal-difference-ratio is calculated when the non-analytic bands are removed. The results can be seen in Table 4.3 (right side, when the non-analytic bands are omitted). By doing this, the weight of non-analytic bands (first and last subbands) in the difference-ratio is quantified. From the table, it is possible to see that most of the difference is occurred because of the first and last subbands. When these subbands are removed, the difference-ratio caused by the energy leakages of opposite frequencies in mid-subbands are much lower. For the forward signals, the mean and standard deviation of difference-ratios are even smaller because the band-limited ESs are unidirectional. These results validate that the proposed methods work well for ESs.

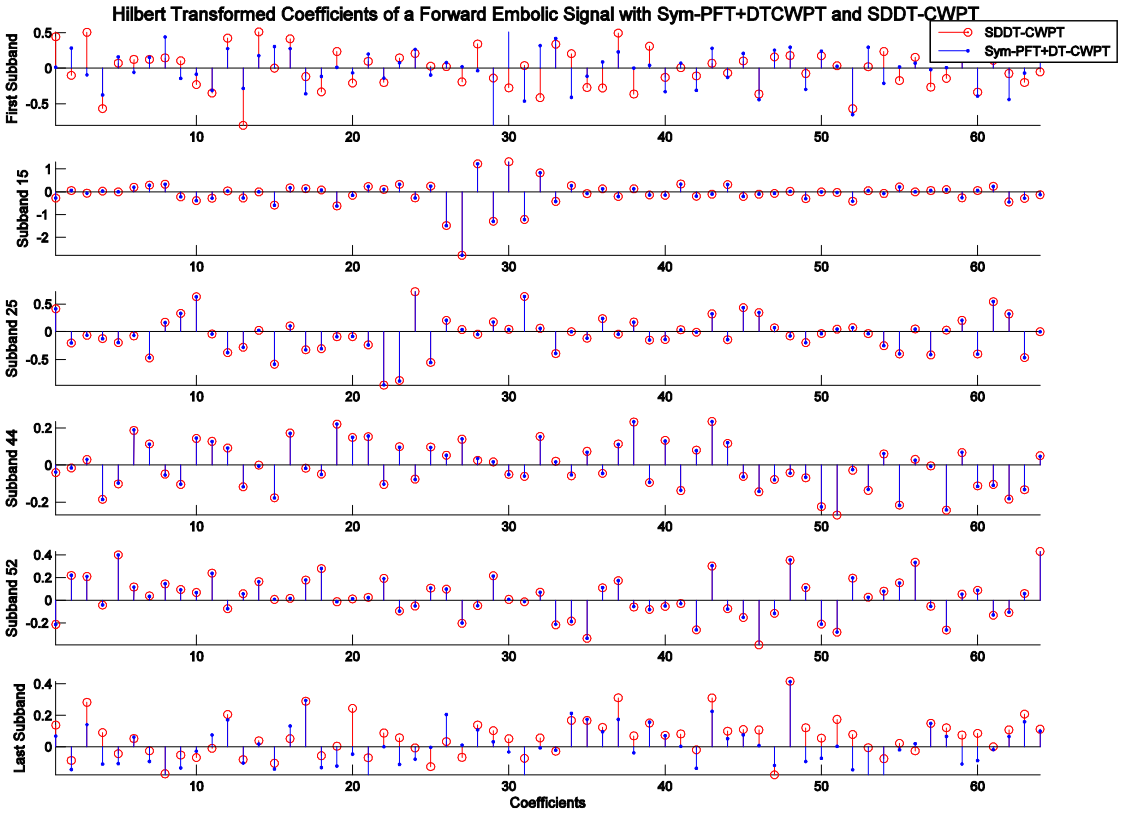

Figure 4.18 Hilbert transformed coefficients of a forward emboli signal obtained with proposed SDDT-CWPT and traditional method.

Table 4.3
Average/Std Signal-Difference Ratios of Forward and Reverse Signals when the non-analytic band are used and not used.

	When All the Bands are Used		When the Non-Analytic Bands are removed	
	Average Difference Ratio	Std of Difference Ratio	Average Difference Ratio	Std of Difference Ratio
Forward Signal	%5.801	%4.448	%1.422	%0.294
Reverse Signal	%11.856	%9.156	%3.412	%1.283

The signal-difference ratio with and without the first and the last subbands for 100 ESs are illustrated in the Figure 4.21. For all signals the signal-difference ratio is smaller when the non-analytical bands are removed. This shows that the proposed methods work well for all subbands except the first and the last. For some signals

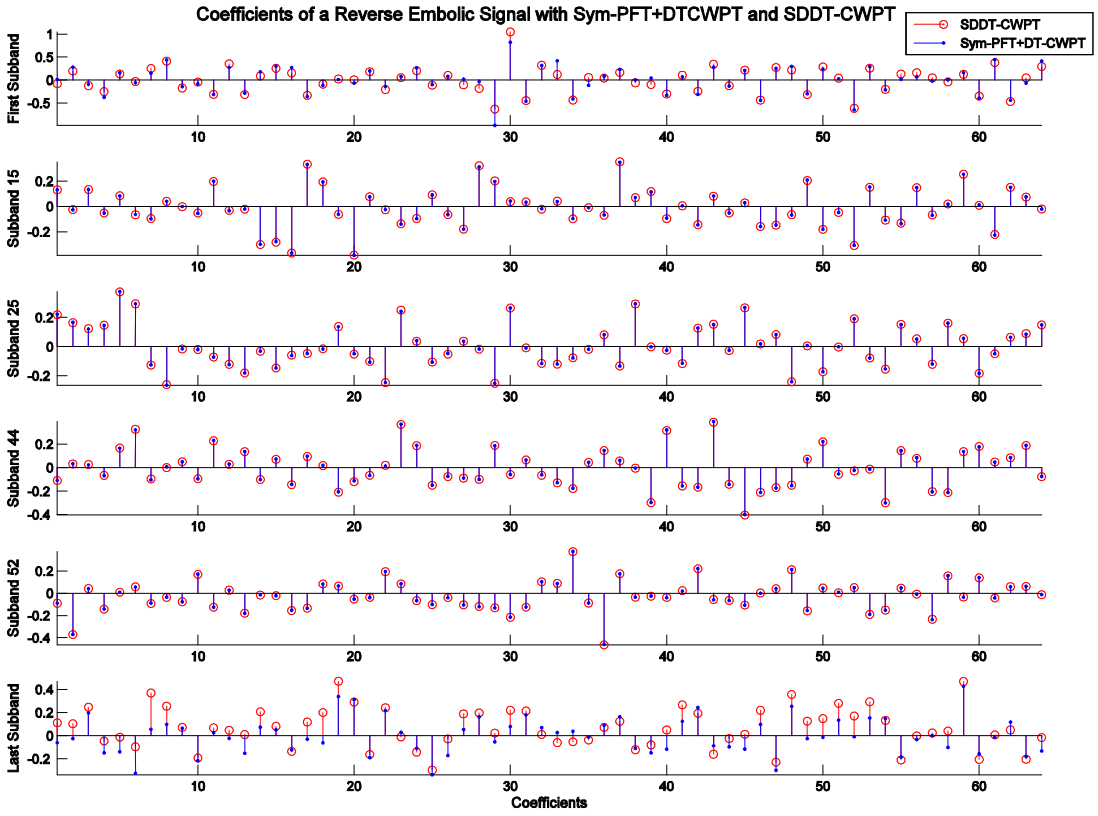

Figure 4.19 Coefficients of a reverse emboli signal obtained with proposed SDDT-CWPT and traditional method.

(for example signals 11, 12, 17, and 18) the signal-difference ratio is much higher. The reason for this is that embolic signal intensity in those signals are relatively smaller and usually some artifacts (some low frequency signals caused by tissue movement, probe tapping, speaking, and any other environmental effects) exist. As an example, in the Figure 4.22, a signal containing a low intensity embolic signal and a large low frequency artifact decomposed and reconstructed by using ADDT-CWPT was compared with the output of traditional Asym-PFT. When the figure is examined, it is possible to see that the difference between the signals is insignificant during the embolic signal, but significant at the other times. This also proves that the proposed methods perform well and can be used for analysis and detection of ESs.

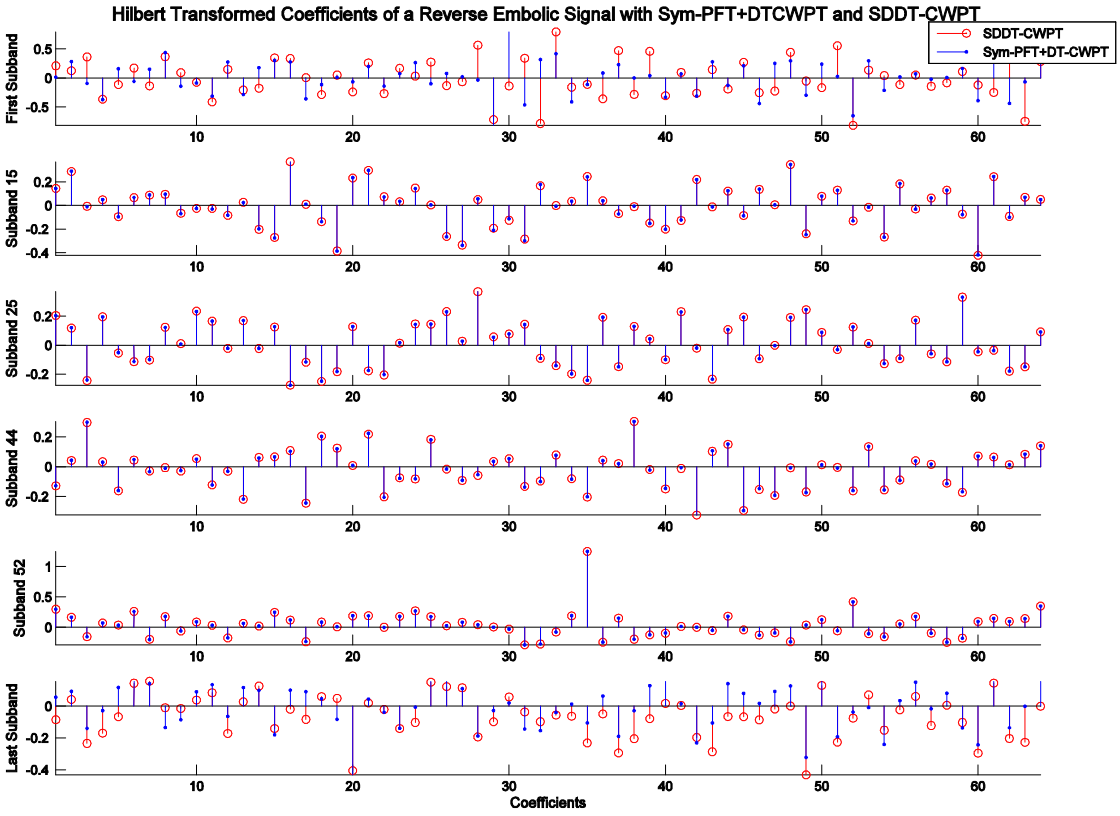

Figure 4.20 Hilbert transformed coefficients of a reverse emboli signal obtained with proposed SDDT-CWPT and traditional method.

4.5.6 Computational Costs of the Proposed Algorithms

In real life implementation of Asym-PFT, a FIR HT filter and a delay filter compensating the time delay caused by the HT filter must be employed. Moreover, in Sym-PFT, two HT filters and two delay filters are needed. In real life applications, usually HT filters comprising considerable numbers of coefficients are employed for obtaining a decent 90 degrees phase shift effect. In order to evaluate the computational efficiency of the proposed methods, HT filters and delay filters having various filter coefficient lengths have been utilized. Time comparisons are done between Asym-PFT + DWPT and ADDT-CWPT, and between Sym-PFT + DT-CWPT and SDDT-CWPT. Two time comparisons are performed. While the first comparison involves the computational complexity of the analysis part (decomposition only), the second comparison includes both the analysis and the synthesis parts (decomposition + reconstruction).

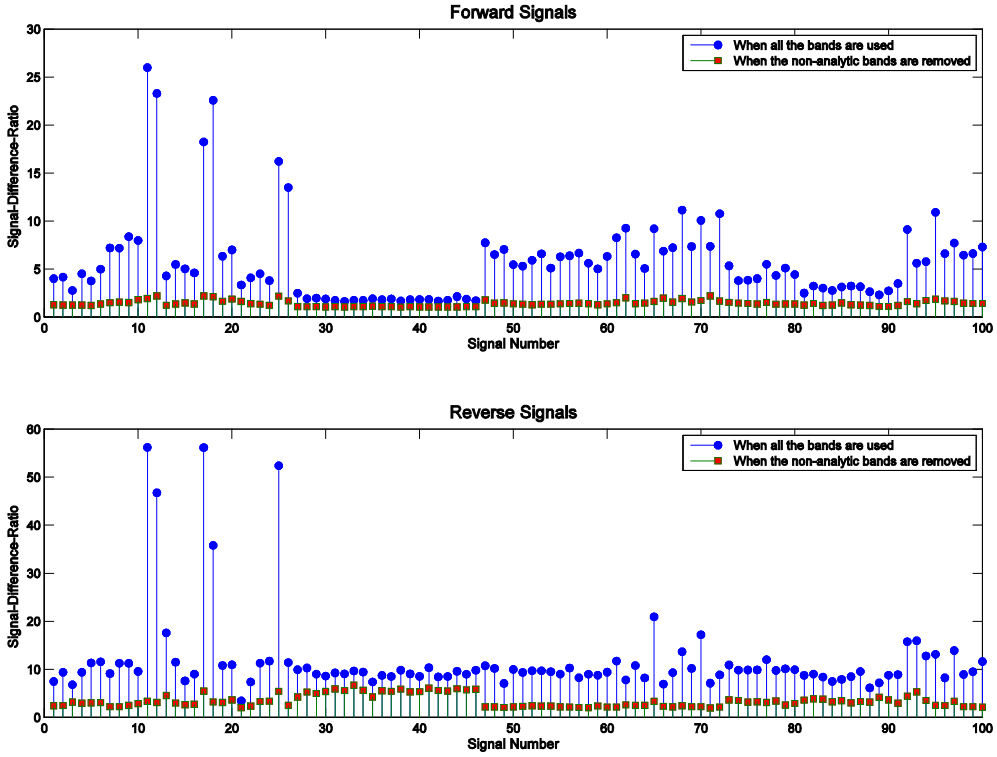

Figure 4.21 The signal-difference ratios of 100 embolic signals when the non-analytic bands are removed and not removed.

For the simulations, in order to minimize background program activity of the computer, a real quadrature embolic signal is chosen and an average result of 10000 time measurements is presented. Evaluations are done on a desktop computer with Intel(R) Core(TM) i3-2120, 3.30 GHz processor and 4 GB RAM.

The differences are quantified by using following formula for both the full tree version and for the only analysis part version,

$$\text{Time enhancement ratio} = \left| \frac{\text{time of traditional method} - \text{time of proposed method}}{\text{time of traditional method}} \right| \times 100 \quad (4.69)$$

In Tables 4.4 and 4.5, the time comparison results of traditional methods and proposed methods are presented. In the Table 4.4, it can be seen that the ADDT-CWPT speeds up the process up to 4.6 percent for the full tree. Moreover this time enhancement can reach up to 34.2 percent in SDDT-CWPT. This is due to the use of only two trees in the SDDT-CWPT during reconstruction, rather than four trees used in the traditional method (Figure 4.7). In the Table 4.5, the results for only analysis

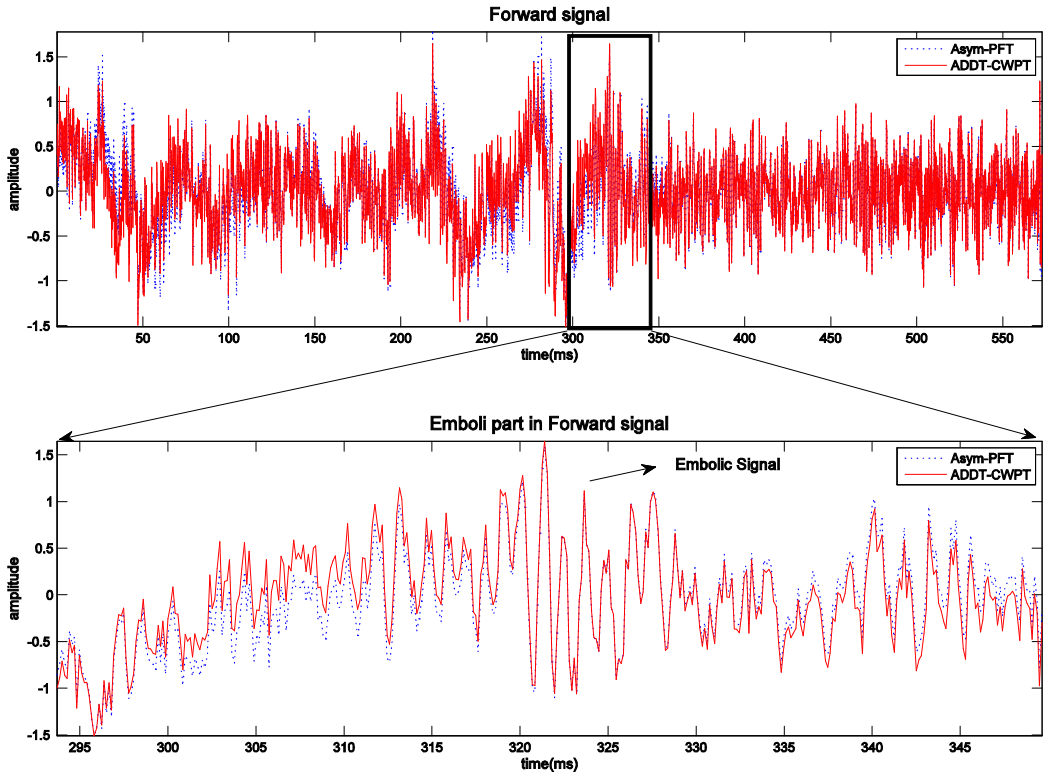

Figure 4.22 A low intensity embolic signal superimposed on a large low frequency artifact.

part are presented. As it can be seen from the table, for both proposed methods, a significant time enhancement up to 11 percent is achieved.

Table 4.4
Time enhancement ratios for full tree.

	with Asymmetrical DDT-CWPT	with Symmetrical DDT-CWPT
coefficient number		
101	%2.255	%32.916
151	%2.884	%33.280
201	%3.743	%33.757
251	%4.595	%34.223

Table 4.5
Time enhancement ratios for only analysis part.

	with Asymmetrical DDT-CWPT	**with Symmetrical DDT-CWPT**
coefficient number		
101	%5.555	%4.580
151	%7.385	%7.322
201	%9.135	%8.496
251	%11.083	%10.277

4.6 Discussion and Conclusions

In this chapter, asymmetrical and symmetrical directional complex discrete wavelet packet transforms, which can be applied directly to quadrature signals and have the ability of extracting directional information during analysis, are introduced. With these proposed directional transforms, the traditional PFT steps, which are used for extracting directional signals prior to wavelet analysis, are eliminated, resulting in a significant reduction in overall computational costs of the analysis system.

In order to measure the performance of proposed methods, synthetic single frequency and narrow-band quadrature signals are constructed. Additionally, a database consisting of 100 real quadrature embolic signals are employed. First, in order to show the effect of non-analytic subbands for both ADDT-CWPT and SDDT-CWPT, a number of decomposition levels are tested by using synthetic single frequency and narrow-band signals and resultant signal-difference-ratios are presented. As it can be seen from the results, the proposed methods work well for signals having narrow-band characteristics.

In real signals case, again both the qualitative and quantitative results of the reconstruction performance are presented. It is possible to see that the proposed methods work well for all subbands except the lowest and highest subbands. Additionally, effect of the proposed method on time-frequency representation of an embolic signal is investigated using short time Fourier transform (STFT). It is seen from the STFT outputs (Figure 4.15) that the position, duration, and intensity of the embolic signal

in the time-frequency plane are almost the same for both the conventional and the proposed methods.

In 4.5.4, by using resulted coefficients the shift-invariance property of proposed SDDT-CWPT is proved. In section 4.5.5, for the embolic signal dataset, the effect of the last and the first subbands on the signal-difference-ratio is calculated and it is shown that the most of the distortion is caused by these non-analytic subbands. It is known that in the ESs, the information carrying parts have band-limited (narrow-band) characteristics. Therefore, in real-world applications, the distorting effect of the energy leakages in the subbands consisting of the embolic signal is negligible and does not corrupt the relevant information. Lastly, in section 4.5.6, a detailed time comparison between the proposed methods and traditional methods is done. From the results of this comparison it is seen that significant computational complexity reduction is achieved with proposed methods.

From the results presented in above sections, it can be concluded that, the proposed directional complex wavelet packet transforms can be confidently used in the quadrature signal processing applications such as noise reduction in blood flow signals, with reduced computational complexity. Additionally, in the future, it will be a challenge to implement these proposed transforms in a real-time asymptomatic embolic signal detection and classification system.

5. DIRECTIONAL DUAL TREE RATIONAL-DILATION COMPLEX WAVELET TRANSFORM

5.1 Introduction

Dyadic discrete wavelet transform (dyadic-DWT), in which the resolution is doubled from each scale to the next scale, is a very effective tool for processing piecewise smooth signals and used as a popular transform in various signal and image processing applications [94, 95]. However, due to its poor frequency resolution and severe frequency aliasing drawbacks, the dyadic-DWT is less effective in the process of signals having more oscillatory behaviour such as speech, biomedical signals like EEG, audio signals and etc. These types of signals are quasi-periodic over short-time intervals. In analyzing these signals, a wavelet transform having better frequency resolution than the dyadic-DWT is needed. Additionally, the dyadic-DWT lacks of shift-invariance property causing considerable distortions in the coefficients resulting in at the end of decomposition stage of wavelet analysis when the input signal is time-shifted.

In order to overcome the drawbacks of the dyadic-DWT in processing oscillatory signals, various overcomplete WTs such as the undecimated WT, the dual tree complex WT and the double density WT have been proposed [30, 96, 97]. Many of these WTs have the capability of increasing only the temporal resolution with limited range of redundancy factors. However in [98], an overcomplete wavelet transform, which is based on rational (non-dyadic) dilation factors, are proposed. This transform is based on a frequency domain design and the implementation is based on fast Fourier transform. Additionally, the transform is appropriate for the discrete-time signals, approximately shift-invariant, and easily invertible. In this transform, various Q-factors and redundancy factors can be attained by changing the dilation factor. Due to its being overcomplete and rational dilation property, this transform is called overcomplete rational dilation wavelet transform (RADWT).

Quadrature signals, which are composed of the in-phase and the quadrature-phase components, are obtained at the detection stage of the systems employing quadrature demodulation technique. In biomedical engineering, Doppler ultrasound systems that are used in blood flow analysis have also quadrature format outputs and the outputs of these systems are frequently used in embolic signal detection. Emboli are small travelling clots which can originate in an artery of the body, traveling up the arterial tree to the brain until it lodges in a blood vessel. The presence of emboli in blood circulation can be the main factor of stroke, which may cause permanent damage or even death. In order to prevent stroke, asymptomatic circulating cerebral emboli can be detected by analyzing quadrature Doppler ultrasound signals.

However, to process quadrature Doppler ultrasound signals, firstly the in-phase and the quadrature-phase components must be decoded into the forward and reverse direction components of blood flow. In literature, the phasing filter technique (PFT) is the most widely used method to obtain directional signals. In the PFT, Hilbert transform (HT) of one of the in-phase and the quadrature-phase components must be taken to introduce 90 degrees phase shift [40, 41]. After obtaining directional signals, Fourier transform and wavelet transform based algorithms are applied for further analysis.

In literature, a complex continuous wavelet transform algorithm which is applied to directly quadrature signals and maps the directional information, while doing the analysis, was introduced in [69]. In the DWT case, a transform which can be applied directly to the in-phase and the quadrature-phase components and has the capability of mapping directional signals in the scale domain during analysis does not exist. To achieve such a property, the DWT must be a complex transform with only one-side frequency spectrum.

In [30] a dual tree complex wavelet transform (DTCWT) was proposed but because of its energy leakages into its negative frequency bands, it cannot achieve desired one-sided frequency spectrum property. In [85, 86, 88, 91] a modified DTCWT is proposed. However, in this transform still an additional HT filter and a delay filter (used in digital circuits to compensate the time delay that occurred because of the

digital HT filter) must be used. Additionally it is still a dyadic-DWT.

Embolic signals (ESs) are usually described as amplitude-modulated sine waves which have very short duration varying between 2 and 100 ms. An example is illustrated in Figure 5.1. In frequency domain, ESs result in an increase in intensity that is focused on a small band of frequencies (behave as a narrow-band signal) in the Doppler spectrum, resulting in a bell-shaped distribution. In [47] the dyadic DWT was applied to directional blood-flow signals in order to detect embolies. However, in order to achieve better detection accuracies for ESs, RADWT, whose Q-factor and redundancy can be adjustable, can be utilized. By tuning the Q-factor (increasing the Q-factor) of the RADWT in decomposition, an optimum oscillatory wavelet behaviour can be set for an embolic signal and a more compact energy distribution of the coefficients can be obtained.

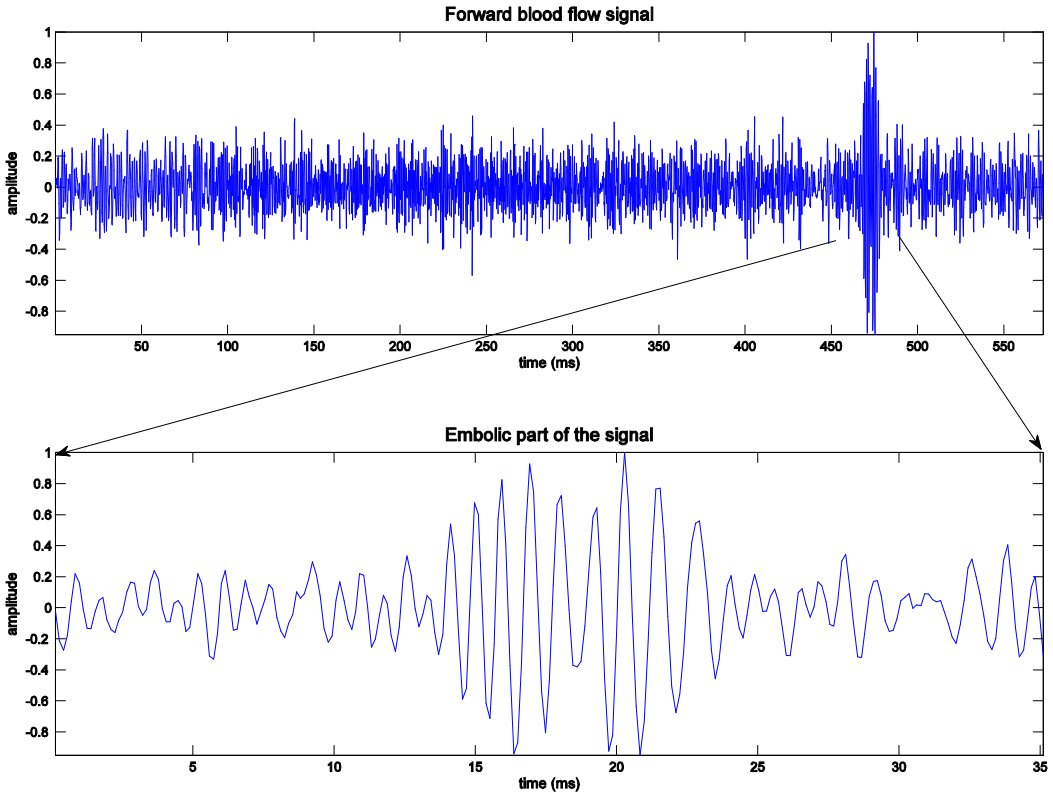

Figure 5.1 A forward blood flow signal (above) and zoomed version of emboli part (below).

In [99] a modified version of RADWT, a dual-tree rational-dilation wavelet transform (DT-RADWT) was introduced that inherits the good frequency resolution and constant-Q property of the RADWT and whose atoms form quadrature pairs. DT-RADWT is realized by two wavelet trees, one is the real tree and the other is imaginary tree, operating in parallel on the same input. In DT-RADWT, the second wavelet filter-banks (FBs of imaginary tree) are designed so that their impulse responses are approximately the discrete HTs of those of the first wavelet FBs (FBs of real tree). Then, to process quadrature signals, this capability of taking HT property of the imaginary tree in DT-RADWT, can be used to obtain 90 degrees phase-shift effect of classical PFT.

In this chapter, we introduce a directional DT-RADWT (DDT-RADWT) that extends the classical DT-RADWT. DDT-RADWT is complex transform which can be directly performed on quadrature signals. Its frequency resolution can be changed by tuning the Q-factor of wavelets according to the behaviour of analyzed signal. Additionally, it is a near shift-invariant transform which is very important in processing quadrature Doppler signals due to the phase relationship of in-phase and quadrature-phase components.

5.2 Rational Dilation Wavelet Transform

In literature, the dyadic DWT and the DTCWT are used successfully in processing signals having non-oscillatory, transient behaviour like pulmonary crackles and brain spike signals [100, 101, 102]. Due to the low Q-factor property of their subbands (low oscillatory nature of wavelet bases), dyadic wavelet transforms are less effective in processing oscillatory signals such as ESs. In this respect, RADWT, which is a fully discrete, easily invertible, energy preserving, approximately shift-invariant, can be employed in the process of oscillatory signals. RADWT provides ability to the user to adjust the Q-factor of wavelet bases. It can be used for high Q-factor analysis or the same low Q-factor analysis as the widely used dyadic-WT. In RADWT, by changing the transform parameters not only the frequency partition manner, but also the time

domain oscillatory nature of the wavelet functions are controlled.

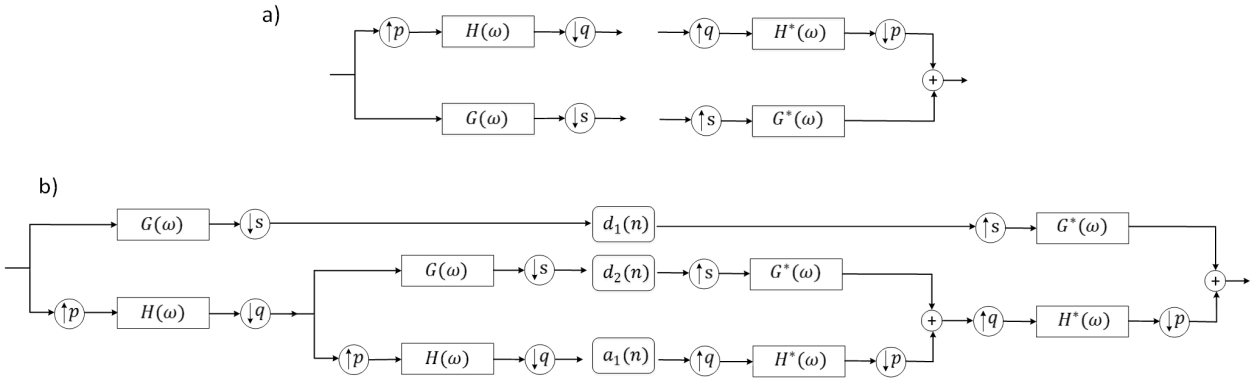

Figure 5.2 a) The analysis and synthesis filter banks used in RADWT.b) The full structure of RADWT including decomposition and reconstruction phases.

Similar to the classical DWT implemented using Mallat's tree-structure filter-bank, the RADWT is also implemented through an iterated two-channel FB as illustrated in Figure 5.2.a. The Q-factor of the wavelet transform depends on the parameters p, q and s. Instead of being based on integer dilations, the dilation factor of the transform is q/p where the numbers q and p are co-prime and satisfy $q > p$. In order to obtain higher frequency resolution, for q and p values, following conditions must be satisfied; $1 < q/p < 2$, q/p ratio must be close to 1, and $s > 1$. When the s is set to 1, classical dyadic DWT with low Q-factor is obtained. In Figure 5.3, in upper left and right parts, the frequency decomposition of the RADWT with a low Q-factor (5 levels) and high Q-factor (18 levels) can be seen. Additionally, in lower left and right parts, associated wavelets from levels 3 to 10 with a low Q-factor and high Q-factor can be seen respectively. As it can be seen, when the Q-factor is increased, in time domain, the wavelets obtained in subbands become more similar to ESs and their frequency responses become more frequency selective. The full structure of RADWT including decomposition and reconstruction phases for two levels can be seen in Figure 5.2.b.

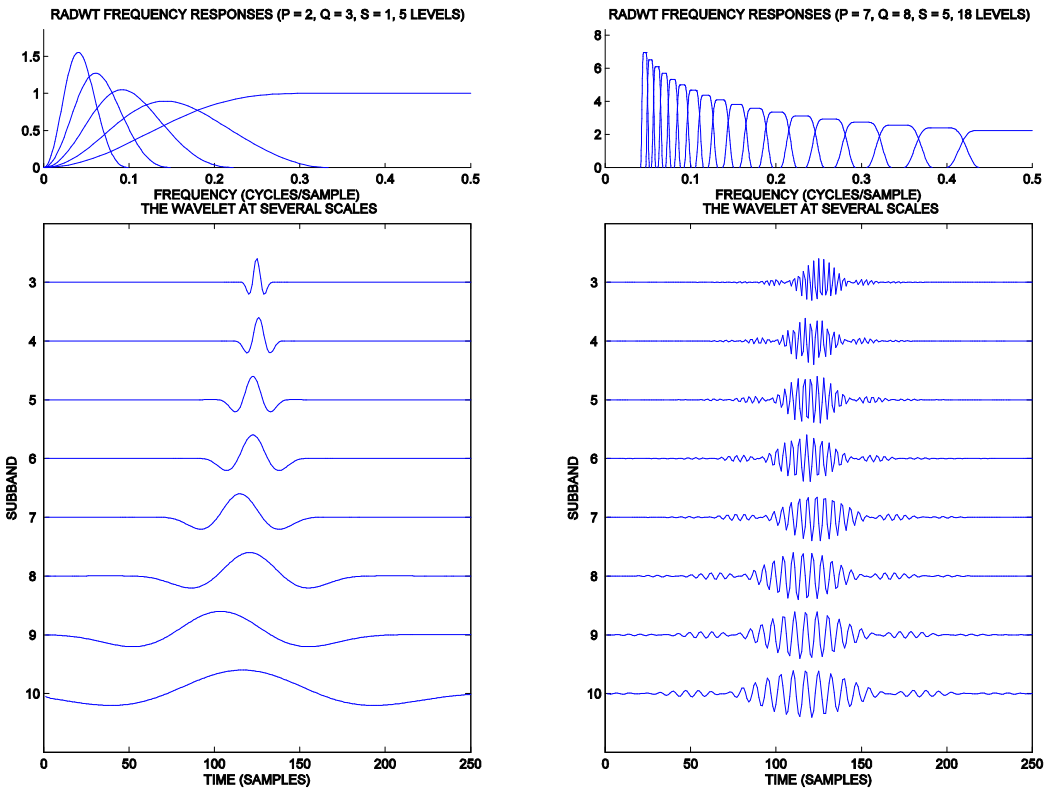

Figure 5.3 Frequency response of decomposed subbands and associated wavelets with low Q-factor (left) and high Q-factor (right).

5.3 Dual Tree Rational-Dilation Complex Wavelet Transform

In [99], the dual-tree rational-dilation complex wavelet transform (DT-RADWT), which employs quadrature pairs of time-frequency atoms similar to the short time Fourier transform (STFT) and the dyadic DTCWT for oscillatory signal processing was introduced. DT-RADWT is a constant-Q transform, a property lacked by the STFT, which in turn makes the introduced transform more suitable for models that depend on scale. Additionally, In the DT-RADWT, the frequency resolution can be adjusted and high Q-factor, a property lacked by the dyadic DTCWT, can be attained. This property makes the DT-RADWT more suitable for processing oscillatory signals such as ESs [99]. DT-RADWT is realized by using two wavelet trees, one is the real tree and the other is imaginary tree, operating in parallel on the same input. In DT-RADWT, the second wavelet FBs (FBs of imaginary tree) are designed so that their impulse responses are approximately the discrete HTs of those of the first wavelet FBs

(FBs of real tree). Then, to process quadrature signals, this capability of taking HT property of the imaginary tree in DT-RADWT, can be used to obtain 90 degrees phase shift effect of the classical PFT. The structure of DT-RADWT is illustrated in Figure 5.4. In the dashed box, real part of the DT-RADWT can be seen.

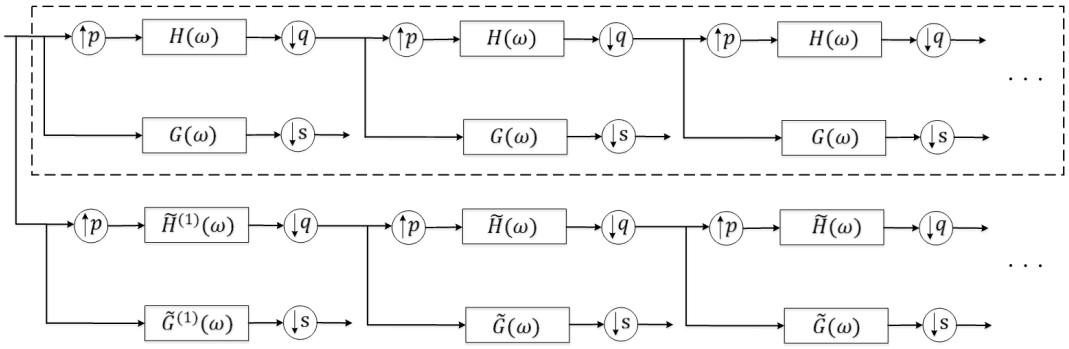

Figure 5.4 The decomposition stage of the DT-RADWT.

5.4 Directional Dual Tree Rational-Dilation Complex Wavelet Transform

Conventionally, in order to utilize RADWT in the analysis of the quadrature Doppler signals, firstly, directional signals (forward signal and reverse signal) must be obtained by using the PFT. Only then, the RADWT can be applied with the aim of emboli detection. This procedure increases the computational cost of the processing system. However, it is possible to reduce the computational cost of the processing system by utilizing the HT property of the analysis and synthesis filters in the imaginary tree of the DT-RADWT. In the proposed method (Directional DT-RADWT), two modifications are made to the conventional DT-RADWT, as illustrated in Figure 5. At the decomposition stage, only the quadrature-phase part ($Q(n)$) is applied to the real tree and only the in-phase part ($D(n)$) is applied to the imaginary tree. Eventually, as an output of real tree, coefficients of $Q(n)$ and as an output of imaginary tree, HT'ed coefficients of $D(n)$ are obtained. Later, the coefficients of $Q(n)$ are subtracted from the HT'ed coefficients of $D(n)$ resulting in the coefficients of reverse signal. Likewise,

HT'ed coefficients of *D(n)* are added to the coefficients of *Q(n)* resulting in the HT'ed coefficients of forward signal. In the decomposition stage, the coefficients of forward and reverse signal are given to synthesis filters of the real tree of DT-RADWT resulting in the forward and reverse directional signals.

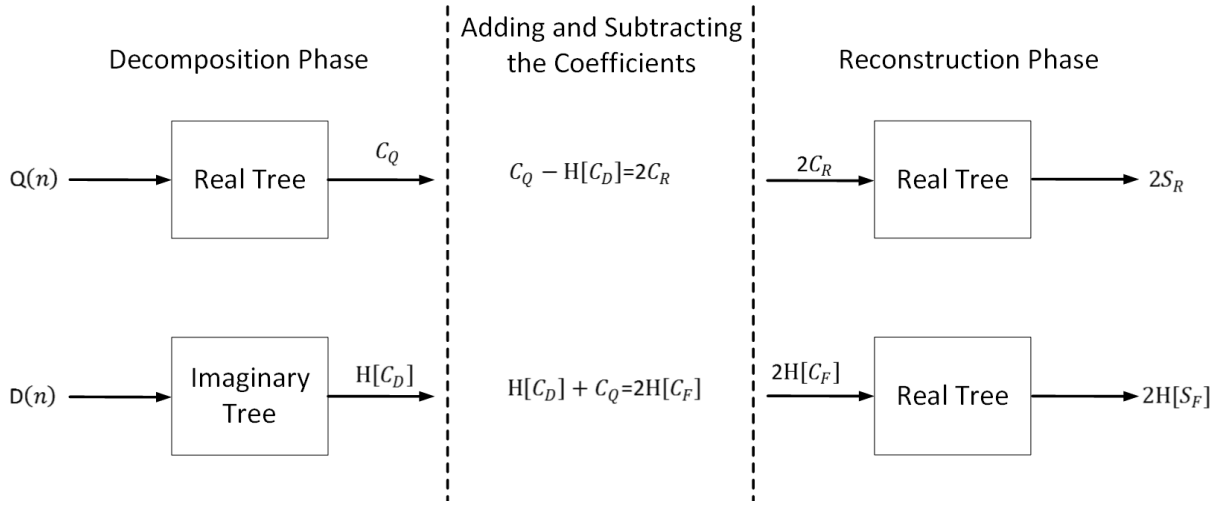

Figure 5.5 The structure of proposed directional DT-RADWT.

5.5 Experimental Results

In order to evaluate proposed method's reconstruction performance and also the ability to extract directional information, a quadrature embolic signal is processed with the traditional PFT and with the directional DT-RADWT (DDT-RADWT). In the DDT-RADWT, the signal is decomposed and reconstructed for 20 levels without any alterations on coefficients. The full obtained forward signals by using the DDT-RADWT and the PFT can be seen in the two upper rows of Figure 5.6. Additionally, to see the reconstruction success on emboli parts, a zoomed version of ESs obtained with the PFT and DDT-RADWT can be seen in the lower third row of Figure 5.6. As it can be seen from the figure, by using the DDT-RADWT, directional signals can be obtained accurately at the end of the proposed transform.

Proposed DDT-RADWT has ability to tune the Q-factor of its wavelet atoms

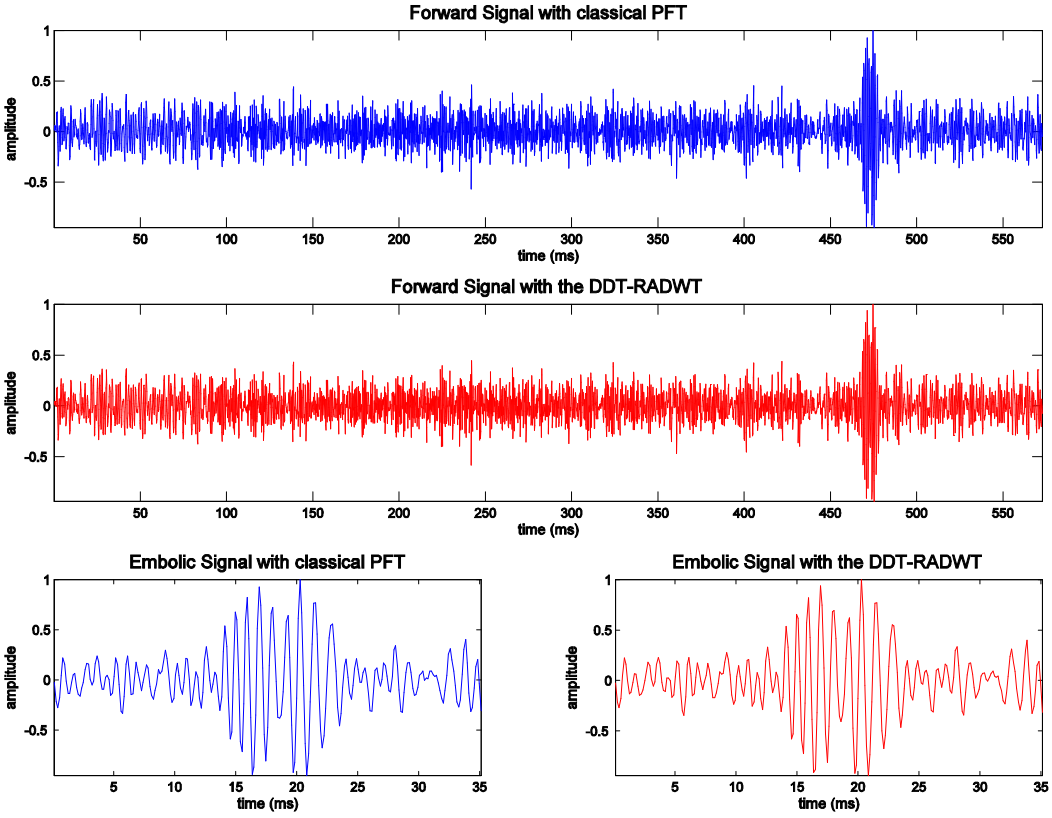

Figure 5.6 In the upper two rows, forward blood flow signals obtained with the classical PFT and proposed directional DT-RADWT are illustrated respectively. In the third row, zoomed embolic signals obtained with the classical PFT and proposed directional DT-RADWT are illustrated.

and this makes the proposed transform more flexible than the traditional dyadic-DWT, which employs low Q-factor wavelet atoms during wavelet analysis. By using DDT-RADWT, wavelet atoms with high Q-factors can be attained resulting in improved frequency resolution. ESs are usually described as amplitude-modulated sine waves and have short time oscillatory time-domain behavior. Therefore, in the Doppler spectrum, ESs behaves as a narrow-band signals that result in a bell-shaped distribution. To obtain sparse representations of ESs in decomposed subbands, by using DDT-RADWT, an adjustable frequency resolution, changing with analyzed emboli information, can be set.

In order to show this property, an ES with an artifact (a low frequency signal caused by tissue movement, probe tapping, speaking, and any other environmental effects) is analyzed with DDT-RADWT. Firstly, we set $p = 1$, $q = 2$, $s = 1$. The

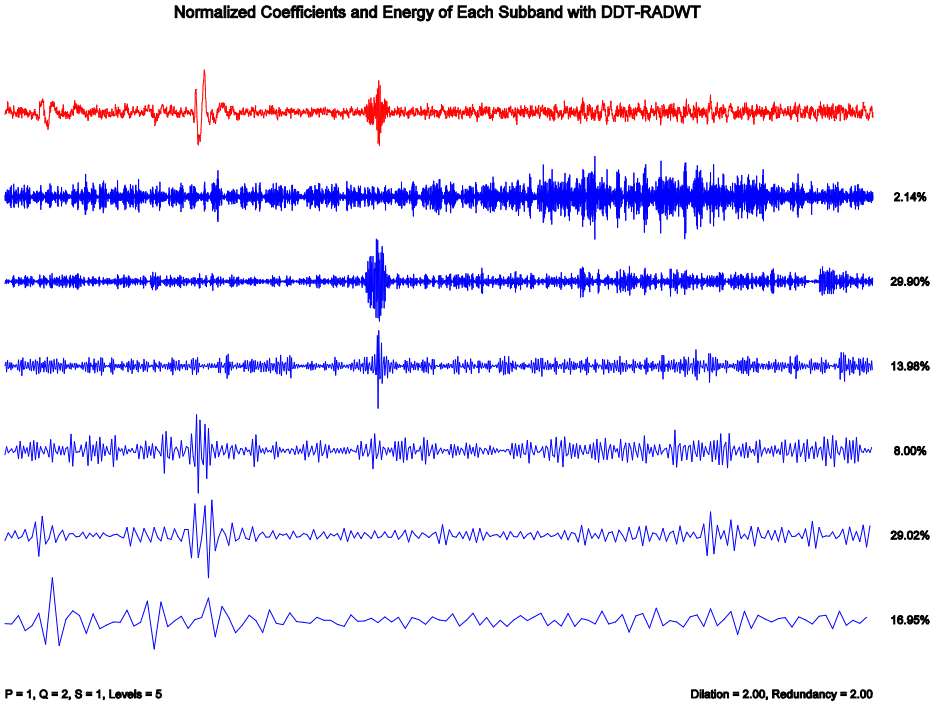

Figure 5.7 Original signal (red, first row) and the normalized coefficients of each subband (blue, rows 2 to 7) by using low Q-factor wavelet analysis (equivalent to dyadic-DWT).

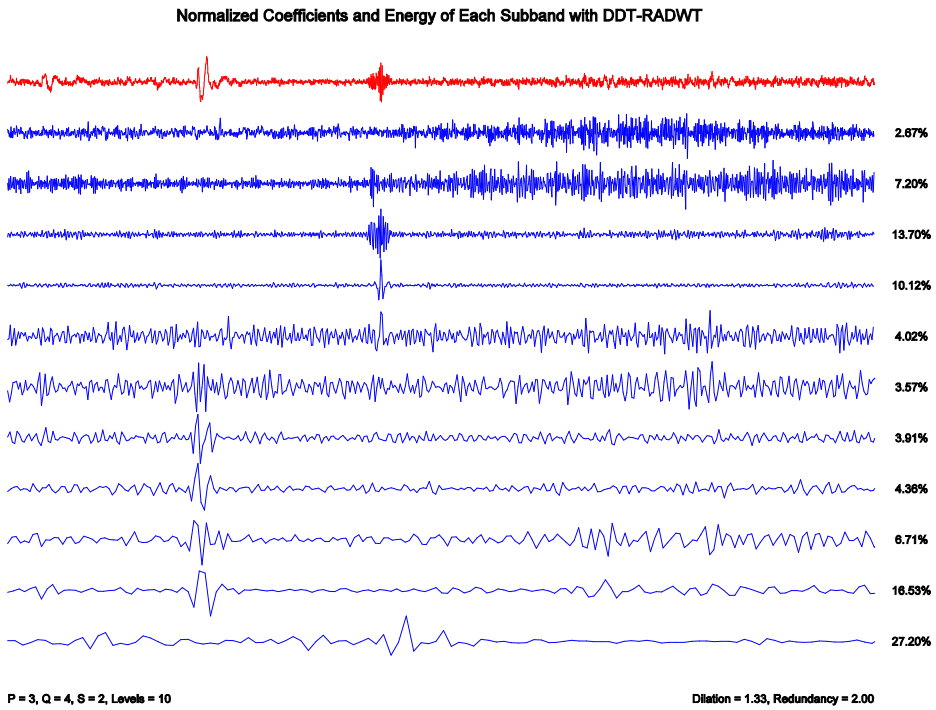

Figure 5.8 Original signal (red, first row) and the normalized coefficients of each subband (blue, rows 2 to 12) by using high Q-factor wavelet analysis.

dilation factor is 2 and the redundancy is 2. When the parameters are chosen in this way, the resultant transform employs low Q-factor wavelets and is equivalent to classic dyadic-DWT. The analysis is done for 5 levels. Secondly, same signal is analyzed with high Q-factor wavelets. We set $p = 3$, $q = 4$, $s = 2$. The dilation factor is $4/3$ and the redundancy is 2. The analysis is done for 10 levels. In Figure 5.7 and Figure 5.8, the original forward signal and the normalized coefficients of each subband, for both low and high Q-factor wavelets, can be seen. The signal energy percents of each subband are given on the right side of each subband.

As expected, in both situations, emboli waveform shows itself in the middle subbands (in the second subband for low Q-factor case and in the second and third subbands for high Q-factor case). In low Q-factor case, a clear emboli waveform representation can not be achieved because of the noise components. On the other hand, a clear representation of emboli information can be achieved when a high Q-factor is employed. Additionally, in Figure 5.9 and Figure 5.10, reconstructed each subband, with both low and high Q-factor wavelets, are given respectively. As it can be seen, in high Q-factor case, a clearer emboli information is achieved and at the last subband artifact waveform is also extracted.

5.6 Discussion and Conclusions

In this chapter, a directional DT-RADWT, which can be applied directly to quadrature signals and have the ability of extracting directional information during analysis, is introduced. With the proposed directional transform, the traditional PFT step, which is used for extracting directional signals prior to wavelet analysis, is eliminated. In the DDT-RADWT, frequency resolution of wavelet atoms can be changed by tuning their Q-factor according to the behavior of analyzed signal. Additionally, the proposed transform has near shift-invariance property, which is very important in processing quadrature Doppler signals due to the phase relationship between their in-phase and quadrature-phase components. In order to measure the performance of the proposed method, a quadrature Doppler signal is processed with both the classical

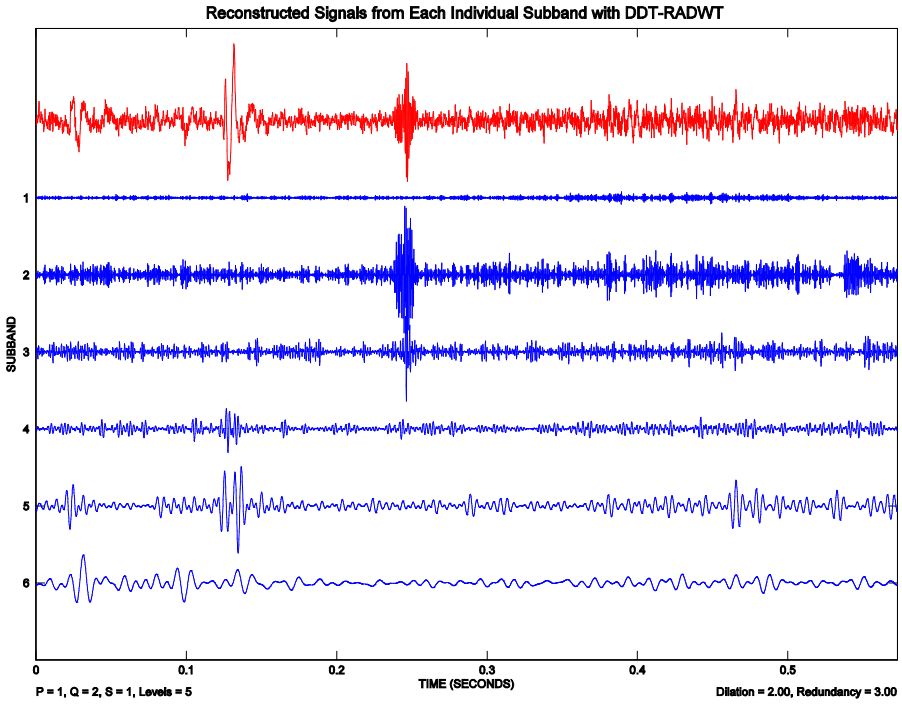

Figure 5.9 Original signal (red, first row) and the recontructed subbands (blue, rows 2 to 7) by using low Q-factor wavelet analysis (equivalent to dyadic-DWT).

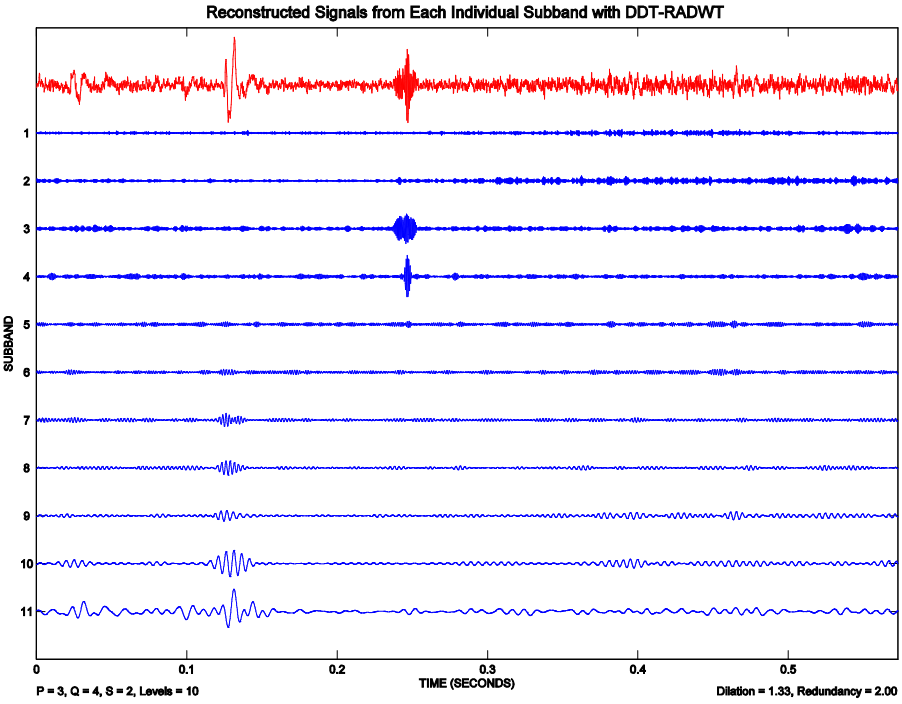

Figure 5.10 Original signal (red, first row) and the recontructed subbands (blue, rows 2 to 12) by using high Q-factor wavelet analysis.

PFT and DDT-RADWT. The results verify that with the DDT-RADWT, directional information can be obtained accurately at the end of the transform without any distortion in the emboli information. Additionally, in order to test the ability of proposed transform in representing emboli information in decomposed subbands, a quadrature Doppler ultrasound signal is analyzed with DDT-RADWT with low and high Q-factors. It is seen that with a high Q-factor analysis, a clear emboli information can be achieved. In the future, proposed DDT-RADWT can be employed in a real-time embolic signal detection algorithm in order to obtain sparse representations of emboli information in decomposed subbands.

6. CONCLUSIONS AND FUTURE WORKS

6.1 General Conclusions

Human body contains many complex systems which perform many physiological processes. These physiological processes constantly produce information about our body condition. This information can be observed through physiological instruments that measure heart rate, blood flow, oxygen saturation levels, blood glucose, lung activity, brain activity and so forth. Traditionally, such measurements are captured at specific points in time and physicians actually see less than one percent of these values, and their treatment decisions are made based upon limited information. However, biomedical signals constantly capture valuable information about these physiological processes as an output of physiological instruments and using digital signal processing techniques, useful supplementary information can be provided from these signals which can improve the success of clinicians' decisions.

Most of the biomedical signals, due to the inherent time-varying character of the underlying physiological processes, are non-stationary, which means their statistical properties are changing with time. Wavelet transform provides a time-scale representation of signals which have good frequency resolution at low frequencies, but also have good time resolution at high frequencies. Because of its adjustable time-frequency representation capability, wavelet transform plays a key role in processing non-stationary biomedical signals.

Automatic computerized analysis of non-stationary biomedical signals has become an active field due to the improvements in digital acquisition systems, computer technology and wavelet based processing techniques in the last three decades. In this thesis, novel Fourier/wavelet transform based biomedical signal processing algorithms, which can be used in automatic diagnosis systems, and novel complex wavelet transforms for processing specific type of biomedical signals are proposed. As biomedical

signals, acoustic lung signals and blood flow signals in quadrature format are employed.

In the first part (Chapter 2) of this thesis, a pulmonary crackle detection method in which the DTCWT is used as a pre-processing step for removing the frequency bands containing no-crackle information is proposed. In this method, various feature sets using TF and TS analysis are extracted and fed to the SVMs, MLP, and k-NN classifiers. It is observed that the overall accuracy and crackle detection performances of the SVMs appear to be superior over the k-NN and MLP on both undenoised and denoised data. Denoising by using DTCWT improves the success of the proposed method in detecting the crackle signals for all classifiers. It is also concluded that ensemble of networks increases the overall and TP accuracy performances of SVMs classifier for all ensemble results.

In the second part (Chapter 3), an emboli detection system in which the forward and reverse blood flow signals are transformed by using FFT, DWT and DTCWT for feature extraction is proposed. In order to get rid of the coefficients which do not contain relevant information, PCA is applied to these extracted features. The resultant new features of the forward flow are fed to SVMs and k-NN classifiers with different training dataset sizes and proportion of variance values. The results show that SVMs based detection methods are superior to k-NN based methods for all the feature extraction methods and the DTCWT is superior to the other coefficient transformation techniques. After proving that the best classification accuracies are yielded by SVMs, the probability distributions obtained by running distinct SVMs on forward and reverse directional signals separately are concatenated and used as a single input to the ensemble system. Using stacking as an ensemble method to take different representations of the data into consideration, namely forward and reverse directional signals, boosts the accuracy rate of the classification.

In the third part (Chapter 4), novel asymmetrical and symmetrical directional complex discrete wavelet packet transforms, which are specially designed for processing quadrature signals, are introduced. They have the ability of extracting directional information during analysis. With these proposed directional transforms, the traditional

PFT steps, which are used for extracting directional signals prior to wavelet analysis, are eliminated, resulting in a significant reduction in overall computational costs of the analysis system. As it can be seen from the results, the proposed methods work well for signals having narrow-band characteristics such as embolic signals.

Lastly in the fourth part (Chapter 5), a novel directional complex rational-dilation wavelet transform, which can be applied directly to quadrature signals and have the ability of extracting directional information during analysis, is introduced. In the proposed transform, frequency resolution of wavelet atoms can be changed by tuning their Q-factor according to the behavior of analyzed signal. Additionally, the proposed transform has near shift-invariance property, which is very important in processing quadrature Doppler signals due to the phase relationship between their in-phase and quadrature-phase components. The results verify that with the proposed transform, directional information can be obtained accurately at the end of the transform without any distortion in the emboli information. It is also seen that by tuning a proper Q-factor, clearer representations of emboli information (with less noise), when compared with the traditional dyadic discrete wavelet transform, are achieved in decomposed subbands with proposed method.

6.2 Future Works

Auscultation of pulmonary sounds via a stethoscope is a widely used, economic and noninvasive diagnostic method for chest diseases. However, it is highly subjective method that depends on the experience of the observer. Stethoscope has limited frequency response resulting in loss of valuable crackle information that found in frequencies above 120 Hz. Moreover, the information obtained with the stethoscope cannot be recorded in computers and is not appropriate for long term monitoring. Therefore, in Chapter 2 an automated crackle detection algorithm that can be reliably used in the analysis of pulmonary signals is proposed. In the future, the proposed crackle detection algorithm can be implemented in real-time as an online crackle detection system, which can be used in the pre-diagnosis of airways diseases such as pneumonia, bronchiecta-

sis, fibrosing alveolitis and asbestosis. For implementation, digital signal processors and field-programmable gate arrays can be employed and by this way portable multi-channel pulmonary sound acquisition devices that are used for home-care patients can be designed. Additionally, this real-time portable device can be used in the diagnosis and treatments of children and pregnant patients for whom radiography may be harmful.

Stroke is a condition causing partial or total paralysis, or death. The most common type of stroke occurs when a blood vessel in or around the brain becomes plugged. The plug can originate in an artery of the brain or somewhere else in the body, often the heart, where it breaks off and travels up the arterial tree to the brain, until it lodges in a blood vessel. These travelling clots, which are particles larger than red blood cells, are called emboli. Traditionally, for detecting embolic signals, visual detection by using individual spectral recordings and acoustic detection by hearing the Doppler shift sound by human experts are the gold standards. However, these types of detection are time consuming (recordings of the patients may last for one hour or more) and subject to observer's experience. As a consequence of these drawbacks, an automated system is required for a reliable and clinically useful emboli detection technique. Therefore, in Chapter 3, an automated blood flow analysis system is introduced, which can be used for predicting whether a signal is emboli, artifact or speckle. As a future direction, the introduced system can be implemented as a real-time application that can be utilized in the asymptomatic circulating cerebral emboli detection, which allows the selection of patients who are prone to stroke and would particularly benefit from preventative treatment.

In Chapters 4 and 5, special directional complex discrete wavelet packet and directional complex rational-dilation wavelet transforms for processing quadrature format signals are proposed respectively. These transforms can be directly applied to quadrature signals and this reduces the computational complexity of quadrature signal processing procedure when compared with existing methods. Embolic signals, which can be used in the diagnosis of stroke, are extracted from quadrature blood flow signals. An important property of the proposed directional transforms is that they have

adjustable time frequency resolution resulting in the ability of obtaining the optimum representation of the analyzed signal. Therefore, in the future, the proposed directional transforms can be applied to quadrature blood flow signals as a denoising or feature extraction operator with the aim of obtaining sparse representations of embolic signals in the scale domain. Additionally, as another future direction, proposed directional transforms can be applied to the other fields of science such as communication, radar, sonar, and MR imaging, where the quadrature format signals are used.

REFERENCES

1. Serbes, G., C. O. Sakar, Y. P. Kahya, and N. Aydin, "Pulmonary crackle detection using time-frequency and time-scale analysis," *Digital Signal Processing*, Vol. 23, no. 3, pp. 1012 – 1021, 2013.

2. Serbes, G., C. Sakar, Y. Kahya, and N. Aydin, "Pulmonary crackle detection using time-frequency analysis," in *Signal Processing and Communications Applications Conference (SIU), 2012 20th*, pp. 1–4, IEEE, 2012.

3. Serbes, G., C. O. Sakar, Y. P. Kahya, and N. Aydin, "Feature extraction using time-frequency/scale analysis and ensemble of feature sets for crackle detection," in *Engineering in Medicine and Biology Society, EMBC, 2011 Annual International Conference of the IEEE*, pp. 3314–3317, IEEE, 2011.

4. Serbes, G., C. O. Sakar, Y. P. Kahya, and N. Aydin, "Effect of different window and wavelet types on the performance of a novel crackle detection algorithm," in *Convergence and Hybrid Information Technology*, pp. 575–581, Springer, 2011.

5. Serbes, G., B. Sakar, N. Aydin, and H. Gulcur, "An emboli detection system based on dual tree complex wavelet transform," in *XIII Mediterranean Conference on Medical and Biological Engineering and Computing 2013*, pp. 819–822, Springer International Publishing, 2014.

6. Serbes, G., B. Sakar, H. Gulcur, and N. Aydin, "An emboli detection system based on the dual tree complex wavelet transform and ensemble learning," *Medical and Biological Engineering and Computing*, 2014. submitted for publication.

7. Serbes, G., N. Aydin, and H. Gulcur, "Directional dual-tree complex wavelet packet transform implementation using band-limited synthetic signals," in *The International Conference on Health Informatics*, pp. 9–12, Springer International Publishing, 2014.

8. Serbes, G., N. Aydin, and H. O. Gulcur, "Directional dual-tree complex wavelet packet transform," in *Engineering in Medicine and Biology Society (EMBC), 2013 35th Annual International Conference of the IEEE*, pp. 3046–3049, IEEE, 2013.

9. Serbes, G., H. Gulcur, and N. Aydin, "Directional dual-tree complex wavelet packet transforms for processing quadrature signals," *Medical and Biological Engineering and Computing*, 2014. submitted for publication.

10. Serbes, G., H. Gulcur, and N. Aydin, "Symmetrical directional dual tree complex wavelet packet transform," in *Proceedings of the Annual International Conference of the IEEE Engineering in Medicine and Biology Society, EMBS*, 2014. submitted for publication.

11. Serbes, G., H. Gulcur, and N. Aydin, "Directional dual tree rational-dilation complex wavelet transform," in *Proceedings of the Annual International Conference of the IEEE Engineering in Medicine and Biology Society, EMBS*, 2014. submitted for publication.

12. Gavriely, N., *Breath Sounds Methodology*, Boca Raton,FL: CRC Press, 1995.

13. Pasterkamp, H., S. Kraman, and G. Wodicka, "Respiratory sounds. advances beyond the stethoscope," *Am. J. Respir. Crit. Care Med.*, Vol. 156, no. 3, pp. 974–987, 1997.

14. Lehrer, S., ed., *Understanding Lung Sounds, 3rd ed.*, WB Saunders Company, 2002.

15. Yeginer, M., and Y. P. Kahya, "Elimination of vesicular sounds from pulmonary crackle waveforms," *Computer Methods and Programs in Biomedicine*, Vol. 89, no. 1, pp. 1 – 13, 2008.

16. Nath, A., L. Capel, H. Fang, and G. He, "Inspiratory crackles: early and late," *Thorax*, Vol. 29, no. 2, pp. 223–227, 1974.

17. Piirila, P., and A. Sovijarvi, "Crackles: Recording, analysis and clinical significance," *European Respiratory Journal*, Vol. 8, no. 12, pp. 2139–2148, 1995.

18. Sovijarvi, A., P. Piirila, and R. Luukkonen, "Separation of pulmonary disorders with two-dimensional discriminant analysis of crackles," *Clinical Physiology*, Vol. 16, no. 2, pp. 171–181, 1996.

19. Vyshedskiy, A., F. Bezares, R. Paciej, M. Ebril, J. Shane, and R. Murphy, "Transmission of crackles in patients with interstitial pulmonary fibrosis, congestive heart failure, and pneumonia," *Chest*, Vol. 128, no. 3, pp. 1468–1474, 2005.

20. Yeginer, M., and Y. P. Kahya, "Feature extraction for pulmonary crackle representation via wavelet networks," *Computers in Biology and Medicine*, Vol. 39, no. 8, pp. 713 – 721, 2009.

21. Sen, I., and Y. Kahya, "A multi-channel device for respiratory sound data acquisition and transient detection," in *Engineering in Medicine and Biology Society, 2005. IEEE-EMBS 2005. 27th Annual International Conference of the*, pp. 6658–6661, Jan 2005.

22. Cohen, L., "Time-frequency distributions-a review," *Proceedings of the IEEE*, Vol. 77, pp. 941–981, Jul 1989.

23. Aydin, N., and H. Markus, "Time-scale analysis of quadrature doppler ultrasound signals," *Science, Measurement and Technology, IEE Proceedings* -, Vol. 148, pp. 15–22, Jan 2001.

24. Harris, F., "On the use of windows for harmonic analysis with the discrete fourier transform," *Proceedings of the IEEE*, Vol. 66, pp. 51–83, Jan 1978.

25. Kay, S. M., *Modern spectral estimation : theory and application / Steven M. Kay*, Englewood Cliffs, N.J. : Prentice Hall, 1988.

26. Aydin, N., and H. S. Markus, "Optimization of processing parameters for the analysis and detection of embolic signals," *European Journal of Ultrasound*, Vol. 12, no. 1, pp. 69 – 79, 2000.

27. Serbes, G., and N. Aydin, "Denoising embolic doppler ultrasound signals using dual tree complex discrete wavelet transform," in *Engineering in Medicine and Biology Society (EMBC), 2010 Annual International Conference of the IEEE*, pp. 1840–1843, Aug 2010.

28. Kingsbury, N., "Shift invariant properties of the dual-tree complex wavelet transform," in *In Proc. IEEE Int. Conf. Acoust., Speech, Signal Processing (ICASSP*, pp. 1221–1224, 1999.

29. Kingsbury, N., "The dual-tree complex wavelet transform: A new technique for shift invariance and directional filters," pp. 319–322, 1998.

30. Selesnick, I., R. Baraniuk, and N. Kingsbury, "The dual-tree complex wavelet transform," *Signal Processing Magazine, IEEE*, Vol. 22, pp. 123–151, Nov 2005.

31. Vapnik, V., *The Nature of Statistical Learning Theory*, Springer, New York, 1995.

32. Alpaydin, E., *Introduction to Machine Learning*, The MIT Press, 2010.

33. Hsu, C.-W., and C.-J. Lin, "A comparison of methods for multiclass support vector machines," *Neural Networks, IEEE Transactions on*, Vol. 13, pp. 415–425, Mar 2002.

34. Warner, B., and M. Misra, "Understanding neural networks as statistical tools," *American Statistician*, Vol. 50, no. 4, pp. 284–293, 1996.

35. Hansen, L. K., and P. Salamon, "Neural network ensembles," *IEEE Trans. Pattern Anal. Mach. Intell.*, Vol. 12, pp. 993–1001, Oct. 1990.

36. Wolpert, D. H., "Stacked generalization," *Neural Networks*, Vol. 5, pp. 241–259, 1992.

37. Markus, H., "Monitoring embolism in real time," *Circulation*, Vol. 102, no. 8, pp. 826–828, 2000.

38. Markus, H., A. Loh, and M. M. Brown, "Computerized detection of cerebral emboli and discrimination from artifact using doppler ultrasound.," *Stroke*, Vol. 24, no. 11, pp. 1667–72, 1993.

39. Ackerstaff, R. G., V. L. Babikian, D. Georgiadis, D. Russell, M. Siebler, M. P. Spencer, and D. Stump, "Basic identification criteria of doppler microembolic signals," *Stroke*, Vol. 26, no. 6, p. 1123, 1995.

40. Aydin, N., and D. Evans, "Implementation of directional doppler techniques using a digital signal processor," *Medical and Biological Engineering and Computing*, Vol. 32, no. 1, pp. 157–164, 1994.

41. Aydin, N., L. Fan, and D. H. Evans, "Quadrature-to-directional format conversion of doppler signals using digital methods," *Physiological Measurement*, Vol. 15, no. 2, p. 181, 1994.

42. Xu, D., and Y. Wang, "An automated feature extraction and emboli detection system based on the pca and fuzzy sets," *Comput. Biol. Med.*, Vol. 37, pp. 861–871, June 2007.

43. Liu, W., T. Wang, S. Chen, L. Luo, and X. Wang, "Complex frequency features for tcd signal analysis," in *World Congress on Medical Physics and Biomedical Engineering May 26-31, 2012, Beijing, China* (Long, M., ed.), Vol. 39 of *IFMBE Proceedings*, pp. 546–549, Springer Berlin Heidelberg, 2013.

44. Roy, E., P. Abraham, S. Montresor, M. Baudry, and J.-L. Saumet, "The narrow band hypothesis: An interesting approach for high-intensity transient signals (hits) detection," *Ultrasound in Medicine and Biology*, Vol. 24, no. 3, pp. 375 – 382, 1998.

45. Roy, E., S. Montresor, P. Abraham, and J.-L. Saumet, "Spectrogram analysis of arterial doppler signals for off-line automated {HITS} detection," *Ultrasound in Medicine and Biology*, Vol. 25, no. 3, pp. 349 – 359, 1999.

46. Aydin, N., S. Padayachee, and H. S. Markus, "The use of the wavelet transform to describe embolic signals," *Ultrasound in Medicine and Biology*, Vol. 25, no. 6, pp. 953 – 958, 1999.

47. Aydin, N., F. Marvasti, and H. S. Markus, "Embolic doppler ultrasound signal detection using discrete wavelet transform," *Trans. Info. Tech. Biomed.*, Vol. 8, pp. 182–190, June 2004.

48. Sakar, C. O., O. Kursun, and F. Gurgen, "A feature selection method based on kernel canonical correlation analysis and the minimum redundancy-maximum relevance filter method," *Expert Systems with Applications*, Vol. 39, no. 3, pp. 3432 – 3437, 2012.

49. Yang, J., and J. yu Yang, "Why can {LDA} be performed in {PCA} transformed space?," *Pattern Recognition*, Vol. 36, no. 2, pp. 563 – 566, 2003.

50. Mo, L. Y. L., and R. S. C. COBBOLD, "A stochastic model of the backscattered doppler ultrasound from blood," *Biomedical Engineering, IEEE Transactions on*, Vol. BME-33, pp. 20–27, Jan 1986.

51. Jones, S. A., and D. P. Giddens, "A simulation of transit time effects in doppler ultrasound signals," *Ultrasound in Medicine and Biology*, Vol. 16, no. 6, pp. 607 – 619, 1990.

52. Daubechies, I., *Ten Lectures on Wavelets*, Philadelphia, PA, USA: Society for Industrial and Applied Mathematics, 1992.

53. Young, R. K., *Wavelet Theory and its Applications*, Norwell, MA: Kluwer., 1993.

54. Mallat, S., *A Wavelet Tour of Signal Processing, Third Edition: The Sparse Way*, Academic Press, 3rd ed., 2008.

55. Strang, G., and T. Nguyen, *Wavelets and Filter Banks*, Cambridge, MA: Wellesley-Cambridge, 1997.

56. Khan, Y. U., and J. Gotman, "Wavelet based automatic seizure detection in intracerebral electroencephalogram.," *Clin Neurophysiol*, Vol. 114, no. 5, pp. 898–908, 2003.

57. Chaplot, S., L. Patnaik, and N. Jagannathan, "Classification of magnetic resonance brain images using wavelets as input to support vector machine and neural network," *Biomedical Signal Processing and Control*, Vol. 1, no. 1, pp. 86 – 92, 2006.

58. Bradley, A., and W. Wilson, "On wavelet analysis of auditory evoked potentials," *Clinical Neurophysiology*, Vol. 115, no. 5, pp. 1114 – 1128, 2004.

59. Selesnick, I., "Hilbert transform pairs of wavelet bases," *Signal Processing Letters, IEEE*, Vol. 8, pp. 170–173, June 2001.

60. Yu, R., and H. Ozkaramanli, "Hilbert transform pairs of orthogonal wavelet bases: necessary and sufficient conditions," *Signal Processing, IEEE Transactions on*, Vol. 53, pp. 4723–4725, Dec 2005.

61. Kingsbury, N., "Image processing with complex wavelets," *Phil. Trans. Royal Society London A*, Vol. 357, pp. 2543–2560, 1997.

62. Friedman, J. H., and U. Fayyad, "On bias, variance, 0/1-loss, and the curse-of-dimensionality," *Data Mining and Knowledge Discovery*, Vol. 1, pp. 55–77, 1997.

63. Belkin, M., and P. Niyogi, "Laplacian eigenmaps for dimensionality reduction and data representation," *Neural Computation*, Vol. 15, pp. 1373–1396, 2002.

64. Zou, H., T. Hastie, and R. Tibshirani, "Sparse principal component analysis," *Journal of Computational and Graphical Statistics*, Vol. 15, p. 2006, 2004.

65. Martinez, A. M., A. M. Mart'inez, and A. C. Kak, "Pca versus lda," *IEEE Transactions on Pattern Analysis and Machine Intelligence*, Vol. 23, pp. 228–233, 2001.

66. Lyons, R. G., *Understanding Digital Signal Processing (3rd Edition)*, Upper Saddle River, NJ, USA: Prentice Hall PTR, 2010.

67. Aydin, N., *Computerised graft monitoring*. PhD thesis, University of Leicester, Leicester, UK, 1994.

68. Serbes, G., "Analysis of quadrature doppler signals with a modified dual-tree complex wavelet transform," Master's thesis, Bahcesehir University, Istanbul, Turkey, 2009.

69. Aydin, N., and H. Markus, "Directional wavelet transform in the context of complex quadrature doppler signals," *IEEE Signal Processing Letters*, Vol. 7, no. 10, pp. 278–280, 2000.

70. Brechet, L., M.-F. Lucas, C. Doncarli, and D. Farina, "Compression of biomedical signals with mother wavelet optimization and best-basis wavelet packet selection," *IEEE Transactions on Biomedical Engineering*, Vol. 54, no. 12, pp. 2186–2192, 2007.

71. Coifman, R. R., and M. V. Wickerhauser, "Entropy-based algorithms for best basis selection," *IEEE Transactions on Information Theory*, Vol. 38, no. 2 pt II, pp. 713–718, 1992.

72. Kannan, R., and M. Vetterli, "Best wavelet packet bases in a rate-distortion sense," *IEEE Transactions on Image Processing*, Vol. 2, no. 2, pp. 160–174, 1993.

73. Vautrin, D., X. Artusi, M. Lucas, and D. Farina, "A novel criterion of wavelet packet best basis selection for signal classification with application to brain-computer interfaces.," *IEEE transactions on bio-medical engineering*, Vol. 56, no. 11 Pt 2, pp. 2734–2738, 2009.

74. Ravier, P., and P.-O. Amblard, "Wavelet packets and de-noising based on higher-order-statistics for transient detection," *Signal Processing*, Vol. 81, no. 9, pp. 1909–1926, 2001.

75. Khushaba, R., S. Kodagoda, S. Lal, and G. Dissanayake, "Driver drowsiness classification using fuzzy wavelet-packet-based feature-extraction algorithm," *IEEE Transactions on Biomedical Engineering*, Vol. 58, no. 1, pp. 121–131, 2011.

76. Kingsbury, N., "Complex wavelets for shift invariant analysis and filtering of signals," *Applied and Computational Harmonic Analysis*, Vol. 10, no. 3, pp. 234–253, 2001.

77. Bayram, I., and I. Selesnick, "On the dual-tree complex wavelet packet and m-band transforms," *IEEE Transactions on Signal Processing*, Vol. 56, no. 6, pp. 2298–2310, 2008.

78. Ozkaramanli, H., and R. Yu, "On the phase condition and its solution for hilbert transform pairs of wavelet bases," *IEEE Transactions on Signal Processing*, Vol. 51, no. 12, pp. 3293–3294, 2003.

79. Jalobeanu, A., L. Blanc-Feraud, and J. Zerubia, "Satellite image deconvolution using complex wavelet packets," in *In Proc. of ICIP*, pp. 809–812, 2000.

80. Jalobeanu, A., L. Blanc-Feraud, and J. Zerubia, "Satellite image deblurring using complex wavelet packets," *International Journal of Computer Vision*, Vol. 51, no. 3, pp. 205–217, 2003.

81. Jalobeanu, A., N. Kingsbury, and J. Zerubia, "Image deconvolution using hidden markov tree modeling of complex wavelet packets," in *IEEE International Conference on Image Processing*, Vol. 1, pp. 201–204, 2001.

82. Xie, Z.-m., E.-f. Wang, G.-h. Zhang, G.-c. Zhao, and X.-g. Chen, "Seismic signal analysis based on the dual-tree complex wavelet packet transform," *Acta Seismologica Sinica*, Vol. 17, no. 1, pp. 117–122, 2004.

83. Oppenheim, A. V., R. W. Schafer, and J. R. Buck, *Discrete-time Signal Processing (2Nd Ed.)*, Upper Saddle River, NJ, USA: Prentice-Hall, Inc., 1999.

84. Marvasti, S., D. Gillies, F. Marvasti, and H. Markus, "Online automated detection of cerebral embolic signals using a wavelet-based system," *Ultrasound in Medicine and Biology*, Vol. 30, no. 5, pp. 647–653, 2004.

85. Serbes, G., and N. Aydin, "A new wavelet transform method for processing doppler signals," in *Proceedings of 2009 14th National Biomedical Engineering Meeting, BIYOMUT 2009*, 2009.

86. Serbes, G., and N. Aydin, "A complex discrete wavelet transform for processing quadrature doppler ultrasound signals," in *9th International Conference on Information Technology and Applications in Biomedicine, ITAB 2009*, 2009.

87. Serbes, G., and N. Aydin, "Denoising performance of modified dual tree complex wavelet transform," in *Proceedings of the IEEE/EMBS Region 8 International Conference on Information Technology Applications in Biomedicine, ITAB*, 2010.

88. Serbes, G., and N. Aydin, "Modified dual tree complex wavelet transform for processing quadrature signals," *Biomedical Signal Processing and Control*, Vol. 6, no. 3, pp. 301–306, 2011.

89. Serbes, G., and N. Aydin, "Symmetrical modified dual tree complex wavelet transform for processing quadrature doppler ultrasound signals," in *Proceedings of the Annual International Conference of the IEEE Engineering in Medicine and Biology Society, EMBS*, pp. 4816–4819, 2011.

90. Serbes, G., and N. Aydin, "Embolic doppler ultrasound signal detection using modified dual tree complex wavelet transform," in *Proceedings - IEEE-EMBS International Conference on Biomedical and Health Informatics: Global Grand Challenge of Health Informatics, BHI 2012*, pp. 945–947, 2012.

91. Serbes, G., and N. Aydin, "Denoising performance of modified dual-tree complex wavelet transform for processing quadrature embolic doppler signals," *Medical and Biological Engineering and Computing*, Vol. 52, no. 1, pp. 29–43, 2014.

92. Weickert, T., C. Benjaminsen, and U. Kiencke, "Analytic wavelet packets - combining the dual-tree approach with wavelet packets for signal analysis and filtering," *IEEE Transactions on Signal Processing*, Vol. 57, no. 2, pp. 493–502, 2009.

93. Goncalves, I. B., A. Leiria, and M. M. M. Moura, "Stft or cwt for the detection of doppler ultrasound embolic signals," *International Journal for Numerical Methods in Biomedical Engineering*, Vol. 29, no. 9, pp. 964–976, 2013.

94. Wang, X.-Y., H.-Y. Yang, and Z.-K. Fu, "A new wavelet-based image denoising using undecimated discrete wavelet transform and least squares support vector machine," *Expert Systems with Applications*, Vol. 37, no. 10, pp. 7040 – 7049, 2010.

95. Wu, P.-C., and L.-G. Chen, "An efficient architecture for two-dimensional discrete wavelet transform," *Circuits and Systems for Video Technology, IEEE Transactions on*, Vol. 11, pp. 536–545, Apr 2001.

96. Selesnick, I., "The double-density dual-tree dwt," *IEEE Transactions on Signal Processing*, Vol. 52, no. 5, pp. 1304–1314, 2004.

97. Chui, C., and W. He, "Compactly supported tight frames associated with refinable functions," *Applied and Computational Harmonic Analysis*, Vol. 8, no. 3, pp. 293–319, 2000.

98. Bayram, I., and I. Selesnick, "Frequency-domain design of overcomplete rational-dilation wavelet transforms," *IEEE Transactions on Signal Processing*, Vol. 57, no. 8, pp. 2957–2972, 2009.

99. Bayram, I., and I. Selesnick, "A dual-tree rational-dilation complex wavelet transform," *IEEE Transactions on Signal Processing*, Vol. 59, no. 12, pp. 6251–6256, 2011.

100. Quiroga, R., Z. Nadasdy, and Y. Ben-Shaul, "Unsupervised spike detection and sorting with wavelets and superparamagnetic clustering," *Neural Computation*, Vol. 16, no. 8, pp. 1661–1687, 2004.

101. Sankur, B., E. Guler, and Y. P. Kahya, "Multiresolution biological transient extraction applied to respiratory crackles," *Computers in Biology and Medicine*, Vol. 26, no. 1, pp. 25 – 39, 1996.

102. Letelier, J. C., and P. P. Weber, "Spike sorting based on discrete wavelet transform coefficients," *Journal of Neuroscience Methods*, Vol. 101, no. 2, pp. 93 – 106, 2000.